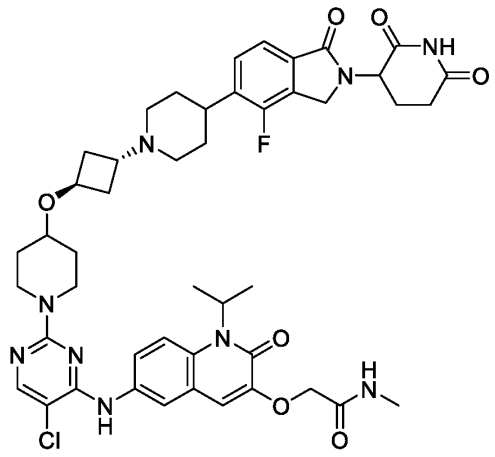
CRYSTALLINE FORMS OF A COMPOUND FOR THE TARGETED DEGRADATION OF BCL6

RELATED APPLICATIONS

This application claims priority to U.S. Provisional Application No. 63/575,269, filed on April 5, 2024. The entire contents of the foregoing application are expressly incorporated herein by reference.

TECHNICAL FIELD

The disclosure provides novel solid forms, solvates and solvate forms, and salts and salt forms of Compound A:



,

and to processes for their preparation. These solid forms, solvates and solid forms, and salts and salt forms are useful as modulators of targeted ubiquitination, especially with respect to a variety of polypeptides and other proteins, which are degraded and/or otherwise inhibited by the salts and salt forms of the present disclosure.

BACKGROUND

Most small molecule drugs bind enzymes or receptors in tight and well-defined pockets. On the other hand, protein-protein interactions are notoriously difficult to target using small molecules due to their large contact surfaces and the shallow grooves or flat interfaces involved. E3 ubiquitin ligases (of which hundreds are known in humans) confer substrate specificity for ubiquitination, and therefore, are more attractive therapeutic targets than general proteasome inhibitors due to their specificity for certain protein substrates. The

development of ligands of E3 ligases has proven challenging, in part due to the fact that they must disrupt protein-protein interactions. However, recent developments have provided specific ligands which bind to these ligases. For example, since the discovery of nutlins, the first small molecule E3 ligase inhibitors, additional compounds have been reported that target E3 ligases but the field remains underdeveloped.

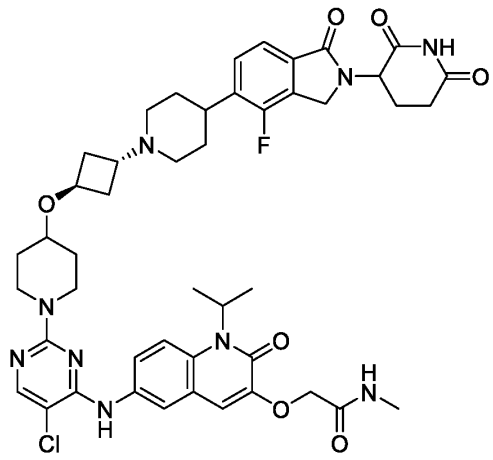
Cereblon is a protein that in humans is encoded by the *CRBN* gene. *CRBN* orthologs are highly conserved from plants to humans, which underscores its physiological importance. Cereblon forms an E3 ubiquitin ligase complex with damaged DNA binding protein 1 (DDB1), Cullin-4A (CUL4A), and regulator of cullins 1 (ROC1). This complex ubiquitinates a number of other proteins. Through a mechanism which has not been completely elucidated, cereblon ubiquitination of target proteins results in increased levels of fibroblast growth factor 8 (FGF8) and fibroblast growth factor 10 (FGF10). FGF8 in turn regulates a number of developmental processes, such as limb and auditory vesicle formation. The net result is that this ubiquitin ligase complex is important for limb outgrowth in embryos. In the absence of cereblon, DDB1 forms a complex with DDB2 that functions as a DNA damage-binding protein.

Bifunctional compounds such as those that are described in U.S. Patent Application Publications 2015-0291562 and 2014-0356322 (incorporated herein by reference), function to recruit endogenous proteins to an E3 ubiquitin ligase for degradation. In particular, the publications describe bifunctional or proteolysis targeting chimeric (PROTAC) compounds, which find utility as modulators of targeted ubiquitination of a variety of polypeptides and other proteins, which are then degraded and/or otherwise inhibited by the bifunctional compounds.

An ongoing need exists in the art for effective treatments for disease associated with (i) aberrant BCL6 expression and/or activity and/or (ii) overexpression or aggregation of B-cell lymphoma 6 protein (BCL6). However, non-specific effects, and the inability to target and modulate BCL6, remain as obstacles to the development of effective treatments. As such, small-molecule therapeutic agents that target BCL6 and that leverage or potentiate E3 ubiquitin ligase (e.g., cereblon's) substrate specificity would be very useful.

SUMMARY

The present disclosure is directed to of Compound A:



(Compound A),

and salts, solvates, solid forms thereof.

In some aspects, the present disclosure is directed to a free base form of Compound A. In some embodiments, Compound A is crystalline. In some embodiments, Compound A is amorphous.

In some aspects, the solid form of Compound A is a crystalline polymorphic form characterized by two or three XRPD signals selected from the group consisting of 8.2 °2θ, 8.7 °2θ, and 13.9 °2θ (±0.2 °2θ; Cu Kα1 radiation).

In some aspects, the solid form of Compound A is a crystalline polymorphic form characterized by XRPD spectra substantially similar to that shown in FIG 3B.

In some aspects, the solid form of Compound A is a crystalline polymorphic form characterized by one, two, three, four, five, six, seven, eight, nine, or ten XRPD signals selected from those in Table 1.

In some aspects, the solid form of Compound A is a crystalline polymorphic form characterized by one, two, three, four, five, six, seven, eight, nine, or ten XRPD signals selected from those in Table 2.

In some aspects, the present disclosure is directed to a salt of Compound A. In some embodiments, the salt of Compound A is crystalline. In some embodiments, the salt of Compound A is amorphous.

In some embodiments, the salt of Compound A is a hydrochloride salt. In some embodiments, the salt of Compound A is a maleate salt. In some embodiments, the salt of Compound A is a phosphate salt. In some embodiments, the salt of Compound A is a 1-hydroxy-2-naphthoate salt. In some embodiments, the salt of Compound A is a tartrate salt. In some embodiments, the salt of Compound A is a fumarate salt. In some embodiments, the salt of Compound A is a citrate salt. In some embodiments, the salt of Compound A is a

tosylate salt. In some embodiments, the salt of Compound A is a mesylate salt. In some embodiments, the salt of Compound A is a malate salt. In some embodiments, the salt of Compound A is a succinate salt.

In some aspects, the present disclosure is directed to a solvate of Compound A. In some embodiments, the solvate is an ethanol solvate. In some embodiments, the solvate of Compound A (e.g., the ethanol solvate of Compound A) is crystalline. In some embodiments, the solvate of Compound A (e.g., the ethanol solvate of Compound A) is amorphous.

In some aspects, the present disclosure is directed to a method of treating a disease or disorder comprising administering to a subject a therapeutically effective amount of a salt, solvate, and/or solid form of Compound A as disclosed herein.

BRIEF DESCRIPTION OF THE DRAWINGS

The accompanying drawings, which are included to provide a further understanding of the present disclosure, are incorporated in and constitute a part of this specification, illustrate aspects of the present disclosure and, together with the detailed description, serve to explain the principles of the present disclosure. The patent or application file contains at least one drawing executed in color. Copies of this patent or patent application publication with color drawing(s) will be provided by the Office upon request and payment of the necessary fee.

FIG. 1 depicts an XRPD diffractogram of the received Compound A (Freebase Pattern 1).

FIG. 2A depicts a post-DVS XRPD diffractogram of the received Compound A.

FIG. 2B depicts the reference XRPD diffractogram of the received Compound A.

FIG. 3A depicts VT-XRPD diffractogram, pattern 1, of Compound A as described in Example 2.

FIG. 3B depicts VT-XRPD diffractogram, pattern 2, of Compound A as described in Example 2.

FIG. 3C depicts VT-XRPD diffractogram, after heating to 30 °C, of Compound A as described in Example 2.

FIG. 3D depicts VT-XRPD diffractogram, after heating to 100 °C, of Compound A as described in Example 2.

FIG. 3E depicts VT-XRPD diffractogram, after heating to 210 °C, of Compound A as described in Example 2.

FIG. 4A depicts VT-XRPD diffractogram, pattern 1, of Compound A as described in Example 2.

FIG. 4B depicts VT-XRPD diffractogram, pattern 2, of Compound A as described in Example 2.

FIG. 4C depicts VT-XRPD diffractogram, after heating to 225 °C, of Compound A as described in Example 2.

FIG. 4D depicts VT-XRPD diffractogram, after heating to 240 °C, of Compound A as described in Example 2.

FIG. 4E depicts VT-XRPD diffractogram, after heating to 255 °C, of Compound A as described in Example 2.

FIG. 5A depicts VT-XRPD diffractogram, pattern 1, of Compound A as described in Example 2.

FIG. 5B depicts VT-XRPD diffractogram, pattern 2, of Compound A as described in Example 2.

FIG. 5C depicts VT-XRPD diffractogram, after heating to 270 °C, of Compound A as described in Example 2.

FIG. 5D depicts VT-XRPD diffractogram, after heating to 280 °C, of Compound A as described in Example 2.

FIG. 5E depicts VT-XRPD diffractogram, after cooling back to 30 °C, of Compound A as described in Example 2.

FIG. 6A depicts XRPD diffractograms of solids recovered from the amorphous preparation trial experiment as described in Example 3.

FIG. 6B depicts the reference XRPD diffractogram of the received Compound A.

FIG. 7A depicts the reference XRPD diffractogram of the received Compound A.

FIG. 7B depicts XRPD diffractogram of solids recovered from the amorphous preparation trial experiment as described in Example 3.

FIG. 8A depicts a XRPD diffractogram, pattern 1, of Compound A as described in Example 4.

FIG. 8B depicts a XRPD diffractogram of the Compound A solids recovered from the 1-propanol solubility assessments described in Example 4.

FIG. 8C depicts a XRPD diffractogram of the Compound A solids recovered from the 2-methyl THF solubility assessments described in Example 4.

FIG. 8D depicts a XRPD diffractogram of the Compound A solids recovered from the 2-propanol solubility assessments described in Example 4.

FIG. 9A depicts a XRPD diffractogram, pattern 1, of the Compound A as described in Example 4.

FIG. 9B depicts a XRPD diffractogram of the Compound A solids recovered from the acetone solubility assessments described in Example 4.

FIG. 9C depicts a XRPD diffractogram of the Compound A solids recovered from the acetonitrile solubility assessments described in Example 4.

FIG. 9D depicts a XRPD diffractogram of the Compound A solids recovered from the dichloroethane solubility assessments described in Example 4.

FIG. 10A depicts a XRPD diffractogram, pattern 1, of the Compound A as described in Example 4.

FIG. 10B depicts a XRPD diffractogram of the Compound A solids recovered from the dichloromethane:methanol (75:25) solubility assessments described in Example 4.

FIG. 10C depicts a XRPD diffractogram of the Compound A solids recovered from the dichloromethane:methanol (25:75) solubility assessments described in Example 4.

FIG. 10D depicts a XRPD diffractogram of the Compound A solids recovered from the dimethylsulfoxide:acetonitrile (1:1) solubility assessments described in Example 4.

FIG. 11A depicts a XRPD diffractogram, pattern 1, of the Compound A as described in Example 4.

FIG. 11B depicts a XRPD diffractogram of the Compound A solids recovered from the ethanol solubility assessments described in Example 4.

FIG. 11C depicts a XRPD diffractogram of the Compound A solids recovered from the ethyl acetate solubility assessments described in Example 4.

FIG. 11D depicts a XRPD diffractogram of the Compound A solids recovered from the heptane solubility assessments described in Example 4.

FIG. 12A depicts a XRPD diffractogram, pattern 1, of the Compound A as described in Example 4.

FIG. 12B depicts a XRPD diffractogram of the Compound A solids recovered from the isopropyl acetate solubility assessments described in Example 4.

FIG. 12C depicts a XRPD diffractogram of the Compound A solids recovered from the methanol solubility assessments described in Example 4.

FIG. 12D depicts a XRPD diffractogram of the Compound A solids recovered from the methyl acetate solubility assessments described in Example 4.

FIG. 13A depicts a XRPD diffractogram, pattern 1, of the Compound A as described in Example 4.

FIG. 13B depicts a XRPD diffractogram of the Compound A solids recovered from the methylethyl ketone solubility assessments described in Example 4.

FIG. 13C depicts a XRPD diffractogram of the Compound A solids recovered from the DMA solubility assessments described in Example 4.

FIG. 13D depicts a XRPD diffractogram of the Compound A solids recovered from the tBME solubility assessments described in Example 4.

FIG. 14A depicts a XRPD diffractogram, pattern 1, of the Compound A as described in Example 4.

FIG. 14B depicts a XRPD diffractogram of the Compound A solids recovered from the THF solubility assessments described in Example 4.

FIG. 14C depicts a XRPD diffractogram of the Compound A solids recovered from the toluene solubility assessments described in Example 4.

FIG. 14D depicts a XRPD diffractogram of the Compound A solids recovered from the water solubility assessments described in Example 4.

FIG. 15A depicts a XRPD diffractogram, pattern 1, of the Compound A as described in Example 4.

FIG. 15B depicts a XRPD diffractogram of the Compound A solids recovered from the NMP solubility assessments described in Example 4.

FIG. 15C depicts a XRPD diffractogram of the Compound A solids recovered from the trifluoroethanol solubility assessments described in Example 4.

FIG. 16A depicts a XRPD diffractogram, pattern 1, of the Compound A as described in Example 5.

FIG. 16B depicts a XRPD diffractogram, pattern 2, of the Compound A as described in Example 5.

FIG. 16C depicts a XRPD diffractogram of the Compound A solids recovered from the dried 2-methyl THF temperature cycling experiments described in Example 5.

FIG. 16D depicts a XRPD diffractogram of the Compound A solids recovered from the wet 2-methyl THF temperature cycling experiments described in Example 5.

FIG. 16E depicts a XRPD diffractogram of the Compound A solids recovered from the wet 2-propanol temperature cycling experiments described in Example 5.

FIG. 16F depicts a XRPD diffractogram of the Compound A solids recovered from the dried 2-propanol temperature cycling experiments described in Example 5.

FIG. 17A depicts a XRPD diffractogram, pattern 1, of the Compound A as described in Example 5.

FIG. 17B depicts a XRPD diffractogram, pattern 2, of the Compound A as described in Example 5.

FIG. 17C depicts a XRPD diffractogram of the Compound A solids recovered from the dried acetone temperature cycling experiments described in Example 5.

FIG. 17D depicts a XRPD diffractogram of the Compound A solids recovered from the wet acetone temperature cycling experiments described in Example 5.

FIG. 17E depicts a XRPD diffractogram of the Compound A solids recovered from the dried acetonitrile temperature cycling experiments described in Example 5.

FIG. 17F depicts a XRPD diffractogram of the Compound A solids recovered from the wet acetonitrile temperature cycling experiments described in Example 5.

FIG. 18A depicts a XRPD diffractogram, pattern 1, of the Compound A as described in Example 5.

FIG. 18B depicts a XRPD diffractogram, pattern 2, of the Compound A as described in Example 5.

FIG. 18C depicts a XRPD diffractogram of the Compound A solids recovered from the dried DCM temperature cycling experiments described in Example 5.

FIG. 18D depicts a XRPD diffractogram of the Compound A solids recovered from the wet DCM temperature cycling experiments described in Example 5.

FIG. 18E depicts a XRPD diffractogram of the Compound A solids recovered from the dried DCM:methanol (90:10) temperature cycling experiments described in Example 5.

FIG. 18F depicts a XRPD diffractogram of the Compound A solids recovered from the wet DCM:methanol (90:10) temperature cycling experiments described in Example 5.

FIG. 19A depicts a XRPD diffractogram, pattern 1, of the Compound A as described in Example 5.

FIG. 19B depicts a XRPD diffractogram, pattern 2, of the Compound A as described in Example 5.

FIG. 19C depicts a XRPD diffractogram of the Compound A solids recovered from the dried DCM:methanol (75:25) temperature cycling experiments described in Example 5.

FIG. 19D depicts a XRPD diffractogram of the Compound A solids recovered from the wet DCM:methanol (75:25) temperature cycling experiments described in Example 5.

FIG. 19E depicts a XRPD diffractogram of the Compound A solids recovered from the dried DCM:methanol (25:75) temperature cycling experiments described in Example 5.

FIG. 19F depicts a XRPD diffractogram of the Compound A solids recovered from the wet DCM:methanol (25:75) temperature cycling experiments described in Example 5.

FIG. 20A depicts a XRPD diffractogram, pattern 1, of the Compound A as described in Example 5.

FIG. 20B depicts a XRPD diffractogram, pattern 2, of the Compound A as described in Example 5.

FIG. 20C depicts a XRPD diffractogram of the Compound A solids recovered from the dried DMSO temperature cycling experiments described in Example 5.

FIG. 20D depicts a XRPD diffractogram of the Compound A solids recovered from the wet DMSO temperature cycling experiments described in Example 5.

FIG. 20E depicts a XRPD diffractogram of the Compound A solids recovered from the dried ethanol temperature cycling experiments described in Example 5.

FIG. 20F depicts a XRPD diffractogram of the Compound A solids recovered from the wet ethanol temperature cycling experiments described in Example 5.

FIG. 21A depicts a XRPD diffractogram, pattern 1, of the Compound A as described in Example 5.

FIG. 21B depicts a XRPD diffractogram, pattern 2, of the Compound A as described in Example 5.

FIG. 21C depicts a XRPD diffractogram of the Compound A solids recovered from the dried ethyl acetate temperature cycling experiments described in Example 5.

FIG. 21D depicts a XRPD diffractogram of the Compound A solids recovered from the wet ethyl acetate temperature cycling experiments described in Example 5.

FIG. 21E depicts a XRPD diffractogram of the Compound A solids recovered from the dried methanol temperature cycling experiments described in Example 5.

FIG. 21F depicts a XRPD diffractogram of the Compound A solids recovered from the wet methanol temperature cycling experiments described in Example 5.

FIG. 22A depicts a XRPD diffractogram, pattern 1, of the Compound A as described in Example 5.

FIG. 22B depicts a XRPD diffractogram, pattern 2, of the Compound A as described in Example 5.

FIG. 22C depicts a XRPD diffractogram of the Compound A solids recovered from the dried methanol:water (50:50) temperature cycling experiments described in Example 5.

FIG. 22D depicts a XRPD diffractogram of the Compound A solids recovered from the wet methanol:water (50:50) temperature cycling experiments described in Example 5.

FIG. 22E depicts a XRPD diffractogram of the Compound A solids recovered from the dried MEK temperature cycling experiments described in Example 5.

FIG. 22F depicts a XRPD diffractogram of the Compound A solids recovered from the wet MEK temperature cycling experiments described in Example 5.

FIG. 23A depicts a XRPD diffractogram, pattern 1, of the Compound A as described in Example 5.

FIG. 23B depicts a XRPD diffractogram, pattern 2, of the Compound A as described in Example 5.

FIG. 23C depicts a XRPD diffractogram of the Compound A solids recovered from the dried DMA temperature cycling experiments described in Example 5.

FIG. 23D depicts a XRPD diffractogram of the Compound A solids recovered from the wet DMA temperature cycling experiments described in Example 5.

FIG. 23E depicts a XRPD diffractogram of the Compound A solids recovered from the dried THF temperature cycling experiments described in Example 5.

FIG. 23F depicts a XRPD diffractogram of the Compound A solids recovered from the wet THF temperature cycling experiments described in Example 5.

FIG. 24A depicts a XRPD diffractogram, pattern 1, of the Compound A as described in Example 5.

FIG. 24B depicts a XRPD diffractogram, pattern 2, of the Compound A as described in Example 5.

FIG. 24C depicts a XRPD diffractogram of the Compound A solids recovered from the dried toluene temperature cycling experiments described in Example 5.

FIG. 24D depicts a XRPD diffractogram of the Compound A solids recovered from the wet toluene temperature cycling experiments described in Example 5.

FIG. 24E depicts a XRPD diffractogram of the Compound A solids recovered from the dried water temperature cycling experiments described in Example 5.

FIG. 24F depicts a XRPD diffractogram of the Compound A solids recovered from the wet water temperature cycling experiments described in Example 5.

FIG. 25A depicts a XRPD diffractogram, pattern 1, of the Compound A as described in Example 5.

FIG. 25B depicts a XRPD diffractogram, pattern 2, of the Compound A as described in Example 5.

FIG. 25C depicts a XRPD diffractogram of the Compound A solids recovered from the dried DMF temperature cycling experiments described in Example 5.

FIG. 25D depicts a XRPD diffractogram of the Compound A solids recovered from the wet DMF temperature cycling experiments described in Example 5.

FIG. 25E depicts a XRPD diffractogram of the Compound A solids recovered from the dried NMP temperature cycling experiments described in Example 5.

FIG. 25F depicts a XRPD diffractogram of the Compound A solids recovered from the wet NMP temperature cycling experiments described in Example 5.

FIG. 26A depicts a XRPD diffractogram, freebase pattern 1, of the Compound A as described in Example 5.

FIG. 26B depicts a XRPD diffractogram, freebase pattern 2, of the Compound A as described in Example 5.

FIG. 26C depicts a XRPD diffractogram of the Compound A solids recovered from the wet DCM:methanol (90:10) evaporation experiments described in Example 5.

FIG. 26D depicts a XRPD diffractogram of the Compound A solids recovered from the wet DCM:methanol (75:25) evaporation experiments described in Example 5.

FIG. 27A depicts a XRPD diffractogram, freebase pattern 1, of the Compound A as described in Example 5.

FIG. 27B depicts a XRPD diffractogram, freebase pattern 2, of the Compound A as described in Example 5.

FIG. 27C depicts a XRPD diffractogram of the Compound A solids recovered from the dried DCM:methanol (90:10) evaporation experiments described in Example 5.

FIG. 27D depicts a XRPD diffractogram of the Compound A solids recovered from the dried DCM:methanol (75:25) evaporation experiments described in Example 5.

FIG. 28A depicts a XRPD diffractogram, freebase pattern 1, of the Compound A as described in Example 5.

FIG. 28B depicts a XRPD diffractogram, freebase pattern 2, of the Compound A as described in Example 5.

FIG. 28C depicts a XRPD diffractogram of the Compound A solids recovered from the dried DMSO evaporation experiments described in Example 5.

FIG. 28D depicts a XRPD diffractogram of the Compound A solids recovered from the wet DMSO evaporation experiments described in Example 5.

FIG. 29A depicts a XRPD diffractogram, freebase pattern 1, of the Compound A as described in Example 5.

FIG. 29B depicts a XRPD diffractogram, freebase pattern 2, of the Compound A as described in Example 5.

FIG. 29C depicts a XRPD diffractogram of the Compound A solids recovered from the dried DMA evaporation experiments described in Example 5.

FIG. 29D depicts a XRPD diffractogram of the Compound A solids recovered from the wet DMA evaporation experiments described in Example 5.

FIG. 30A depicts a XRPD diffractogram, freebase pattern 1, of the Compound A as described in Example 5.

FIG. 30B depicts a XRPD diffractogram, freebase pattern 2, of the Compound A as described in Example 5.

FIG. 30C depicts a XRPD diffractogram of the Compound A solids recovered from the dried trifluoroethanol evaporation experiments described in Example 5.

FIG. 30D depicts a XRPD diffractogram of the Compound A solids recovered from the wet trifluoroethanol evaporation experiments described in Example 5.

FIG. 31A depicts a XRPD diffractogram, freebase pattern 1, of the Compound A as described in Example 5.

FIG. 31B depicts a XRPD diffractogram, freebase pattern 2, of the Compound A as described in Example 5.

FIG. 31C depicts a XRPD diffractogram of the Compound A solids recovered from the wet DCM:methanol (75:25) antisolvent addition experiments described in Example 5.

FIG. 31D depicts a XRPD diffractogram of the Compound A solids recovered from the dried DCM:methanol (75:25) antisolvent addition experiments described in Example 5.

FIG. 32A depicts a XRPD diffractogram, freebase pattern 1, of the Compound A as described in Example 5.

FIG. 32B depicts a XRPD diffractogram, freebase pattern 2, of the Compound A as described in Example 5.

FIG. 32C depicts a XRPD diffractogram of the Compound A solids recovered from the wet DMSO antisolvent addition experiments described in Example 5.

FIG. 32D depicts a XRPD diffractogram of the Compound A solids recovered from the dried DMSO antisolvent addition experiments described in Example 5.

FIG. 33A depicts a XRPD diffractogram, freebase pattern 1, of the Compound A as described in Example 5.

FIG. 33B depicts a XRPD diffractogram, freebase pattern 2, of the Compound A as described in Example 5.

FIG. 33C depicts a XRPD diffractogram of the Compound A solids recovered from the wet DMA antisolvent addition experiments described in Example 5.

FIG. 33D depicts a XRPD diffractogram of the Compound A solids recovered from the dried DMA antisolvent addition experiments described in Example 5.

FIG. 34A depicts a XRPD diffractogram, freebase pattern 1, of the Compound A as described in Example 5.

FIG. 34B depicts a XRPD diffractogram, freebase pattern 2, of the Compound A as described in Example 5.

FIG. 34C depicts a XRPD diffractogram of the Compound A solids recovered from the wet DCM:tBME (75:25) antisolvent addition experiments described in Example 5.

FIG. 34D depicts a XRPD diffractogram of the Compound A solids recovered from the dried DCM:tBME (75:25) antisolvent addition experiments described in Example 5.

FIG. 35A depicts a XRPD diffractogram, freebase pattern 1, of the Compound A as described in Example 5.

FIG. 35B depicts a XRPD diffractogram, freebase pattern 2, of the Compound A as described in Example 5.

FIG. 35C depicts a XRPD diffractogram of the Compound A solids recovered from the wet trifluoroethanol antisolvent addition experiments described in Example 5.

FIG. 35D depicts a XRPD diffractogram of the Compound A solids recovered from the dried trifluoroethanol antisolvent addition experiments described in Example 5.

FIG. 36A depicts a XRPD diffractogram, freebase pattern 1, of the Compound A as described in Example 5.

FIG. 36B depicts a XRPD diffractogram, freebase pattern 2, of the Compound A as described in Example 5.

FIG. 36C depicts a XRPD diffractograms of the Compound A solids recovered from the wet IPA:trifluoroethanol (25:75) slow cooling experiments described in Example 5.

FIG. 36D depicts a XRPD diffractograms of the Compound A solids recovered from the dried IPA:trifluoroethanol (25:75) slow cooling experiments described in Example 5.

FIG. 37A depicts a XRPD diffractogram, freebase pattern 1, of the Compound A as described in Example 5.

FIG. 37B depicts a XRPD diffractogram, freebase pattern 2, of the Compound A as described in Example 5.

FIG. 37C depicts a XRPD diffractograms of the Compound A solids recovered from the wet DCM:methanol (90:10) slow cooling experiments described in Example 5.

FIG. 37D depicts a XRPD diffractograms of the Compound A solids recovered from the dried DCM:methanol (90:10) slow cooling experiments described in Example 5.

FIG. 38A depicts a XRPD diffractogram, freebase pattern 1, of the Compound A as described in Example 5.

FIG. 38B depicts a XRPD diffractogram, freebase pattern 2, of the Compound A as described in Example 5.

FIG. 38C depicts a XRPD diffractograms of the Compound A solids recovered from the wet DCM:methanol (75:25) slow cooling experiments described in Example 5.

FIG. 38D depicts a XRPD diffractograms of the Compound A solids recovered from the dried DCM:methanol (75:25) slow cooling experiments described in Example 5.

FIG. 39A depicts a XRPD diffractogram, freebase pattern 1, of the Compound A as described in Example 5.

FIG. 39B depicts a XRPD diffractogram, freebase pattern 2, of the Compound A as described in Example 5.

FIG. 39C depicts a XRPD diffractograms of the Compound A solids recovered from the wet DMSO:water (75:25) slow cooling experiments described in Example 5.

FIG. 39D depicts a XRPD diffractograms of the Compound A solids recovered from the dried DMSO:water (75:25) slow cooling experiments described in Example 5.

FIG. 40A depicts a XRPD diffractogram, freebase pattern 1, of the Compound A as described in Example 5.

FIG. 40B depicts a XRPD diffractogram, freebase pattern 2, of the Compound A as described in Example 5.

FIG. 40C depicts a XRPD diffractograms of the Compound A solids recovered from the wet DMA slow cooling experiments described in Example 5.

FIG. 40D depicts a XRPD diffractograms of the Compound A solids recovered from the dried DMA slow cooling experiments described in Example 5.

FIG. 41A depicts a XRPD diffractogram, freebase pattern 1, of the Compound A as described in Example 5.

FIG. 41B depicts a XRPD diffractogram, freebase pattern 2, of the Compound A as described in Example 5.

FIG. 41C depicts a XRPD diffractograms of the Compound A solids recovered from the wet DMA:tBME (75:25) slow cooling experiments described in Example 5.

FIG. 41D depicts a XRPD diffractograms of the Compound A solids recovered from the dried DMA:tBME (75:25) slow cooling experiments described in Example 5.

FIG. 42A depicts a XRPD diffractogram, freebase pattern 1, of the Compound A as described in Example 5.

FIG. 42B depicts a XRPD diffractogram, freebase pattern 2, of the Compound A as described in Example 5.

FIG. 42C depicts a XRPD diffractograms of the Compound A solids recovered from the wet trifluoroethanol slow cooling experiments described in Example 5.

FIG. 42D depicts a XRPD diffractograms of the Compound A solids recovered from the dried trifluoroethanol slow cooling experiments described in Example 5.

FIG. 43A depicts a XRPD diffractogram of the Compound A solids recovered from the 1-propanol solvent drop experiments described in Example 5 before drying.

FIG. 43B depicts a XRPD diffractogram of the Compound A solids recovered from the 2-methyl THF solvent drop experiments described in Example 5 before drying.

FIG. 43C depicts a XRPD diffractogram of the Compound A solids recovered from the 2-propanol solvent drop experiments described in Example 5 before drying.

FIG. 43D depicts a XRPD diffractogram of the Compound A solids recovered from the acetone solvent drop experiments described in Example 5 before drying.

FIG. 43E depicts a XRPD diffractogram of the Compound A solids recovered from the acetonitrile solvent drop experiments described in Example 5 before drying.

FIG. 44A depicts a XRPD diffractogram of the Compound A solids recovered from the 1-propanol solvent drop experiments described in Example 5 after drying.

FIG. 44B depicts a XRPD diffractogram of the Compound A solids recovered from the 2-methyl THF solvent drop experiments described in Example 5 after drying.

FIG. 44C depicts a XRPD diffractogram of the Compound A solids recovered from the 2-propanol solvent drop experiments described in Example 5 after drying.

FIG. 44D depicts a XRPD diffractogram of the Compound A solids recovered from the acetone solvent drop experiments described in Example 5 after drying.

FIG. 44E depicts a XRPD diffractogram of the Compound A solids recovered from the acetonitrile solvent drop experiments described in Example 5 after drying.

FIG. 45A depicts a XRPD diffractogram of the Compound A solids recovered from the anisole solvent drop experiments described in Example 5 before drying.

FIG. 45B depicts a XRPD diffractogram of the Compound A solids recovered from the dichloromethane solvent drop experiments described in Example 5 before drying.

FIG. 45C depicts a XRPD diffractogram of the Compound A solids recovered from the DCM:methanol (90:10) solvent drop experiments described in Example 5 before drying.

FIG. 45D depicts a XRPD diffractogram of the Compound A solids recovered from the DCM:methanol (75:25) solvent drop experiments described in Example 5 before drying.

FIG. 45E depicts a XRPD diffractogram of the Compound A solids recovered from the DCM:methanol (25:75) solvent drop experiments described in Example 5 before drying.

FIG. 46A depicts a XRPD diffractogram of the Compound A solids recovered from the anisole solvent drop experiments described in Example 5 after drying.

FIG. 46B depicts a XRPD diffractogram of the Compound A solids recovered from the dichloromethane solvent drop experiments described in Example 5 after drying.

FIG. 46C depicts a XRPD diffractogram of the Compound A solids recovered from the DCM:methanol (90:10) solvent drop experiments described in Example 5 after drying.

FIG. 46D depicts a XRPD diffractogram of the Compound A solids recovered from the DCM:methanol (75:25) solvent drop experiments described in Example 5 after drying.

FIG. 46E depicts a XRPD diffractogram of the Compound A solids recovered from the DCM:methanol (25:75) solvent drop experiments described in Example 5 after drying.

FIG. 47A depicts a XRPD diffractogram of the Compound A solids recovered from the dimethysulfoxide solvent drop experiments described in Example 5 before drying.

FIG. 47B depicts a XRPD diffractogram of the Compound A solids recovered from the DMSO:acetonitrile solvent drop experiments described in Example 5 before drying.

FIG. 47C depicts a XRPD diffractogram of the Compound A solids recovered from the ethanol solvent drop experiments described in Example 5 before drying.

FIG. 47D depicts a XRPD diffractogram of the Compound A solids recovered from the ethyl acetate solvent drop experiments described in Example 5 before drying.

FIG. 47E depicts a XRPD diffractogram of the Compound A solids recovered from the heptane solvent drop experiments described in Example 5 before drying.

FIG. 48A depicts a XRPD diffractogram of the Compound A solids recovered from the dimethysulfoxide solvent drop experiments described in Example 5 after drying.

FIG. 48B depicts a XRPD diffractogram of the Compound A solids recovered from the DMSO:acetonitrile solvent drop experiments described in Example 5 after drying.

FIG. 48C depicts a XRPD diffractogram of the Compound A solids recovered from the ethanol solvent drop experiments described in Example 5 after drying.

FIG. 48D depicts a XRPD diffractogram of the Compound A solids recovered from the ethyl acetate solvent drop experiments described in Example 5 after drying.

FIG. 48E depicts a XRPD diffractogram of the Compound A solids recovered from the heptane solvent drop experiments described in Example 5 after drying.

FIG. 49A depicts a XRPD diffractogram of the Compound A solids recovered from the isopropyl acetate solvent drop experiments described in Example 5 before drying.

FIG. 49B depicts a XRPD diffractogram of the Compound A solids recovered from the methanol solvent drop experiments described in Example 5 before drying.

FIG. 49C depicts a XRPD diffractogram of the Compound A solids recovered from the methyl acetate solvent drop experiments described in Example 5 before drying.

FIG. 49D depicts a XRPD diffractogram of the Compound A solids recovered from the methylethyl ketone solvent drop experiments described in Example 5 before drying.

FIG. 49E depicts a XRPD diffractogram of the Compound A solids recovered from the DMA solvent drop experiments described in Example 5 before drying.

FIG. 50A depicts a XRPD diffractogram of the Compound A solids recovered from the isopropyl acetate solvent drop experiments described in Example 5 after drying.

FIG. 50B depicts a XRPD diffractogram of the Compound A solids recovered from the methanol solvent drop experiments described in Example 5 after drying.

FIG. 50C depicts a XRPD diffractogram of the Compound A solids recovered from the methyl acetate solvent drop experiments described in Example 5 after drying.

FIG. 50D depicts a XRPD diffractogram of the Compound A solids recovered from the methylethyl ketone solvent drop experiments described in Example 5 after drying.

FIG. 50E depicts a XRPD diffractogram of the Compound A solids recovered from the DMA solvent drop experiments described in Example 5 after drying.

FIG. 51A depicts a XRPD diffractogram of the Compound A solids recovered from the tBME solvent drop experiments described in Example 5 before drying.

FIG. 51B depicts a XRPD diffractogram of the Compound A solids recovered from the THF solvent drop experiments described in Example 5 before drying.

FIG. 51C depicts a XRPD diffractogram of the Compound A solids recovered from the toluene solvent drop experiments described in Example 5 before drying.

FIG. 51D depicts a XRPD diffractogram of the Compound A solids recovered from the water solvent drop experiments described in Example 5 before drying.

FIG. 51E depicts a XRPD diffractogram of the Compound A solids recovered from the trifluoroethanol solvent drop experiments described in Example 5 before drying.

FIG. 52A depicts a XRPD diffractogram of the Compound A solids recovered from the tBME solvent drop experiments described in Example 5 after drying.

FIG. 52B depicts a XRPD diffractogram of the Compound A solids recovered from the THF solvent drop experiments described in Example 5 after drying.

FIG. 52C depicts a XRPD diffractogram of the Compound A solids recovered from the toluene solvent drop experiments described in Example 5 after drying.

FIG. 52D depicts a XRPD diffractogram of the Compound A solids recovered from the water solvent drop experiments described in Example 5 after drying.

FIG. 52E depicts a XRPD diffractogram of the Compound A solids recovered from the trifluoroethanol solvent drop experiments described in Example 5 after drying.

FIG. 53A depicts a XRPD diffractogram, pattern 1, of the Compound A as described in Example 6.

FIG. 53B depicts a XRPD diffractogram, pattern 2, of the Compound A as described in Example 6.

FIG. 53C depicts the XRPD diffractogram of the first attempt of freebase pattern 2 scale-up subsample solids as described in Example 6.

FIG. 54A depicts a XRPD diffractogram, pattern 2, of the Compound A as described in Example 6.

FIG. 54B depicts the XRPD diffractogram of the Compound A subsample solids recovered from the second freebase Pattern 2 scale up experiment as described in Example 6.

FIG. 54C depicts the XRPD diffractogram of the Compound A wet solids recovered from the second freebase Pattern 2 scale up experiment as described in Example 6.

FIG. 54D depicts the XRPD diffractogram of the Compound A dried solids recovered from the second freebase Pattern 2 scale up experiment as described in Example 6.

FIG. 55A depicts a XRPD diffractogram, pattern 2, of the Compound A as described in Example 6 (initial peaks excluded).

FIG. 55B depicts the XRPD diffractogram of the Compound A subsample solids recovered from the second freebase Pattern 2 scale up experiment as described in Example 6 (initial peaks excluded).

FIG. 55C depicts the XRPD diffractogram of the Compound A wet solids recovered from the second freebase Pattern 2 scale up experiment as described in Example 6 (initial peaks excluded).

FIG. 55D depicts the XRPD diffractogram of the Compound A dried solids recovered from the second freebase Pattern 2 scale up experiment as described in Example 6 (initial peaks excluded).

FIG. 56A depicts a XRPD diffractogram, freebase pattern 1, of the Compound A as described in Example 7.

FIG. 56B depicts a XRPD diffractogram, freebase pattern 2, of the Compound A as described in Example 7.

FIG. 56C depicts a XRPD diffractogram, freebase pattern 3, of the Compound A as described in Example 7.

FIG. 56D depicts a XRPD diffractogram of the Compound A solids recovered from the DCM:methanol (75:25) 20 °C competitive slurry experiments described in Example 7 before drying.

FIG. 57A depicts a XRPD diffractogram, freebase pattern 1, of the Compound A as described in Example 7.

FIG. 57B depicts a XRPD diffractogram, freebase pattern 2, of the Compound A as described in Example 7.

FIG. 57C depicts a XRPD diffractogram, freebase pattern 3, of the Compound A as described in Example 7.

FIG. 57D depicts a XRPD diffractogram of the Compound A solids recovered from the DCM:methanol (75:25) 20 °C competitive slurry experiments described in Example 7 after drying.

FIG. 58A depicts a XRPD diffractogram, freebase pattern 1, of the Compound A as described in Example 7.

FIG. 58B depicts a XRPD diffractogram, freebase pattern 2, of the Compound A as described in Example 7.

FIG. 58C depicts a XRPD diffractogram of the Compound A solids recovered from the 2-propanol 20 °C competitive slurry experiments described in Example 7 after 2 days before drying.

FIG. 58D depicts a XRPD diffractogram of the Compound A solids recovered from the 2-propanol 20 °C competitive slurry experiments described in Example 7 after 9 days before drying.

FIG. 59A depicts a XRPD diffractogram, freebase pattern 1, of the Compound A as described in Example 7.

FIG. 59B depicts a XRPD diffractogram, freebase pattern 2, of the Compound A as described in Example 7.

FIG. 59C depicts a XRPD diffractogram of the Compound A solids recovered from the 2-propanol 20 °C competitive slurry experiments described in Example 7 after 2 days after drying.

FIG. 59D depicts a XRPD diffractogram of the Compound A solids recovered from the 2-propanol 20 °C competitive slurry experiments described in Example 7 after 9 days after drying.

FIG. 60A depicts a XRPD diffractogram, freebase pattern 1, of the Compound A as described in Example 7.

FIG. 60B depicts a XRPD diffractogram, freebase pattern 2, of the Compound A as described in Example 7.

FIG. 60C depicts a XRPD diffractogram of the Compound A solids recovered from the acetone 20 °C competitive slurry experiments described in Example 7 after 2 days before drying.

FIG. 60D depicts a XRPD diffractogram of the Compound A solids recovered from the acetone 20 °C competitive slurry experiments described in Example 7 after 9 days before drying.

FIG. 61A depicts a XRPD diffractogram, freebase pattern 1, of the Compound A as described in Example 7.

FIG. 61B depicts a XRPD diffractogram, freebase pattern 2, of the Compound A as described in Example 7.

FIG. 61C depicts a XRPD diffractogram of the Compound A solids recovered from the acetone 20 °C competitive slurry experiments described in Example 7 after 2 days after drying.

FIG. 61D depicts a XRPD diffractogram of the Compound A solids recovered from the acetone 20 °C competitive slurry experiments described in Example 7 after 9 days after drying.

FIG. 62A depicts a XRPD diffractogram, freebase pattern 1, of the Compound A as described in Example 7.

FIG. 62B depicts a XRPD diffractogram, freebase pattern 2, of the Compound A as described in Example 7.

FIG. 62C depicts a XRPD diffractogram of the Compound A solids recovered from the DMSO 20 °C competitive slurry experiments described in Example 7 after 2 days before drying.

FIG. 62D depicts a XRPD diffractogram of the Compound A solids recovered from the DMSO 20 °C competitive slurry experiments described in Example 7 after 9 days before drying.

FIG. 63A depicts a XRPD diffractogram, freebase pattern 1, of the Compound A as described in Example 7.

FIG. 63B depicts a XRPD diffractogram, freebase pattern 2, of the Compound A as described in Example 7.

FIG. 63C depicts a XRPD diffractogram of the Compound A solids recovered from the DMSO 20 °C competitive slurry experiments described in Example 7 after 2 days after drying.

FIG. 63D depicts a XRPD diffractogram of the Compound A solids recovered from the DMSO 20 °C competitive slurry experiments described in Example 7 after 9 days after drying.

FIG. 64A depicts a XRPD diffractogram, freebase pattern 1, of the Compound A as described in Example 7.

FIG. 64B depicts a XRPD diffractogram, freebase pattern 2, of the Compound A as described in Example 7.

FIG. 64C depicts a XRPD diffractogram of the Compound A solids recovered from the ethyl acetate 20 °C competitive slurry experiments described in Example 7 after 2 days before drying.

FIG. 64D depicts a XRPD diffractogram of the Compound A solids recovered from the ethyl acetate 20 °C competitive slurry experiments described in Example 7 after 9 days before drying.

FIG. 65A depicts a XRPD diffractogram, freebase pattern 1, of the Compound A as described in Example 7.

FIG. 65B depicts a XRPD diffractogram, freebase pattern 2, of the Compound A as described in Example 7.

FIG. 65C depicts a XRPD diffractogram of the Compound A solids recovered from the ethyl acetate 20 °C competitive slurry experiments described in Example 7 after 2 days after drying.

FIG. 65D depicts a XRPD diffractogram of the Compound A solids recovered from the ethyl acetate 20 °C competitive slurry experiments described in Example 7 after 9 days after drying.

FIG. 66A depicts a XRPD diffractogram, freebase pattern 1, of the Compound A as described in Example 7.

FIG. 66B depicts a XRPD diffractogram, freebase pattern 2, of the Compound A as described in Example 7.

FIG. 66C depicts a XRPD diffractogram of the Compound A solids recovered from the methanol:water (50:50) 20 °C competitive slurry experiments described in Example 7 after 2 days before drying.

FIG. 66D depicts a XRPD diffractogram of the Compound A solids recovered from the methanol:water (50:50) 20 °C competitive slurry experiments described in Example 7 after 9 days before drying.

FIG. 67A depicts a XRPD diffractogram, freebase pattern 1, of the Compound A as described in Example 7.

FIG. 67B depicts a XRPD diffractogram, freebase pattern 2, of the Compound A as described in Example 7.

FIG. 67C depicts a XRPD diffractogram of the Compound A solids recovered from the methanol:water (50:50) 20 °C competitive slurry experiments described in Example 7 after 2 days after drying.

FIG. 67D depicts a XRPD diffractogram of the Compound A solids recovered from the methanol:water (50:50) 20 °C competitive slurry experiments described in Example 7 after 9 days after drying.

FIG. 68A depicts a XRPD diffractogram, freebase pattern 1, of the Compound A as described in Example 7.

FIG. 68B depicts a XRPD diffractogram, freebase pattern 2, of the Compound A as described in Example 7.

FIG. 68C depicts a XRPD diffractogram of the Compound A solids recovered from the 2-propanol 35 °C competitive slurry experiments described in Example 7 before drying.

FIG. 68D depicts a XRPD diffractogram of the Compound A solids recovered from the 2-propanol 35 °C competitive slurry experiments described in Example 7 after drying.

FIG. 69A depicts a XRPD diffractogram, freebase pattern 1, of the Compound A as described in Example 7.

FIG. 69B depicts a XRPD diffractogram, freebase pattern 2, of the Compound A as described in Example 7.

FIG. 69C depicts a XRPD diffractogram of the Compound A solids recovered from the acetone 35 °C competitive slurry experiments described in Example 7 before drying.

FIG. 69D depicts a XRPD diffractogram of the Compound A solids recovered from the acetone 35 °C competitive slurry experiments described in Example 7 after drying.

FIG. 70A depicts a XRPD diffractogram, freebase pattern 1, of the Compound A as described in Example 7.

FIG. 70B depicts a XRPD diffractogram, freebase pattern 2, of the Compound A as described in Example 7.

FIG. 70C depicts a XRPD diffractogram of the Compound A solids recovered from the DMSO 35 °C competitive slurry experiments described in Example 7 before drying.

FIG. 70D depicts a XRPD diffractogram of the Compound A solids recovered from the DMSO 35 °C competitive slurry experiments described in Example 7 after drying.

FIG. 71A depicts a XRPD diffractogram, freebase pattern 1, of the Compound A as described in Example 7.

FIG. 71B depicts a XRPD diffractogram, freebase pattern 2, of the Compound A as described in Example 7.

FIG. 71C depicts a XRPD diffractogram of the Compound A solids recovered from the ethyl acetate 35 °C competitive slurry experiments described in Example 7 before drying.

FIG. 71D depicts a XRPD diffractogram of the Compound A solids recovered from the ethyl acetate 35 °C competitive slurry experiments described in Example 7 after drying.

FIG. 72A depicts a XRPD diffractogram, freebase pattern 1, of the Compound A as described in Example 7.

FIG. 72B depicts a XRPD diffractogram, freebase pattern 2, of the Compound A as described in Example 7.

FIG. 72C depicts a XRPD diffractogram of the Compound A solids recovered from the methanol:water (50:50) 35 °C competitive slurry experiments described in Example 7 before drying.

FIG. 72D depicts a XRPD diffractogram of the Compound A solids recovered from the methanol:water (50:50) 35 °C competitive slurry experiments described in Example 7 after drying.

FIG. 73A depicts a XRPD diffractogram, freebase pattern 1, of the Compound A as described in Example 8.

FIG. 73B depicts a XRPD diffractogram of freebase Pattern 3 of the Compound A solids obtained from DCM:methanol antisolvent addition as described in Example 8 before drying.

FIG. 73C depicts a XRPD diffractogram of freebase Pattern 3 of the Compound A solids obtained from DCM:methanol antisolvent addition as described in Example 8 after drying.

FIG. 74A depicts a XRPD diffractogram, freebase pattern 1, of the Compound A as described in Example 8.

FIG. 74B depicts a XRPD diffractogram of the Compound A solids obtained from 2-propanol 20 °C competitive slurry experiment as described in Example 8 before drying.

FIG. 74C depicts a XRPD diffractogram of the Compound A solids obtained from DCM:methanol antisolvent addition as described in Example 8 after drying.

FIG. 75A depicts a XRPD diffractogram, freebase pattern 1, of the Compound A as described in Example 9.

FIG. 75B depicts a XRPD diffractogram, freebase pattern 2, of the Compound A as described in Example 9.

FIG. 75C depicts a XRPD diffractogram of the Compound A solids recovered from the primary salt screen (HCl in ethyl acetate) before drying.

FIG. 75D depicts a XRPD diffractogram of the Compound A solids recovered from the primary salt screen (HCl in ethyl acetate) after drying

FIG. 75E depicts a XRPD diffractogram of the Compound A solids recovered from the primary salt screen (HCl in ethyl acetate) after 16 h of 40°C/ 75% RH storage.

FIG. 76A depicts a XRPD diffractogram, freebase pattern 1, of the Compound A as described in Example 9.

FIG. 76B depicts a XRPD diffractogram, freebase pattern 2, of the Compound A as described in Example 9.

FIG. 76C depicts a XRPD diffractogram of the Compound A solids recovered from the primary salt screen (HCl in MEK) before drying.

FIG. 76D depicts a XRPD diffractogram of the Compound A solids recovered from the primary salt screen (HCl in MEK) after drying

FIG. 76E depicts a XRPD diffractogram of the Compound A solids recovered from the primary salt screen (HCl in MEK) after 16 h of 40°C/ 75% RH storage.

FIG. 77A depicts a XRPD diffractogram, freebase pattern 1, of the Compound A as described in Example 9.

FIG. 77B depicts a XRPD diffractogram, freebase pattern 2, of the Compound A as described in Example 9.

FIG. 77C depicts a XRPD diffractogram of the solids of the Compound A recovered from the primary salt screen (maleic acid in ethyl acetate) as described in Example 9 before drying.

FIG. 77D depicts a XRPD diffractogram of the solids of the Compound A recovered from the primary salt screen (maleic acid in MEK) as described in Example 9 before drying.

FIG. 78A depicts a XRPD diffractogram, freebase pattern 1, of the Compound A as described in Example 9.

FIG. 78B depicts a XRPD diffractogram, freebase pattern 2, of the Compound A as described in Example 9.

FIG. 78C depicts a XRPD diffractogram of the solids of the Compound A recovered from the primary salt screen (phosphoric acid in 75:25 DCM:methanol) as described in Example 9 before drying.

FIG. 78D depicts a XRPD diffractogram of the solids of the Compound A recovered from the primary salt screen (phosphoric acid in 90:10 THF:water) as described in Example 9 before drying.

FIG. 79A depicts a XRPD diffractogram, freebase pattern 1, of the Compound A as described in Example 9.

FIG. 79B depicts a XRPD diffractogram, freebase pattern 2, of the Compound A as described in Example 9.

FIG. 79C depicts a XRPD diffractogram of the solids of the Compound A recovered from the primary salt screen (1-hydroxy-2-naphthoic acid in 90:10 THF:water) as described in Example 9 before drying.

FIG. 79D depicts a XRPD diffractogram of the solids of the Compound A recovered from the primary salt screen (1-hydroxy-2-naphthoic acid in methanol) as described in Example 9 before drying.

FIG. 79E depicts a XRPD diffractogram of the solids of the Compound A recovered from the primary salt screen (1-hydroxy-2-naphthoic acid in 75:25 DCM:methanol) as described in Example 9 before drying.

FIG. 80A depicts a XRPD diffractogram, freebase pattern 1, of the Compound A as described in Example 9.

FIG. 80B depicts a XRPD diffractogram, freebase pattern 2, of the Compound A as described in Example 9.

FIG. 80C depicts a XRPD diffractogram of the solids of the Compound A recovered from the primary salt screen (L-tartaric acid in 75:25 DCM:methanol) as described in Example 9 before drying.

FIG. 80D depicts a XRPD diffractogram of the solids of the Compound A recovered from the primary salt screen (L-tartaric acid in 75:25 DCM:methanol) as described in Example 9 after drying.

FIG. 80E depicts a XRPD diffractogram of the solids of the Compound A recovered from the primary salt screen (L-tartaric acid in 75:25 DCM:methanol) as described in Example 9 after 16 h of 40°C/ 75% RH storage.

FIG. 81A depicts a XRPD diffractogram, freebase pattern 1, of the Compound A as described in Example 9.

FIG. 81B depicts a XRPD diffractogram, freebase pattern 2, of the Compound A as described in Example 9.

FIG. 81C depicts a XRPD diffractogram of the solids of the Compound A recovered from the primary salt screen (fumaric acid in 90:10 THF:water) as described in Example 9 before drying.

FIG. 81D depicts a XRPD diffractogram of the solids of the Compound A recovered from the primary salt screen (fumaric acid in MEK) as described in Example 9 before drying.

FIG. 81E depicts a XRPD diffractogram of the solids of the Compound A recovered from the primary salt screen (fumaric acid in methanol) as described in Example 9 before drying.

FIG. 81F depicts a XRPD diffractogram of the solids of the Compound A recovered from the primary salt screen (fumaric acid in trifluoroethanol) as described in Example 9 before drying.

FIG. 82A depicts a XRPD diffractogram, freebase pattern 1, of the Compound A as described in Example 9.

FIG. 82B depicts a XRPD diffractogram, freebase pattern 2, of the Compound A as described in Example 9.

FIG. 82C depicts a XRPD diffractogram of the solids of the Compound A recovered from the primary salt screen (citric acid in MEK) as described in Example 9 before drying.

FIG. 82D depicts a XRPD diffractogram of the solids of the Compound A recovered from the primary salt screen (citric acid in MEK) as described in Example 9 after drying.

FIG. 82E depicts a XRPD diffractogram of the solids of the Compound A recovered from the primary salt screen (citric acid in MEK) as described in Example 9 after 16 h of 40°C/ 75% RH storage.

FIG. 83A depicts a XRPD diffractogram, freebase pattern 1, of the Compound A as described in Example 9.

FIG. 83B depicts a XRPD diffractogram, freebase pattern 2, of the Compound A as described in Example 9.

FIG. 83C depicts a XRPD diffractogram of the solids of the Compound A recovered from the primary salt screen (p-toluenesulfonic acid in MEK) as described in Example 9 before drying.

FIG. 83D depicts a XRPD diffractogram of the solids of the Compound A recovered from the primary salt screen (p-toluenesulfonic acid in trifluoroethanol) as described in Example 9 before drying.

FIG. 83E depicts a XRPD diffractogram of the solids of the Compound A recovered from the primary salt screen (p-toluenesulfonic acid in 75:25 DCM:methanol) as described in Example 9 before drying.

FIG. 84A depicts a XRPD diffractogram, freebase pattern 1, of the Compound A as described in Example 9.

FIG. 84B depicts a XRPD diffractogram, freebase pattern 2, of the Compound A as described in Example 9.

FIG. 84C depicts a XRPD diffractogram of the solids of the Compound A recovered from the primary salt screen (methanesulfonic acid in 75:25 DCM:methanol) as described in Example 9 before drying.

FIG. 84D depicts a XRPD diffractogram of the solids of the Compound A recovered from the primary salt screen (methanesulfonic acid in 75:25 DCM:methanol) as described in Example 9 after drying.

FIG. 84E depicts a XRPD diffractogram of the solids of the Compound A recovered from the primary salt screen (methanesulfonic acid in 75:25 DCM:methanol) as described in Example 9 after 16 h of 40°C/ 75% RH storage.

FIG. 85A depicts a XRPD diffractogram, freebase pattern 1, of the Compound A as described in Example 9.

FIG. 85B depicts a XRPD diffractogram, freebase pattern 2, of the Compound A as described in Example 9.

FIG. 85C depicts a XRPD diffractogram of the solids of the Compound A recovered from the primary salt screen (L-malic acid in ethyl acetate) as described in Example 9 before drying.

FIG. 85D depicts a XRPD diffractogram of the solids of the Compound A recovered from the primary salt screen (L-malic acid in methanol) as described in Example 9 before drying.

FIG. 86A depicts a XRPD diffractogram, freebase pattern 1, of the Compound A as described in Example 9.

FIG. 86B depicts a XRPD diffractogram, freebase pattern 2, of the Compound A as described in Example 9.

FIG. 86C depicts a XRPD diffractogram of the solids of the Compound A recovered from the primary salt screen (succinic acid in ethyl acetate) as described in Example 9 before drying.

FIG. 86D depicts a XRPD diffractogram of the solids of the Compound A recovered from the primary salt screen (succinic acid in methanol) as described in Example 9 before drying.

FIG. 86E depicts a XRPD diffractogram of the solids of the Compound A recovered from the primary salt screen (succinic acid in 75:25 DCM:methanol) as described in Example 9 before drying.

FIG. 87A depicts a XRPD diffractogram, freebase pattern 1, of the Compound A as described in Example 10.

FIG. 87B depicts a XRPD diffractogram, tosylate pattern 3, of the Compound A as described in Example 10.

FIG. 87C depicts a XRPD diffractogram of the solids recovered from the tosylate Pattern 3 mini scale-up experiment as described in Example 10 before drying.

FIG. 87D depicts a XRPD diffractogram of the solids recovered from the tosylate Pattern 3 mini scale-up experiment as described in Example 10 after drying.

FIG. 88A depicts a XRPD diffractogram, freebase pattern 1, of the Compound A as described in Example 10.

FIG. 88B depicts a XRPD diffractogram, freebase pattern 2, of the Compound A as described in Example 10.

FIG. 88C depicts a XRPD diffractogram, hydrochloride pattern 1, of the Compound A as described in Example 10.

FIG. 88D depicts a XRPD diffractogram of the initial solids recovered from the hydrochloride Pattern 1 mini scale-up experiment as described in Example 10 before drying.

FIG. 88E depicts a XRPD diffractogram of the solids recovered after the addition of more acid from the hydrochloride Pattern 1 mini scale-up experiment as described in Example 10 before drying.

FIG. 88F depicts a XRPD diffractogram of the solids recovered after the addition of water from the hydrochloride Pattern 1 mini scale-up experiment as described in Example 10 before drying.

FIG. 88G depicts a XRPD diffractogram of the solids recovered from the hydrochloride Pattern 1 mini scale-up experiment as described in Example 10 after drying.

FIG. 89A depicts a XRPD diffractogram, freebase pattern 1, of the Compound A as described in Example 10.

FIG. 89B depicts a XRPD diffractogram, freebase pattern 2, of the Compound A as described in Example 10.

FIG. 89C depicts a XRPD diffractogram, maleate pattern 1, of the Compound A as described in Example 10.

FIG. 89D depicts a XRPD diffractogram of the initial solids recovered from the maleate Pattern 1 mini scale-up experiment as described in Example 10 before drying.

FIG. 89E depicts a XRPD diffractogram of the solids recovered after the addition of more acid from the maleate Pattern 1 mini scale-up experiment as described in Example 10 before drying.

FIG. 89F depicts a XRPD diffractogram of the solids recovered after the addition of water from the maleate Pattern 1 mini scale-up experiment as described in Example 10 before drying.

FIG. 89G depicts a XRPD diffractogram of the solids recovered from the maleate Pattern 1 mini scale-up experiment as described in Example 10 after drying.

FIG. 90A depicts a XRPD diffractogram, freebase pattern 1, of the Compound A as described in Example 10.

FIG. 90B depicts a XRPD diffractogram, freebase pattern 2, of the Compound A as described in Example 10.

FIG. 90C depicts a XRPD diffractogram, phosphate pattern 1, of the Compound A as described in Example 10.

FIG. 90D depicts a XRPD diffractogram of the initial solids recovered from the phosphate Pattern 1 mini scale-up experiment as described in Example 10 before drying.

FIG. 90E depicts a XRPD diffractogram of the solids recovered after the addition of more acid from the phosphate Pattern 1 mini scale-up experiment as described in Example 10 before drying.

FIG. 90F depicts a XRPD diffractogram of the solids recovered after the addition of water from the phosphate Pattern 1 mini scale-up experiment as described in Example 10 before drying.

FIG. 90G depicts a XRPD diffractogram of the solids recovered from the phosphate Pattern 1 mini scale-up experiment as described in Example 10 after drying.

FIG. 91A depicts a XRPD diffractogram, freebase pattern 1, of the Compound A as described in Example 10.

FIG. 91B depicts a XRPD diffractogram, freebase pattern 2, of the Compound A as described in Example 10.

FIG. 91C depicts a XRPD diffractogram, 1-hydroxy-2-naphthoate pattern 3, of the Compound A as described in Example 10.

FIG. 91D depicts a XRPD diffractogram of the initial solids recovered from the 1-hydroxy-2-naphthoate Pattern 3 mini scale-up experiment as described in Example 10 before drying.

FIG. 91E depicts a XRPD diffractogram of the solids recovered after further temperature-cycling from the 1-hydroxy-2-naphthoate Pattern 3 mini scale-up experiment as described in Example 10 before drying.

FIG. 91F depicts a XRPD diffractogram of the solids recovered from the 1-hydroxy-2-naphthoate Pattern 3 mini scale-up experiment as described in Example 10 after drying.

FIG. 92A depicts a XRPD diffractogram, freebase pattern 1, of the Compound A as described in Example 10.

FIG. 92B depicts a XRPD diffractogram, freebase pattern 2, of the Compound A as described in Example 10.

FIG. 92C depicts a XRPD diffractogram, fumarate pattern 3, of the Compound A as described in Example 10.

FIG. 92D depicts a XRPD diffractogram of the initial solids recovered from the fumarate pattern 3 mini scale-up experiment as described in Example 10 before drying.

FIG. 92E depicts a XRPD diffractogram of the solids recovered after further temperature-cycling from the fumarate pattern 3 mini scale-up experiment as described in Example 10 before drying.

FIG. 92F depicts a XRPD diffractogram of the solids recovered from the fumarate pattern 3 mini scale-up experiment as described in Example 10 after drying.

FIG. 93A depicts a XRPD diffractogram, freebase pattern 1, of the Compound A as described in Example 10.

FIG. 93B depicts a XRPD diffractogram, freebase pattern 2, of the Compound A as described in Example 10.

FIG. 93C depicts a XRPD diffractogram, malate pattern 1, of the Compound A as described in Example 10.

FIG. 93D depicts a XRPD diffractogram of the initial solids recovered from the malate Pattern 1 mini scale-up experiment as described in Example 10 before drying.

FIG. 93E depicts a XRPD diffractogram of the solids recovered after the addition of more acid from the malate Pattern 1 mini scale-up experiment as described in Example 10 before drying.

FIG. 93F depicts a XRPD diffractogram of the solids recovered after the addition of water from the malate Pattern 1 mini scale-up experiment as described in Example 10 before drying.

FIG. 93G depicts a XRPD diffractogram of the solids recovered from the malate Pattern 1 mini scale-up experiment as described in Example 10 after drying.

FIG. 94A depicts a XRPD diffractogram, freebase pattern 1, of the Compound A as described in Example 10.

FIG. 94B depicts a XRPD diffractogram, freebase pattern 2, of the Compound A as described in Example 10.

FIG. 94C depicts a XRPD diffractogram, succinate pattern 2, of the Compound A as described in Example 10.

FIG. 94D depicts a XRPD diffractogram of the initial solids recovered from the succinate pattern 2 mini scale-up experiment as described in Example 10 before drying.

FIG. 94E depicts a XRPD diffractogram of the solids recovered after the addition of more acid from the succinate pattern 2 mini scale-up experiment as described in Example 10 before drying.

FIG. 94F depicts a XRPD diffractogram of the solids recovered after the addition of water from the succinate pattern 2 mini scale-up experiment as described in Example 10 before drying.

FIG. 94G depicts a XRPD diffractogram of the solids recovered from the succinate pattern 2 mini scale-up experiment as described in Example 10 after drying.

FIG. 95A depicts a XRPD diffractogram, freebase pattern 1, of the Compound A as described in Example 10.

FIG. 95B depicts a XRPD diffractogram, freebase pattern 2, of the Compound A as described in Example 10.

FIG. 95C depicts a XRPD diffractogram, tartrate pattern 1, of the Compound A as described in Example 10.

FIG. 95D depicts a XRPD diffractogram of the initial solids recovered from the tartrate pattern 1 mini scale-up experiment as described in Example 10 before drying.

FIG. 95E depicts a XRPD diffractogram of the solids recovered after the addition of more acid from the tartrate pattern 1 mini scale-up experiment as described in Example 10 before drying.

FIG. 95F depicts a XRPD diffractogram of the solids recovered after the addition of water from the tartrate pattern 1 mini scale-up experiment as described in Example 10 before drying.

FIG. 95G depicts a XRPD diffractogram of the solids recovered from the tartrate pattern 1 mini scale-up experiment as described in Example 10 after drying.

FIG. 96A depicts a XRPD diffractogram, freebase pattern 1, of the Compound A as described in Example 10.

FIG. 96B depicts a XRPD diffractogram, freebase pattern 2, of the Compound A as described in Example 10.

FIG. 96C depicts a XRPD diffractogram, citrate pattern 1, of the Compound A as described in Example 10.

FIG. 96D depicts a XRPD diffractogram of the initial solids recovered from the citrate pattern 1 mini scale-up experiment as described in Example 10 before drying.

FIG. 96E depicts a XRPD diffractogram of the solids recovered after the addition of more acid from the citrate pattern 1 mini scale-up experiment as described in Example 10 before drying.

FIG. 96F depicts a XRPD diffractogram of the solids recovered after the addition of water from the citrate pattern 1 mini scale-up experiment as described in Example 10 before drying.

FIG. 96G depicts a XRPD diffractogram of the solids recovered from the citrate pattern 1 mini scale-up experiment as described in Example 10 after drying.

FIG. 97A depicts a XRPD diffractogram, maleate pattern 1, of the Compound A as described in Example 11.

FIG 97B depicts a XRPD diffractogram of the aqueous solubility 200 mg maleate Pattern 1 preparation experiment before drying.

FIG 97C depicts a XRPD diffractogram of the aqueous solubility 200 mg maleate Pattern 1 preparation experiment after drying.

FIG. 98A depicts a XRPD diffractogram, tosylate pattern 3, of the Compound A as described in Example 11.

FIG 98B depicts a XRPD diffractogram of the aqueous solubility 200 mg tosylate pattern 3 preparation experiment before drying.

FIG 98C depicts a XRPD diffractogram of the aqueous solubility 200 mg tosylate pattern 3 preparation experiment after drying.

FIG. 99A depicts a XRPD diffractogram, fumarate pattern 5, of the Compound A as described in Example 11.

FIG 99B depicts a XRPD diffractogram of the aqueous solubility 200 mg fumarate pattern 5 preparation experiment before drying.

FIG 99C depicts a XRPD diffractogram of the aqueous solubility 200 mg fumarate pattern 5 preparation experiment after drying.

FIG. 100A depicts a XRPD diffractogram, maleate pattern 1, of the Compound A as described in Example 11.

FIG 100B depicts a XRPD diffractogram of the solids recovered from the aqueous solubility maleate Pattern 1 experiment after 30 minutes as described in Example 11.

FIG 100C depicts a XRPD diffractogram of the solids recovered from the aqueous solubility maleate Pattern 1 experiment after 24 hours as described in Example 11.

FIG. 101A depicts a XRPD diffractogram, tosylate pattern 3, of the Compound A as described in Example 11.

FIG 101B depicts a XRPD diffractogram of the solids recovered from the aqueous solubility tosylate pattern 3 experiment after 30 minutes as described in Example 11.

FIG 101C depicts a XRPD diffractogram of the solids recovered from the aqueous solubility tosylate pattern 3 experiment after 24 hours as described in Example 11.

FIG. 102A depicts a XRPD diffractogram, fumarate pattern 6, of the Compound A as described in Example 11.

FIG. 102B depicts a XRPD diffractogram, fumarate pattern 5, of the Compound A as described in Example 11.

FIG 102C depicts a XRPD diffractogram of the solids recovered from the aqueous solubility fumarate pattern 5 experiment after 30 minutes as described in Example 11.

FIG 102D depicts a XRPD diffractogram of the solids recovered from the aqueous solubility fumarate pattern 5 experiment after 24 hours as described in Example 11.

FIG. 103A depicts a XRPD diffractogram, freebase pattern 1, of the Compound A as described in Example 11.

FIG 103B depicts a XRPD diffractogram of the solids recovered from the aqueous solubility freebase pattern 1 experiment after 30 minutes as described in Example 11.

FIG 103C depicts a XRPD diffractogram of the solids recovered from the aqueous solubility freebase pattern 1 experiment after 24 hours as described in Example 11.

FIG. 104A depicts a XRPD diffractogram, freebase pattern 2, of the Compound A as described in Example 11.

FIG 104B depicts a XRPD diffractogram of the solids recovered from the aqueous solubility freebase pattern 2 experiment after 30 minutes as described in Example 11.

FIG 104C depicts a XRPD diffractogram of the solids recovered from the aqueous solubility freebase pattern 2 experiment after 24 hours as described in Example 11.

FIG. 105A depicts a XRPD diffractogram, freebase pattern 1, of the Compound A as described in Example 12.

FIG. 105B depicts a XRPD diffractogram, freebase pattern 2, of the Compound A as described in Example 12.

FIG. 105C depicts a XRPD diffractogram of the solids recovered from the freebase Pattern 2 secondary screen scale-up experiment before drying as described in Example 12.

FIG. 105D depicts a XRPD diffractogram of the solids recovered from the freebase Pattern 2 secondary screen scale-up experiment after drying as described in Example 12.

FIG. 106A depicts a XRPD diffractogram, freebase pattern 2, of the Compound A as described in Example 12.

FIG. 106B depicts the post-DVS analysis XRPD diffractogram of the solids recovered from the freebase Pattern 2 secondary screen scale-up experiment as described in Example 12.

FIG. 107A depicts a XRPD diffractogram, tosylate pattern 3, of the Compound A as described in Example 12.

FIG. 107B depicts a XRPD diffractogram of the solids recovered from the tosylate pattern 3 secondary screen scale-up experiment before drying as described in Example 12.

FIG. 107C depicts a XRPD diffractogram of the solids recovered from the tosylate pattern 3 secondary screen scale-up experiment after drying as described in Example 12.

FIG. 108A depicts a XRPD diffractogram, tosylate pattern 3, of the Compound A as described in Example 12.

FIG. 108B depicts the post-DVS analysis XRPD diffractogram of the solids recovered from the tosylate Pattern 3 secondary screen scale-up experiment as described in Example 12.

FIG. 109A depicts a XRPD diffractogram of the resulting freebase Pattern 2 after 40°C/ 75% RH storage in an open vial for 1 week as described in Example 12.

FIG. 109B depicts a XRPD diffractogram of the resulting freebase Pattern 2 after 80 °C storage in a closed vial for 1 week as described in Example 12.

FIG. 109C depicts a XRPD diffractogram of the resulting freebase Pattern 2 after storage in an open vial at ambient conditions for 1 week as described in Example 12.

FIG. 110A depicts a XRPD diffractogram of the resulting tosylate pattern 3 after 40°C/ 75% RH storage in an open vial for 1 week as described in Example 12.

FIG. 110B depicts a XRPD diffractogram of the resulting tosylate pattern 3 after 80 °C storage in a closed vial for 1 week as described in Example 12.

FIG. 110C depicts a XRPD diffractogram of the resulting tosylate pattern 3 after storage in an open vial at ambient conditions for 1 week as described in Example 12.

FIG. 111A depicts a XRPD diffractogram, freebase pattern 1, of the Compound A as described in Example 12.

FIG. 111B depicts a XRPD diffractogram, freebase pattern 2, of the Compound A as described in Example 12.

FIG. 111C depicts a XRPD diffractogram of the solids recovered from the freebase Pattern 2 pH solubility assessment at pH 1.2.

FIG. 111D depicts a XRPD diffractogram of the solids recovered from the freebase Pattern 2 pH solubility assessment at pH 4.5.

FIG. 111E depicts a XRPD diffractogram of the solids recovered from the freebase Pattern 2 pH solubility assessment at pH 6.8.

FIG. 112A depicts a XRPD diffractogram, freebase pattern 1, of the Compound A as described in Example 12.

FIG. 112B depicts a XRPD diffractogram, freebase pattern 2, of the Compound A as described in Example 12.

FIG. 112C depicts a XRPD diffractogram, tosylate pattern 3, of the Compound A as described in Example 12.

FIG. 112D depicts a XRPD diffractogram of the solids recovered from the tosylate pattern 3 pH solubility assessment at pH 1.2.

FIG. 112E depicts a XRPD diffractogram of the solids recovered from the tosylate pattern 3 pH solubility assessment at pH 4.5.

FIG. 112F depicts a XRPD diffractogram of the solids recovered from the tosylate pattern 3 pH solubility assessment at pH 6.8.

FIG. 113 depicts overlaid XRPD patterns of Form P2 of Compound A (Batches A & B).

FIG. 114 depicts the XRPD pattern of Form P2 of Compound A (Batch B).

FIG. 115 depicts a DSC thermogram of Form P2 of Compound A.

FIG. 116 depicts a TGA thermogram of Form P2 Compound A.

FIG. 117 depicts an XRPD pattern of a crystalline ethanol solvate form of Compound A – Batch A.

FIG. 118 depicts an XRPD pattern of a crystalline ethanol solvate form of Compound A – Batch B.

FIG. 119 depicts a TGA thermogram of a crystalline ethanol solvate form of Compound A – Batch A.

FIG. 120 depicts a DSC thermogram of a crystalline ethanol solvate form of Compound A – Batch A.

FIG. 121 depicts a DVS change in mass plot for a crystalline ethanol solvate form of Compound A – Batch A.

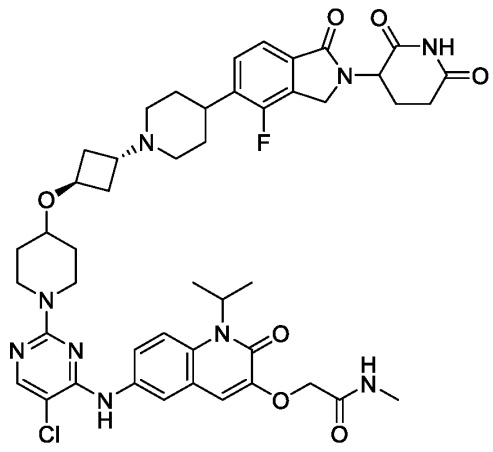
FIG. 122 depicts a DVS isotherm plot for a crystalline ethanol solvate form of Compound A – Batch A.

DETAILED DESCRIPTION

The present disclosure provides salts and polymorphic salt forms of Compound A that are useful in the preparation of a medicament and/or as pharmaceutical agents. In some embodiments, one or more of the salts and/or salt forms described herein can be formulated into a pharmaceutical composition.

Definitions

Compound A of the present disclosure refers to 2-((6-((5-chloro-2-(4-((1r,3r)-3-(4-(2-(2,6-dioxopiperidin-3-yl)-4-fluoro-1-oxoisoindolin-5-yl)piperidin-1-yl)cyclobutoxy)piperidin-1-yl)pyrimidin-4-yl)amino)-1-isopropyl-2-oxo-1,2-dihydroquinolin-3-yl)oxy)-N-methylacetamide, which has the following structure:



(Compound A).

In some embodiments, Compound A can be prepared as described in US Patent Application Publication No. 2022-0395576 A1, which is incorporated herein by reference in its entirety.

The terms "powder X-ray diffraction pattern", "PXRD pattern", "X-ray powder diffraction pattern", and "XRPD pattern" are used interchangeably and refer to the experimentally observed diffractogram or parameters derived therefrom. Powder X-ray diffraction patterns are typically characterized by peak positions (abscissa) and peak intensities (ordinate). The term "peak intensities" refers to relative signal intensities within a given X-ray diffraction pattern. Factors which can affect the relative peak intensities are sample thickness and preferred orientation (i.e., the crystalline particles are not distributed randomly). The term "peak positions" as used herein refers to X-ray reflection positions as measured and observed in powder X-ray diffraction experiments. Peak positions are directly related to the dimensions of the unit cell. The peaks, identified by their respective peak positions, are extracted from the diffraction patterns for the various polymorphic forms of salts of Compound A.

The terms "2 theta value", "2θ", "2 θ", "°2θ", or "°2 θ" refer to the peak position in degrees based on the experimental setup of the X-ray diffraction experiment and is a common abscissa unit in diffraction patterns. In general, the experimental setup requires that if a reflection is diffracted when the incoming beam forms an angle theta (θ) with a certain lattice plane, the reflected beam is recorded at an angle 2 theta (2 θ). It should be understood that reference herein to specific 2θ values for a specific polymorphic form is intended to mean the 2θ values (in degrees) as measured using the X-ray diffraction experimental conditions as described herein.

"Preferred orientation effects" refer to variable peak intensities or relative intensity differences between different XRPD measurements of the same samples that can be due to the orientation of the particles. Without wishing to be bound by theory, in XRPD it can be desirable to have a sample in which particles are oriented randomly (e.g., a powder). However, it can be difficult or in some cases impossible to achieve truly random particle orientations in practice. As particle size increases, the randomness of particle orientation can decrease, leading to increased challenges with achieving a preferred orientation. Without wishing to be bound by theory, a smaller particle size can reduce technical challenges associated with preferred orientation and allow for more accurate representation of peaks. However, one of skill in the art will understand how to reduce or mitigate preferred orientation effects and will recognize preferred orientation effects that can exist even between two different measurements of the same sample. For instance, in some embodiments,

differences in resolution or relative peak intensities can be attributed to preferred orientation effects.

As used herein, the term "substantially pure" with reference to a particular salt (or to a mixture of two or more salts) of a compound indicates the salt (or a mixture) includes less than 10%, less than 5%, less than 3%, less than 1%, less than 0.5%, less than 0.2%, or less than 0.1% by weight of impurities, including other salt forms of the compound. Such purity may be determined, for example, by powder X-ray diffraction.

As used herein, the term "polymorph" or "salt form" refers to different crystalline forms of the same compound and other solid state molecular forms including pseudo-polymorphs, such as hydrates (e.g., bound water present in the crystalline structure) and solvates (e.g., bound solvents other than water) of the same compound. Different crystalline polymorphs have different crystal structures due to a different packing of the molecules in the lattice. This results in a different crystal symmetry and/or unit cell parameters which directly influences its physical properties such as the X-ray diffraction characteristics of crystals or powders. A different polymorph, for example, will in general diffract at a different set of angles and will give different values for the intensities. Therefore, X-ray powder diffraction can be used to identify different polymorphs, or a solid form that comprises more than one polymorph, in a reproducible and reliable way (S. Byrn et al, Pharmaceutical Solids: A Strategic Approach to Regulatory Considerations, Pharmaceutical research, Vol. 12, No. 7, p. 945-954, 1995; J. K. Haleblian and W. McCrone, Pharmaceutical Applications of Polymorphism, Journal of Pharmaceutical Sciences, Vol. 58, No. 8, p. 91 1 -929, 1969).

Crystalline polymorphic forms are of interest to the pharmaceutical industry and especially to those involved in the development of suitable dosage forms. If the polymorphic form is not held constant during clinical or stability studies, the exact dosage form used or studied may not be comparable from one lot to another. It is also desirable to have processes for producing a compound with the selected polymorphic form in high purity when the compound is used in clinical studies or commercial products since impurities present may produce undesired toxicological effects. Certain polymorphic forms may exhibit enhanced thermodynamic stability or may be more readily manufactured in high purity in large quantities, and thus are more suitable for inclusion in pharmaceutical formulations. Certain polymorphs may display other advantageous physical properties such as lack of hygroscopic tendencies, improved solubility, and enhanced rates of dissolution due to different lattice energies.

The term "amorphous" refers to any solid substance which (i) lacks order in three dimensions, or (ii) exhibits order in less than three dimensions, order only over short distances (e.g., less than 10 Å), or both. Thus, amorphous substances include partially crystalline materials and crystalline mesophases with, e.g., one- or two-dimensional translational order (liquid crystals), orientational disorder (orientationally disordered crystals), or conformational disorder (conformationally disordered crystals). Amorphous solids may be characterized by known techniques, including X-ray powder diffraction (XRRD) crystallography, solid state nuclear magnet resonance (ssNMR) spectroscopy, differential scanning calorimetry (DSC), or some combination of these techniques. Amorphous solids give diffuse XRPD patterns, typically comprised of one or two broad peaks (i.e., peaks having base widths of about 5° 2 θ or greater).

The term "crystalline" refers to any solid substance exhibiting three-dimensional order, which in contrast to an amorphous solid substance, gives a distinctive XRPD pattern with sharply defined peaks.

The term "ambient temperature" refers to a temperature condition typically encountered in a laboratory setting. This includes the approximate temperature range of about 20 ° to about 30 °C.

The term "detectable amount" refers to an amount or amount per unit volume that can be detected using conventional techniques, such as X-ray powder diffraction, differential scanning calorimetry, HPLC, Fourier Transform Infrared Spectroscopy (FT- IR), Raman spectroscopy, and the like.

The term "solvate" describes a molecular complex comprising the drug substance and a stoichiometric or non-stoichiometric amount of one or more solvent molecules (e.g., ethanol). When the solvent is tightly bound to the drug the resulting complex will have a well-defined stoichiometry that is independent of humidity. When, however, the solvent is weakly bound, as in channel solvates and hygroscopic compounds, the solvent content will be dependent on humidity and drying conditions. In such cases, the complex may be non-stoichiometric.

The term "hydrate" describes a solvate comprising the drug substance and a stoichiometric or non-stoichiometric amount of water.

The term "relative humidity" refers to the ratio of the amount of water vapor in air at a given temperature to the maximum amount of water vapor that can be held at that temperature and pressure, expressed as a percentage.

The term "relative intensity" refers to an intensity value derived from a sample X-ray diffraction pattern. The complete ordinate range scale for a diffraction pattern is assigned a value of 100. A peak having intensity falling between about 50% to about 100% on this scale intensity is termed very strong (vs); a peak having intensity falling between about 50% to about 25% is termed strong (s). Additional weaker peaks are present in typical diffraction patterns and are also characteristic of a given polymorph, wherein the additional peaks are termed medium (m), weak (w) and very weak (vw).

The term "slurry" refers to a solid substance suspended in a liquid medium, typically water or an organic solvent.

The term "under vacuum" refers to typical pressures obtainable by a laboratory oil or oil-free diaphragm vacuum pump.

The term "pharmaceutical composition" refers to a composition comprising one or more of the polymorphic forms of salts of Compound A described herein, and other chemical components, such as physiologically/pharmaceutically acceptable carriers, diluents, vehicles and/or excipients. The purpose of a pharmaceutical composition is to facilitate administration of a compound to an organism, such as a human or other mammals.

The term "pharmaceutically acceptable" "carrier", "diluent", "vehicle", or "excipient" refers to a material (or materials) that may be included with a particular pharmaceutical agent to form a pharmaceutical composition, and may be solid or liquid. Exemplary solid carriers are lactose, sucrose, talc, gelatin, agar, pectin, acacia, magnesium stearate, stearic acid and the like. Exemplary liquid carriers are syrup, peanut oil, olive oil, water and the like. Similarly, the carrier or diluent may include time-delay or time-release material known in the art, such as glyceryl monostearate or glyceryl distearate alone or with a wax, ethylcellulose, hydroxypropyl methylcellulose, methylmethacrylate and the like.

The term "treating", as used herein, unless otherwise indicated, means reversing, alleviating, or inhibiting the progress of the disorder or condition to which such term applies, or one or more symptoms of such disorder or condition. The term "treatment", as used herein, unless otherwise indicated, refers to the act of "treating" as defined immediately above. For example, the terms "treat", "treating" and "treatment" can refer to a method of alleviating or abrogating a particular disorder and/or one or more of its attendant symptoms.

As used herein, "subject" means a human or animal (in the case of an animal, the subject can be a mammal). In one aspect, the subject is a human. In one aspect, the subject is a male.

The term "about" is used herein to mean approximately, in the region of, roughly or around. When the term "about" is used in conjunction with a numerical range, it modifies that range by extending the boundaries above and below the numerical values set forth. In general, the term "about" is used herein to modify a numerical value above and below the stated value by a variance of 20%, a variance of 10%, a variance of 5%, a variance of 3%, or a variance of 1%. When used in the context of XRPD peak values, the term "about" can indicate a peak value ±0.20, ±0.15, ±0.10, ±0.05, or ±0.01 °2θ. In some embodiments, when used in the context of XRPD peak values "about" can indicate a peak value at substantially exactly the disclosed peak value.

Crystalline Forms of Compound A

As set forth below, Compound A can form salts with different acids, and may also form solvates. In some embodiments, the salts and solvates of Compound A described herein exist in various crystalline forms. All XRPD peaks described herein are in °2θ ((±0.5 °2θ; ±0.2 °2θ; ±0.1 °2θ; or ±0.0 °2θ; Cu Kα1 radiation). Additionally, all XRPD spectra are obtained using Cu Kα1 X-rays at a wavelength of 1.5406 Å.

Compound A Free Base – Batch A

In some embodiments, the present disclosure provides solid forms of Compound A, e.g., crystalline forms of Compound A free base Pattern 2. In some embodiments, the Compound A free base Pattern 2 XRPD profile is substantially similar to that shown in FIG. 113.

In some embodiments, the solid form of Compound A free base Pattern 2 is crystalline Compound A free base Pattern 2 characterized by two or three XRPD signals selected from the group consisting of 8.2 °2θ, 8.6 °2θ, and 13.9 °2θ (±0.2 °2θ; ±0.1 °2θ; or ±0.0 °2θ; Cu Kα1 radiation). In some embodiments, the solid form of Compound A free base Pattern 2 is crystalline Compound A free base Pattern 2 characterized by XRPD signals at 8.2 °2θ, 8.7 °2θ, and 13.9 °2θ (±0.2 °2θ; ±0.1 °2θ; or ±0.0 °2θ; Cu Kα1 radiation).

In some embodiments, the solid form of Compound A free base Pattern 2 is crystalline Compound A free base Pattern 2 characterized by two or three XRPD signals selected from the group consisting of 5.3 °2θ, 8.2 °2θ, and 13.9 °2θ (±0.2 °2θ; ±0.1 °2θ; or ±0.0 °2θ; Cu Kα1 radiation). In some embodiments, the solid form of Compound A free base Pattern 2 is crystalline Compound A free base Pattern 2 characterized by XRPD signals at 5.3 °2θ, 8.2 °2θ, and 13.9 °2θ (±0.2 °2θ; ±0.1 °2θ; or ±0.0 °2θ; Cu Kα1 radiation).

In some embodiments, the solid form of Compound A free base Pattern 2 is crystalline Compound A free base Pattern 2 characterized by two or more, or three or more XRPD signals selected from the group consisting of 8.0 °2θ, 8.2 °2θ, 8.6 °2θ, 13.9 °2θ, and 16.0 °2θ (±0.2 °2θ; ±0.1 °2θ; or ±0.0 °2θ; Cu Kα1 radiation). In some embodiments, the solid form of Compound A free base Pattern 2 is crystalline Compound A free base Pattern 2 characterized by XRPD signals at 8.0 °2θ, 8.2 °2θ, 8.6 °2θ, 13.9 °2θ, and 16.0 °2θ (±0.2 °2θ; ±0.1 °2θ; or ±0.0 °2θ; Cu Kα1 radiation).

In some embodiments, the solid form of Compound A free base Pattern 2 is crystalline Compound A free base Pattern 2 characterized by two or more, or three or more XRPD signals selected from the group consisting of 5.3 °2θ, 8.2 °2θ, 8.6 °2θ, 13.9 °2θ, and 16.0 °2θ (±0.2 °2θ; ±0.1 °2θ; or ±0.0 °2θ; Cu Kα1 radiation). In some embodiments, the solid form of Compound A free base Pattern 2 is crystalline Compound A free base Pattern 2 characterized by XRPD signals at 5.3 °2θ, 8.2 °2θ, 8.6 °2θ, 13.9 °2θ, and 16.0 °2θ (±0.2 °2θ; ±0.1 °2θ; or ±0.0 °2θ; Cu Kα1 radiation).

In some embodiments, the solid form of Compound A free base Pattern 2 is crystalline Compound A free base Pattern 2 characterized by two or more, or three or more XRPD signals selected from the group consisting of 8.0 °2θ, 8.2 °2θ, 8.6 °2θ, 13.9 °2θ, 16.0 °2θ, 16.4 °2θ, and 18.6 °2θ (±0.2 °2θ; ±0.1 °2θ; or ±0.0 °2θ; Cu Kα1 radiation). In some embodiments, the solid form of Compound A free base Pattern 2 is crystalline Compound A free base Pattern 2 characterized by XRPD signals at 8.0 °2θ, 8.2 °2θ, 8.6 °2θ, 13.9 °2θ, 16.0 °2θ, 16.4 °2θ, and 18.6 °2θ (±0.2 °2θ; ±0.1 °2θ; or ±0.0 °2θ; Cu Kα1 radiation).

In some embodiments, the solid form of Compound A free base Pattern 2 is crystalline Compound A free base Pattern 2 characterized by two or more, or three or more XRPD signals selected from the group consisting of 5.3 °2θ, 8.0 °2θ, 8.2 °2θ, 8.6 °2θ, 13.9 °2θ, 16.0 °2θ, and 18.6 °2θ (±0.2 °2θ; ±0.1 °2θ; or ±0.0 °2θ; Cu Kα1 radiation). In some embodiments, the solid form of Compound A free base Pattern 2 is crystalline Compound A free base Pattern 2 characterized by XRPD signals at 5.3 °2θ, 8.0 °2θ, 8.2 °2θ, 8.6 °2θ, 13.9 °2θ, 16.0 °2θ, and 18.6 °2θ (±0.2 °2θ; ±0.1 °2θ; or ±0.0 °2θ; Cu Kα1 radiation).

In some embodiments, the solid form of Compound A free base Pattern 2 is crystalline Compound A free base Pattern 2 characterized by two or more, or three or more XRPD signals selected from the group consisting of 3.6 °2θ, 3.9 °2θ, 5.3 °2θ, 8.0 °2θ, 8.2 °2θ, 8.6 °2θ, 13.9 °2θ, 16.0 °2θ, 16.4 °2θ, and 18.6 °2θ (±0.2 °2θ; ±0.1 °2θ; or ±0.0 °2θ; Cu Kα1 radiation). In some embodiments, the solid form of Compound A free base Pattern 2 is crystalline Compound A free base Pattern 2 characterized by XRPD signals at 3.6 °2θ, 3.9

°2θ, 5.3 °2θ, 8.0 °2θ, 8.2 °2θ, 8.6 °2θ, 13.9 °2θ, 16.0 °2θ, 16.4 °2θ, and 18.6 °2θ (±0.2 °2θ; ±0.1 °2θ; or ±0.0 °2θ; Cu Kα1 radiation).

In some embodiments, the crystalline Compound A free base Pattern 2 is characterized by one, two, three, four, five, six, seven, eight, nine, or ten XRPD signals selected from those set forth in Table 1.

Table 1: XRPD peak table of Compound A free base Pattern 2 – Batch A

No.	Pos. [°2θ]	Net Intensity
1	3.554	29300.2
2	3.913	24533.1
3	5.276	12399.8
4	7.953	2538.21
5	8.220	5774.88
6	8.649	3998.35
7	13.857	4501.51
8	16.014	3947.73
9	16.382	1179.92
10	18.615	1603.10

Compound A Free Base– Batch B

In some embodiments, the present disclosure provides solid forms of Compound A, e.g., crystalline forms of Compound A free base. In some embodiments, the Compound A free base XRPD profile is substantially similar to that shown in FIG. 114. In some embodiments, the Compound A free base TGA profile is substantially similar to that shown in FIG. 116. In some embodiments, the Compound A free base DSC profile is substantially similar to that shown in FIG. 115.

In some embodiments, the solid form of Compound A free base is crystalline Compound A free base characterized by two or three XRPD signals selected from the group consisting of 8.3 °2θ, 13.9 °2θ, and 16.0 °2θ (±0.2 °2θ; ±0.1 °2θ; or ±0.0 °2θ; Cu Kα1 radiation). In some embodiments, the solid form of Compound A free base is crystalline Compound A free base characterized by XRPD signals at 8.3 °2θ, 13.9 °2θ, and 16.0 °2θ (±0.2 °2θ; ±0.1 °2θ; or ±0.0 °2θ; Cu Kα1 radiation).

In some embodiments, the solid form of Compound A free base is crystalline Compound A free base characterized by two or three XRPD signals selected from the group consisting of 5.3 °2θ, 8.3 °2θ, and 13.9 °2θ (±0.2 °2θ; ±0.1 °2θ; or ±0.0 °2θ; Cu Kα1 radiation). In some embodiments, the solid form of Compound A free base is crystalline

Compound A free base characterized by XRPD signals at 5.3 °2θ, 8.3 °2θ, and 13.9 °2θ (±0.2 °2θ; ±0.1 °2θ; or ±0.0 °2θ; Cu Kα1 radiation).

In some embodiments, the solid form of Compound A free base is crystalline Compound A free base characterized by two or more, or three or more XRPD signals selected from the group consisting of 8.0 °2θ, 8.3 °2θ, 8.7 °2θ, 13.9 °2θ, and 16.0 °2θ (±0.2 °2θ; ±0.1 °2θ; or ±0.0 °2θ; Cu Kα1 radiation). In some embodiments, the solid form of Compound A free base is crystalline Compound A free base characterized by XRPD signals at 8.0 °2θ, 8.3 °2θ, 8.7 °2θ, 13.9 °2θ, and 16.0 °2θ (±0.2 °2θ; ±0.1 °2θ; or ±0.0 °2θ; Cu Kα1 radiation).

In some embodiments, the solid form of Compound A free base is crystalline Compound A free base characterized by two or more, or three or more XRPD signals selected from the group consisting of 5.3 °2θ, 8.3 °2θ, 8.7 °2θ, 13.9 °2θ, and 16.0 °2θ (±0.2 °2θ; ±0.1 °2θ; or ±0.0 °2θ; Cu Kα1 radiation). In some embodiments, the solid form of Compound A free base is crystalline Compound A free base characterized by XRPD signals at 5.3 °2θ, 8.3 °2θ, 8.7 °2θ, 13.9 °2θ, and 16.0 °2θ (±0.2 °2θ; ±0.1 °2θ; or ±0.0 °2θ; Cu Kα1 radiation).

In some embodiments, the solid form of Compound A free base is crystalline Compound A free base characterized by two or more, or three or more XRPD signals selected from the group consisting of 8.0 °2θ, 8.3 °2θ, 8.7 °2θ, 13.9 °2θ, 16.0 °2θ, 16.4 °2θ, and 18.6 °2θ (±0.2 °2θ; ±0.1 °2θ; or ±0.0 °2θ; Cu Kα1 radiation). In some embodiments, the solid form of Compound A free base is crystalline Compound A free base characterized by XRPD signals at 8.0 °2θ, 8.3 °2θ, 8.7 °2θ, 13.9 °2θ, 16.0 °2θ, 16.4 °2θ, and 18.6 °2θ (±0.2 °2θ; ±0.1 °2θ; or ±0.0 °2θ; Cu Kα1 radiation).

In some embodiments, the solid form of Compound A free base is crystalline Compound A free base characterized by two or more, or three or more XRPD signals selected from the group consisting of 5.3 °2θ, 8.0 °2θ, 8.3 °2θ, 8.7 °2θ, 13.9 °2θ, 16.0 °2θ, and 18.6 °2θ (±0.2 °2θ; ±0.1 °2θ; or ±0.0 °2θ; Cu Kα1 radiation). In some embodiments, the solid form of Compound A free base is crystalline Compound A free base characterized by XRPD signals at 5.3 °2θ, 8.0 °2θ, 8.3 °2θ, 8.7 °2θ, 13.9 °2θ, 16.0 °2θ, and 18.6 °2θ (±0.2 °2θ; ±0.1 °2θ; or ±0.0 °2θ; Cu Kα1 radiation).

In some embodiments, the solid form of Compound A free base is crystalline Compound A free base characterized by two or more, or three or more XRPD signals selected from the group consisting of 3.6 °2θ, 4.0 °2θ, 5.3 °2θ, 8.0 °2θ, 8.3 °2θ, 8.7 °2θ, 13.9 °2θ, 16.0 °2θ, 16.4 °2θ, and 18.6 °2θ (±0.2 °2θ; ±0.1 °2θ; or ±0.0 °2θ; Cu Kα1 radiation). In some embodiments, the solid form of Compound A free base is crystalline Compound A free base

characterized by XRPD signals at 3.6 °2θ, 4.0 °2θ, 5.3 °2θ, 8.0 °2θ, 8.3 °2θ, 8.7 °2θ, 13.9 °2θ, 16.0 °2θ, 16.4 °2θ, and 18.6 °2θ (±0.2 °2θ; ±0.1 °2θ; or ±0.0 °2θ; Cu Kα1 radiation).

In some embodiments, the crystalline Compound A free base is characterized by one, two, three, four, five, six, seven, eight, nine, or ten XRPD signals selected from those set forth in Table 2.

Table 2: XRPD peak table of Compound A free base – Batch B

No.	Pos. [°2θ]	Net Intensity
1	3.630	24193.5
2	3.995	16422.2
3	5.334	7964.39
4	8.015	2540.30
5	8.293	5079.22
6	8.707	3097.80
7	13.899	3701.47
8	16.042	3118.30
9	16.379	1266.84
10	18.631	2468.05

Compound A crystalline ethanol solvate form – Batch A

In some embodiments, the present disclosure provides solid forms of an ethanol solvate of Compound A, e.g., crystalline forms of Compound A free base. In some embodiments, the Compound A free base XRPD profile is substantially similar to that shown in FIG. 117.

In some embodiments, the solid form of Compound A free base is crystalline Compound A free base characterized by two or more, or three or more XRPD signals selected from the group consisting of 4.0 °2θ, 4.2 °2θ, 5.4 °2θ, 5.5 °2θ, 5.6 °2θ, 8.4 °2θ, and 8.7 °2θ (±0.2 °2θ; ±0.1 °2θ; or ±0.0 °2θ; Cu Kα1 radiation). In some embodiments, the solid form of Compound A free base is crystalline Compound A free base characterized by XRPD signals at 4.0 °2θ, 4.2 °2θ, 5.4 °2θ, 5.5 °2θ, 5.6 °2θ, 8.4 °2θ, and 8.7 °2θ (±0.2 °2θ; ±0.1 °2θ; or ±0.0 °2θ; Cu Kα1 radiation).

In some embodiments, the crystalline Compound A free base is characterized by one, two, three, four, five, six, seven, eight, nine, or ten XRPD signals selected from those set forth in Table 1E.

Table 1E: XRPD peak table of Compound A crystalline ethanol solvate form – Batch A

No.	Pos. [°2θ]	Height [cts]	FWHM Left [°2θ]	d-spacing [Å]	Rel. Int. [%]
1	3.9664	27024.41	0.1476	22.27748	100.00
2	4.1948	3309.66	0.0984	21.06485	12.25
3	5.4354	7338.62	0.0689	16.25938	27.16
4	5.5014	8245.52	0.0787	16.06445	30.51
5	5.5599	6250.49	0.0394	15.89553	23.13
6	6.7106	40.96	0.2362	13.17227	0.15
7	7.7017	2038.32	0.2165	11.47927	7.54
8	8.3621	3154.90	0.0984	10.57404	11.67
9	8.7223	4393.18	0.0984	10.13815	16.26
10	10.3916	386.23	0.3149	8.51306	1.43
11	10.9878	653.16	0.1574	8.05245	2.42
12	11.4804	2210.88	0.2362	7.70801	8.18
13	12.2064	2677.23	0.2755	7.25114	9.91
14	13.9176	1800.27	0.1771	6.36321	6.66
15	14.8242	1866.07	0.1771	5.97600	6.91
16	15.3943	1409.11	0.1574	5.75597	5.21
17	15.8640	1863.08	0.1378	5.58658	6.89
18	17.0067	1514.96	0.2362	5.21371	5.61
19	17.6637	2165.61	0.1378	5.02124	8.01
20	18.4606	853.87	0.1574	4.80625	3.16
21	18.9131	1369.65	0.1771	4.69227	5.07
22	19.4321	1182.37	0.3936	4.56809	4.38
23	19.9936	687.01	0.1181	4.44106	2.54
24	20.7887	1726.25	0.2165	4.27296	6.39
25	22.1977	689.90	0.2755	4.00483	2.55
26	23.1025	715.18	0.2362	3.84998	2.65
27	23.9667	759.64	0.1378	3.71308	2.81
28	25.9025	1226.20	0.2362	3.43981	4.54
29	26.9849	1069.18	0.2362	3.30424	3.96
30	27.7022	904.84	0.3149	3.22030	3.35
31	28.9455	732.38	0.1378	3.08474	2.71
32	29.7557	282.06	0.2755	3.00256	1.04

Compound A crystalline ethanol solvate form – Batch B

In some embodiments, the present disclosure provides solid forms of an ethanol solvate of Compound A, e.g., crystalline forms of Compound A free base. In some embodiments, the Compound A free base XRPD profile is substantially similar to that shown in FIG. 118.

In some embodiments, the solid form of Compound A free base is crystalline Compound A free base characterized by two or more, or three or more XRPD signals selected

from the group consisting of 3.9 °2θ, 4.2 °2θ, 8.4 °2θ, 14.8 °2θ, 16.9 °2θ, 17.3 °2θ, and 17.7 °2θ (±0.2 °2θ; ±0.1 °2θ; or ±0.0 °2θ; Cu Kα1 radiation). In some embodiments, the solid form of Compound A free base is crystalline Compound A free base characterized by XRPD signals at 3.9 °2θ, 4.2 °2θ, 8.4 °2θ, 14.8 °2θ, 16.9 °2θ, 17.3 °2θ, and 17.7 °2θ (±0.2 °2θ; ±0.1 °2θ; or ±0.0 °2θ; Cu Kα1 radiation).

In some embodiments, the crystalline Compound A free base is characterized by one, two, three, four, five, six, seven, eight, nine, or ten XRPD signals selected from those set forth in Table 2E.

Table 2E: XRPD peak table of the Compound A crystalline ethanol solvate form – Batch B

No.	Pos. [°2θ]	Height [cts]	FWHM Left [°2θ]	d-spacing [Å]	Rel. Int. [%]
1	3.9390	13696.87	0.0984	22.43191	100.00
2	4.1550	10849.50	0.1476	21.26653	79.21
3	5.3014	1583.69	0.1771	16.67008	11.56
4	6.7127	192.26	0.2362	13.16814	1.40
5	7.5039	610.24	0.1968	11.78132	4.46
6	8.3527	7523.66	0.0492	10.58592	54.93
7	8.4102	7886.87	0.0590	10.51373	57.58
8	8.7955	1003.80	0.0984	10.05396	7.33
9	10.5368	756.84	0.4723	8.39601	5.53
10	11.3057	518.86	0.1574	7.82671	3.79
11	12.2140	949.08	0.1574	7.24664	6.93
12	12.8071	893.01	0.1968	6.91235	6.52
13	13.3976	787.02	0.3149	6.60897	5.75
14	14.8350	4003.94	0.2558	5.97170	29.23
15	16.1581	1061.23	0.2362	5.48556	7.75
16	16.8646	1586.27	0.1968	5.25730	11.58
17	17.3292	2243.53	0.2755	5.11742	16.38
18	17.6824	1835.96	0.1574	5.01599	13.40
19	19.2659	900.51	0.1968	4.60712	6.57
20	20.5377	1031.97	0.1968	4.32462	7.53
21	21.2191	1172.60	0.2755	4.18726	8.56
22	22.0063	540.91	0.2755	4.03921	3.95
23	23.4679	1102.75	0.1968	3.79086	8.05
24	23.8982	1014.14	0.1968	3.72357	7.40
25	24.4496	604.80	0.1968	3.64083	4.42
26	25.0610	650.39	0.3149	3.55338	4.75
27	26.1610	1084.32	0.2362	3.40640	7.92
28	27.5933	684.46	0.4723	3.23276	5.00
29	28.8047	405.06	0.3936	3.09949	2.96

Methods of ubiquitinating/degrading a target protein in a cell

The present disclosure provides a method of ubiquitinating/degrading a target protein in a cell.

In some embodiments, the method comprises administering a solid form of Compound A of the disclosure or a salt form of Compound A of the disclosure, wherein Compound A is a bifunctional compound comprising an E3 ubiquitin ligase binding moiety and a protein targeting moiety linked via a linker moiety.

In some embodiments, the E3 ubiquitin ligase binding moiety is coupled to the protein targeting moiety via a linker moiety, and wherein the E3 ubiquitin ligase binding moiety recognizes a ubiquitin pathway protein (e.g., an ubiquitin ligase, preferably an E3 ubiquitin ligase) and the protein targeting moiety recognizes the target protein such that degradation of the target protein will occur when the target protein is placed in proximity to the ubiquitin ligase, thus resulting in degradation/inhibition of the effects of the target protein and the control of protein levels. The control of protein levels afforded by the present disclosure provides treatment of a disease state or condition, which is modulated through the target protein by lowering the level of that protein in the cells of a patient.

In some embodiments, this application provides a solid form of Compound A of the disclosure or a salt form of Compound A of the disclosure that degrades BCL6.

In some embodiments, the present disclosure is directed to a method of treating a patient in need for a disease state or condition modulated through a protein where the degradation of that protein (e.g. BCL6) will produce a therapeutic effect in that patient, the method comprising administering to a patient in need an effective amount of a solid form of Compound A of the disclosure or a salt form of Compound A of the disclosure, optionally in combination with another anti-cancer agent. The disease state or condition may be a disease caused by overexpression of a protein, which leads to a disease state and/or condition.

Methods of Treatment

In an additional aspect, the description provides therapeutic compositions comprising an effective amount of a solid form of Compound A of the disclosure or a salt form of Compound A of the disclosure, and a pharmaceutically acceptable carrier. The therapeutic compositions modulate protein degradation in a patient or subject, for example, an animal such

as a human, and can be used for treating or ameliorating disease states or conditions which are modulated through the degraded protein (e.g. BCL6).

The terms "treat", "treating", and "treatment", etc., as used herein, refer to any action providing a benefit to a patient for which the solid form of Compound A of the disclosure or a salt form of Compound A of the disclosure may be administered, including the treatment of any disease state or condition which is modulated through the protein to which the solid form of Compound A of the disclosure or a salt form of Compound A of the disclosure bind. Disease states or conditions, including cancer, which may be treated using a solid form of Compound A of the disclosure or a salt form of Compound A of the disclosure according to the present disclosure are set forth hereinabove.

The description provides therapeutic compositions as described herein for effectuating the degradation of a protein of interest (e.g. BCL6) for the treatment or amelioration of a disease, e.g. cancer.

In some embodiments, the method comprises administering a solid form of Compound A of the disclosure or a salt form of Compound A of the disclosure, wherein Compound A is a bifunctional compound comprising an E3 ubiquitin ligase binding moiety and a protein targeting moiety linked via a linker moiety.

In some embodiments, the E3 ubiquitin ligase binding moiety is coupled to the protein targeting moiety via a linker moiety, and wherein the E3 ubiquitin ligase binding moiety recognizes a ubiquitin pathway protein (e.g., an ubiquitin ligase, preferably an E3 ubiquitin ligase) and the protein targeting moiety recognizes the target protein such that degradation of the target protein will occur when the target protein is placed in proximity to the ubiquitin ligase, thus resulting in degradation/inhibition of the effects of the target protein and the control of protein levels. The control of protein levels afforded by the present disclosure provides treatment of a disease state or condition, which is modulated through the target protein by lowering the level of that protein in the cells of a patient. In certain embodiments, the method comprises administering an effective amount of a solid form of Compound A of the disclosure or a salt form of Compound A of the disclosure, as described herein, optionally including a pharmaceutically acceptable excipient, carrier, adjuvant, another bioactive agent or combination thereof.

In additional embodiments, the description provides methods for treating or ameliorating a disease, disorder or symptom thereof in a subject or a patient, e.g., an animal such as a human, comprising administering to a subject in need thereof a composition comprising an effective amount, e.g., a therapeutically effective amount, of a solid form of

Compound A of the disclosure or a salt form of Compound A of the disclosure, described herein, and a pharmaceutically acceptable excipient, carrier, adjuvant, another bioactive agent or combination thereof, wherein the composition is effective for treating or ameliorating the disease or disorder or symptom thereof in the subject.

In any aspect or embodiment described herein, the disease or disorder is associated with aberrant BCL6 expression and or activity.

In any aspect or embodiment described herein, the disease or disorder is a cancer associated with aberrant BCL6 expression and or activity.

In any aspect or embodiment described herein, the disease or disorder is associated with BCL6 accumulation and aggregation.

In any aspect or embodiment described herein, the disease or disorder is a cancer associated with BCL6 accumulation and aggregation.

In another aspect, the description provides methods for identifying the effects of the degradation of the protein of interest (e.g. BCL6) in a biological system using a solid form of Compound A of the disclosure or a salt form of Compound A of the disclosure according to the present disclosure.

In another embodiment, the present disclosure is directed to a method of treating a human patient in need for a disease state or condition modulated through a protein (e.g. BCL6) where the degradation of that BCL6 protein will produce a therapeutic effect in the patient, the method comprising administering to a patient in need an effective amount of a solid form of Compound A of the disclosure or a salt form of Compound A of the disclosure, according to the present disclosure, optionally in combination with another bioactive agent. The disease state or condition may be a disease caused by a microbial agent or other exogenous agent such as a virus, bacteria, fungus, protozoa or other microbe or may be a disease state, which is caused by overexpression of a protein, which leads to a disease state and/or condition.

The term “disease state or condition” is used to describe any disease state or condition wherein protein dysregulation (i.e., the amount of protein expressed in a patient is elevated) occurs and where degradation of one or more proteins in a patient may provide beneficial therapy or relief of symptoms to a patient in need thereof. In certain instances, the disease state or condition may be cured.

Disease states or conditions which may be treated using a solid form of Compound A of the disclosure or a salt form of Compound A of the disclosure, according to the present disclosure include, for example, malignant lymphoma, Burkitt's lymphoma, non-Hodgkin's

lymphoma, Large B-cell Lymphoma, follicular lymphoma, angioimmunoblastic T-cell lymphoma, or diffuse large B-cell lymphoma (DLBCL).

The term "neoplasia" or "cancer" is used throughout the specification to refer to the pathological process that results in the formation and growth of a cancerous or malignant neoplasm, i.e., abnormal tissue that grows by cellular proliferation, often more rapidly than normal and continues to grow after the stimuli that initiated the new growth cease. Malignant neoplasms show partial or complete lack of structural organization and functional coordination with the normal tissue and most invade surrounding tissues, metastasize to several sites, and are likely to recur after attempted removal and to cause the death of the patient unless adequately treated. As used herein, the term neoplasia is used to describe all cancerous disease states and embraces or encompasses the pathological process associated with malignant hematogenous, ascitic and solid tumors.

Exemplary cancers which may be treated by the solid form of Compound A of the disclosure or a salt form of Compound A of the disclosure either alone or in combination with at least one additional anti-cancer agent include advanced lymphoma, relapsed/refractory (R/R) lymphoma, malignant lymphoma, Burkitt's lymphoma, non-Hodgkin's lymphoma, advanced non-Hodgkin Lymphoma, B-cell advanced non-Hodgkin Lymphoma, Large B-cell Lymphoma, follicular lymphoma, intravascular large B-cell lymphoma, transformed follicular lymphoma, angioimmunoblastic T-cell lymphoma, diffuse large B-cell lymphoma (DLBCL), high grade B-cell lymphoma, germinal center B-cell (GCB) DLBCL, activated B-cell (ABC) DLBCL, non-Hodgkin's lymphoma not otherwise specified, solid tumors (e.g. breast cancer, lung cancer, ovarian cancer, neuroblastoma, and glioblastoma), Kaposi advanced non-Hodgkin's lymphoma (NHL), relapsed/refractory (R/R) non-Hodgkin's lymphoma (NHL), relapsed/refractory (R/R) B cell non-Hodgkin's Lymphoma, advanced relapsed/refractory (R/R) non-Hodgkin's lymphoma (NHL), nodal T-follicular helper cell lymphoma - angioimmunoblastic type (nTFHL-AI) / advanced angioimmunoblastic T-cell lymphoma (AITL), relapsed/refractory (R/R) nodal T-follicular helper cell lymphoma - angioimmunoblastic type (nTFHL-AI) / angioimmunoblastic T-cell lymphoma (AITL), nodal T-follicular helper cell lymphoma (nTFHL), relapsed/refractory (R/R) nodal T-follicular helper cell lymphoma (nTFHL), advanced nTFHL, R/R nTFHL, nodal T-follicular helper cell lymphoma-angioimmunoblastic type (nTFHL-AI), advanced nTFHL-AI, R/R nTFHL-AI, T-lineage lymphoblastic Lymphoma (T-LL), Peripheral T-cell lymphoma, or Pre-B Lymphoma.

In one aspect, the cancer which may be treated by the solid form of Compound A of the disclosure or a salt form of Compound A of the disclosure either alone or in combination

with at least one additional anti-cancer agent include diffuse large B-cell lymphoma (DLBCL), relapsed/refractory DLBCL and high grade B-cell lymphoma.

In one aspect, the present application pertains to a method of treating and/or preventing cancer comprising administering to a subject in need thereof a therapeutically effective amount of a solid form of Compound A of the disclosure or a salt form of Compound A of the disclosure, in combination with one or more additional anti-cancer agents.

The term "pharmaceutically acceptable salt" is used throughout the specification to describe, where applicable, a salt form of one or more of the compounds described herein which are presented to increase the solubility of the compound in the gastic juices of the patient's gastrointestinal tract in order to promote dissolution and the bioavailability of the compounds. Pharmaceutically acceptable salts include those derived from pharmaceutically acceptable inorganic or organic bases and acids, where applicable. Suitable salts include those derived from alkali metals such as potassium and sodium, alkaline earth metals such as calcium, magnesium and ammonium salts, among numerous other acids and bases well known in the pharmaceutical art. Sodium and potassium salts are particularly preferred as neutralization salts of the phosphates according to the present disclosure.

The term "pharmaceutically acceptable derivative" is used throughout the specification to describe any pharmaceutically acceptable prodrug form (such as an ester, amide other prodrug group), which, upon administration to a patient, provides directly or indirectly the present compound or an active metabolite of the present compound.

EXAMPLES

Abbreviations used:

DCM	dichloromethane
DMF	dimethylformamide
DMSO	dimethylsulfoxide
EtOAc	ethyl acetate
IPA	isopropyl alcohol
MeOH	methanol
MEK	methylethyl ketone
DMA	N,N-dimethylacetamide
NMP	N-methyl-2-pyrrolidone
NMP	N-methylpyrrolidone
t-BME or tBME	tert-butyl methyl ether
THF	tetrahydrofuran

THF	tetrahydrofuran

Example 1. General Methods of Analysis

X-ray Powder Diffraction (XRPD) – Method 1

For some samples, XRPD data was collected under ambient conditions on a Bruker D2 Phaser diffractometer with a low power X-ray generator of 300w. Powder patterns were collected on a zero background sample holder with a 0.5s/step with total of 1837, two theta at 0.01°C per step at 30 kV and 10 mA. The X-ray tube of Cu (Kα) was employed.

Differential Scanning Calorimetry (DSC) – Method 2

For some samples, DSC was performed with a TA Discovery series DSC using approximately a few milligrams of material in a Tzero aluminum pan sealed with a Tzero hermetic lid. The sample was analyzed using a heating rate of 10 °C per minute from 25 °C to 300 °C under nitrogen flow.

Thermogravimetric Analysis (TGA) – Method 3

For some samples, TGA was also performed with a TA Discovery series TGA. The sample was also analyzed using a heating rate of 10 °C per minute from 25 °C to 300 °C under nitrogen flow.

X-ray Powder Diffraction (XRPD) – Method 4

For some samples, XRPD analysis was carried out on a PANalytical X'pert pro with PIXcel detector (128 channels), scanning the samples between 3 and 35° 2θ. The material was gently ground to release any agglomerates and loaded onto a multi-well plate with Mylar polymer film to support the sample. The multi-well plate was then placed into the diffractometer and analysed using Cu K radiation (α_1 λ = 1.54060 Å; α_2 = 1.54443 Å; β = 1.39225 Å; α_1: α_2 ratio = 0.5) running in transmission mode (step size 0.0130° 2θ, step time 18.87s) using 40 kV / 40 mA generator settings. Data were visualized and images generated using the HighScore Plus 4.9 desktop application (PANalytical, 2020).

The following temperature profile was used for the VT-XRPD:

Table 3: Temperature Profile for VT-XRPD of Compound A

Temperature / °C	Heating Rate / °C/min	Hold Time Before Scan / min
30	n/a	n/a
100	10	5
210	10	5
225	2	5
240	2	5
255	2	5
270	2	5
280	2	5
30	n/a	0

Polarised Light Microscopy (PLM) – Method 5

For some samples, The presence of crystallinity (birefringence) was determined using an Olympus BX53 microscope, equipped with cross-polarising lenses and a Motic camera. Images were captured using Motic Images Plus 3.0. All images were recorded using the 20x objective, unless otherwise stated.

Thermogravimetric Analysis/ Differential Scanning Calorimetry (TGA/DSC) – Method 6

For some samples, 5 – 10 mg of material was added into a pre-tared open aluminium pan and loaded into a TA Instruments Discovery SDT 650 Auto - Simultaneous DSC and held at room temperature. The sample was then heated at a rate of 10 °C/min from 30 °C to 400 °C during which time the change in sample weight was recorded along with the heat flow response (DSC). Nitrogen was used as the sample purge gas, at a flow rate of 200 cm^3/min.

Thermogravimetric/Differential Thermal Analysis (TG/DTA) – Method 7

For some samples, 2 – 5 mg of material was weighed into an open aluminium pan and loaded into a simultaneous thermogravimetric/differential thermal analyser (TG/DTA) and held at room temperature. The sample was then heated at a rate of 10°C/min from 20°C to 400°C during which time the change in sample weight was recorded along with any differential thermal events (DTA). Nitrogen was used as the purge gas, at a flow rate of 300 cm^3/min.

Differential Scanning Calorimetry (DSC) – Method 8

For some samples, 1 – 5 mg of material was weighed into an aluminium DSC pan and sealed non-hermetically with an aluminium lid. The sample pan was then loaded into a TA Instruments Discovery DSC 2500 differential scanning calorimeter equipped with a RC90 cooler. The sample and reference were heated to a specified upper limit (sample dependent)

at a scan rate of 10°C/min and the resulting heat flow response monitored. The sample was re-cooled to -80°C and then reheated again to the upper limit all at 10 °C/min. Nitrogen was used as the purge gas, at a flow rate of 50 cm^3/min.

Karl Fischer Coulometric Titration (KF) – Method 9

For some samples, Solids were analyzed using a vaporizer method:

Approximately 10 mg of material was weighed into a 10 mL glass vial and tightly sealed with a screw cap. The water content of the samples was analyzed using an In Motion KF Oven Autosampler, at 170 °C. The samples were run in duplicate, and an average moisture content reported.

Blank	Oven Temperature	170 °C
	Source for Drift	Determination
	Max. Start Drift	10 µg/min
	Carrier Gas Flow Rate	80 mL/min
	Transfer Tube Heating	No
	Mix Time	60 s
	Stir Speed	45%
	Drift Termination	10 s (Delay Time)
	Max. Titration Time	600 s
Sample	Oven Temperature	170 °C
	Source for Drift	Determination
	Max. start Drift	10 µg/min
	Carrier Gas Flow Rate	80 mL/min
	Mix Time	60 s
	Stir Speed	45%
	Drift Termination	10 s (Delay Time)
	Max. Titration Time	600 s

Nuclear Magnetic Resonance (NMR) – Method 10

For some samples, NMR experiments were performed on a Bruker AVIIIHD spectrometer equipped with a PRODIGY cryoprobe operating at 500.12 MHz for protons. Experiments were performed in deuterated DMSO, and each sample was prepared to *ca.* 10 mM concentration.

Infrared Spectroscopy (IR) – Method 11

For some samples, Infrared spectroscopy was carried out on a Bruker ALPHA P spectrometer. Sufficient material was placed onto the center of the plate of the spectrometer and the spectra were obtained using the following parameters:

Resolution:	4 cm^{-1}
Background Scan Time:	16 scans
Sample Scan Time:	16 scans
Data Collection:	4000 to 400 cm^{-1}
Result Spectrum:	Transmittance
Software:	OPUS version 6

Dynamic Vapor Sorption (DVS) – Method 12

For some samples, 10 – 20 mg of sample was placed into a mesh vapor sorption balance pan and loaded into a DVS Intrinsic dynamic vapor sorption balance by Surface Measurement Systems. The sample was subjected to a ramping profile from 40 – 90% relative humidity (RH) at 10% increments, maintaining the sample at each step until a stable weight had been achieved (dm/dt 0.004%, minimum step length 30 minutes, maximum step length 500 minutes) at 25°C. After completion of the sorption cycle, the sample was dried using the same procedure to 0% RH and then a second sorption cycle back to 40% RH. Two cycles were performed. The weight change during the sorption/desorption cycles were plotted, allowing for the hygroscopic nature of the sample to be determined. XRPD analysis was then carried out on any solid retained.

Variable Temperature X-ray powder diffraction (VT-XRPD) – Method 13

For some samples, VT-XRPD analysis was carried out on a Philips X'Pert Pro Multipurpose diffractometer equipped with a temperature chamber. The samples were scanned between 4 and 35.99 °2θ using Cu K radiation (α_1 λ = 1.54060 Å; α_2 = 1.54443 Å; β = 1.39225 Å; α_1:α_2 ratio = 0.5) running in Bragg-Brentano geometry (step size 0.008 °2θ) using 40 kV / 40 mA generator settings. Measurements were performed following specific temperature programs.

High Performance Liquid Chromatography-Ultraviolet Detection (HPLC-UV) – Method 14

Column	Halo C18 100x4.6mm 2.7µm
Column Temperature (°C)	40
Flow Rate (mL/min)	1.5
Column Pressure at start of Run (Bar)	~300
Injection Volume (µL)	3
Autosampler Temperature (°C)	Ambient
Detection parameters	236nm/210nm
Sampling Rate	25Hz
Mobile Phase A	0.05% TFA in Water
Mobile Phase B	0.05% TFA in 9:1 ACN:THF
Diluent	DMSO
Needle Wash	Acetonitrile

Gradient program:

Time (min)	%MP A	%MP B
0	90	10
2.5	65	35
4.5	65	35
6.0	5	95
8.0	5	95
8.1	90	10
12	90	10

X-ray Powder Diffraction (XRPD) – Method 15

Anchor Scan Parameters

Scan Axis Gonio
Start Position [°2θ] 2.0023
End Position [°2θ] 39.9623
Step Size [°2θ] 0.0100
Scan Step Time [s] 96.0000
Scan Type Pre-set time
Offset [°2θ] 0.0000
Divergence Slit Type Fixed
Divergence Slit Size [°] 1.0000
Specimen Length [mm] 10.00
Receiving Slit Size [mm] 0.1000
Measurement Temperature [°C] 25.00
Anode Material Cu
Intended Wavelength Type K-Alpha
K-Alpha1 [Å] 1.54060
K-Alpha2 [Å] 1.54443
K-Beta [Å] 1.39225
K-A2 / K-A1 Ratio 0.50000
Generator Settings 0 mA, 0 kV

Diffractometer Number	0
Goniometer Radius [mm]	240.00
Dist. Focus-Diverg. Slit [mm]	91.00
Incident Beam Monochromator	No
Spinning	No

Example 2. Initial Characterization

Compound A was synthesized according to standard methods and characterized to provide reference data. The following results were obtained:

- XRPD analysis (Method 4) indicated the material was crystalline, with peaks consistent with the reference data. The solid form was assigned as Pattern 1.
- PLM analysis (Method 5; taken with 20× magnification), showed small particles with no clear morphology. Aggregation and birefringence were also present.
- TG analysis showed a 0.69% weight loss between outset (*ca.* 20 °C) and 110 °C, with decomposition above *ca.* 330 °C. A shallow exothermic event with an onset of 210 °C and a peak at 216 °C was observed in the DSC. This was followed by a melting event at an onset of 242 °C, with a peak at 254 °C.
- During the DSC first heat (Method 8), a complex thermal event was observed at an onset of 200 °C, with an endothermic peak at 210 °C and an exothermic peak at 217 °C. This was followed by a large melt with an onset of 243 °C, with 2 peaks at 253 °C and 256 °C. In the cooling step, a glass transition with a mid-point half-height of 145 °C followed by vitrification was observed. During the second heat, a glass transition with a mid-point half-height of 151 °C was observed.
- DVS analysis (Method 12) indicated a *c.a.* 9 wt.% uptake at 80 %RH and a classification of moderately hygroscopic. XRPD analysis of the post-DVS sample was consistent with the input material.
- An FT-IR spectrum was recorded for reference using IR Method 11.
- ^{1}H and ^{19}F NMR analysis were consistent with the supplied structure, and were carried out using NMR Method 10.
- HPLC analysis (Method 14) determined the solids had a chemical purity of 98.54 %area.
- VT-XRPD analysis (Method 13) indicated that Pattern 1 was maintained up to at least 100 °C.

- By 210 °C, partial conversion to the newly identified Pattern 2 was observed (a mixture of Pattern 1 and 2 was observed). At 225 °C, the solids had converted to a form similar to Pattern 2 (extra peaks were observed).
- At 240 °C, the material was observed to be poorly crystalline, with degradation observed by 255 °C.

Example 3. Preparation of Amorphous Compound A Free Base

PRELIMINARY SOLUBILITY ASSESSMENT

Prior to the preparation of amorphous material, a preliminary solubility assessment was carried out on the crystalline freebase. This was to determine the suitable solvent system and protocol for the amorphous preparation.

- *Ca.* 10 mg of Compound A was added to 7 × 1.5 mL screw cap vials.
- Solvent was added to each vial in 50 µL aliquots until the solid dissolved or a total of *ca.* 1 mL had been added.
- After each addition the vial was heated to 40 °C, with mixing to check for dissolution at elevated temperature.

Table 4: Solvent systems assessed during the preliminary solubility studies

Solvent system
Dichloromethane (DCM)
Methanol
1,4-Dioxane
Water
DCM:MeOH (50:50 v/v)
DCM:MeOH (75:25 v/v)
DCM:MeOH (25:75 v/v)

The following results were obtained:

- A slurry was observed at a concentration of 10 mg/mL in dichloromethane, methanol, 1,4-Dioxane, water and DCM:MeOH 25:75 v/v.
- Dissolution was observed at 36 mg/mL in DCM:MeOH 75:25 v/v.
- Dissolution was observed at 14 mg/mL in DCM:MeOH 50:50 v/v

AMORPHOUS PREPARATION

The crystalline Compound A free base was observed to dissolve in the DCM:MeOH mixtures (36 to 54 mg/mL at 75:25 v/v). Amorphous preparation was attempted in this solvent system:

- Ca. 60 mg of Compound A was added to a 20 mL scintillation vial.

- DCM:MeOH (75:25 v/v) (ca. 2 mL) was added the vial and stirred at ambient temperature (*c.a.* 20 °C) until complete dissolution was observed.
    - Concentration = 30 mg/mL
- The solution was then rotary evaporated and a solid was recovered.
- The solid was then analyzed by XRPD (Method 4) to confirm if the material was amorphous.

This procedure was successful and repeated as necessary to produce the required amorphous Compound A.

The following results were obtained:

- XRPD analysis (Method 4) of the recovered solids indicated that they were amorphous.

A procedure for generating the amorphous Compound A required to fund the various experiments carried out on the amorphous Compound A freebase was developed. The results of using this procedure are as follows.

- XRPD analysis (Method 4) of the recovered solids indicated that they were amorphous.

Example 4. Approximate Solubility Assessments of Compound A

Using amorphous Compound A prepared in Section 5.2.2, the approximate solubility assessment was carried out in 24 solvent systems using the following procedure:

- 10 mg of amorphous Compound A were weighed into 24 × 2 mL vials.
- Solvent was added to each experiment at ambient temperature in 20 µL (2 vol.) aliquots until dissolution was observed or a total of 1 mL (100 vol.) had been added.
    - Aliquot size was increased to 100 µL (10 vol.) after 200 µL (20 vol.) of solvent had been added.
- Each experiment was heated to 40 °C between each aliquot addition to assess dissolution at elevated temperature.
    - The DCM experiment was not heated to 40 °C due to the solvent's low boiling point.
- After solvent addition, the experiments were stirred at 40 °C for *c.a.* 3 days.
- After 3 days, the resulting slurries were isolated via centrifugation and analyzed by XRPD (Method 4).

Table 5: Solvent systems explored in the approximate solubility assessment

Solvent systems	
1-Propanol	Ethanol
2-Methyl THF	Ethyl Acetate
2-Propanol	Heptane
Acetone	Isopropyl Acetate
Acetonitrile	Methanol
Anisole	Methyl Acetate
Dichloromethane (DCM)	Methylethyl Ketone (MEK)
DCM:MeOH (90:10 v/v)	N,N-Dimethylacetamide (DMA)
DCM:MeOH (75:25 v/v)	tert-Butylmethyl Ether (t-BME)
DCM:MeOH (25:75 v/v)	Tetrahydrofuran (THF)
Dimethylsulfoxide (DMSO)	Toluene
DMSO:Acetonitirile (50:50 v/v)	Water

An approximate solubility assessment was also carried out on 3 additional solvents, using the following procedure:

- 3 × 10 mg samples of amorphous Compound A were weighed into 3 × 2 mL vials.
- Solvent was added to each experiment at ambient temperature in 20 µL (2 vol.) aliquots until dissolution was observed or 1 mL (100 vol.) had been added.
    - Aliquot size was increased to 100 µL (10 vol.) after 200 µL (20 vol.) of solvent had been added.
- Each experiment was heated to 40 °C between each aliquot addition.
- Experiments where dissolution was observed were dried under vacuum at 40 °C, the resulting solids were analyzed by XRPD (Method 4).

Table 6: Additional solvents used in the approximate solubility assessment experiment

Solvent system
Dimethylformamide (DMF)
N-methylpyrrolidone (NMP)
Trifluoroethanol

The results of this experiment are as follows:

- The amorphous solids were observed to exhibit low solubility (<10 mg/mL) in most of the solvent systems assessed.
    - High solubility (≥167 mg/mL) was observed in NMP and trifluoroethanol (dissolution observed at 40 °C).
    - Moderate solubility (25 – 50 mg/mL) was observed in DCM:MeOH 90:10 v/v, DCM:MeOH 75:25 v/v, DMSO and DMA.

XRPD analysis (Method 4) indicated that most of the experiments produced solids consistent with Pattern 2.

- Poorly crystalline solids similar to Pattern 1 were recovered from DCM:MeOH 25:75 v/v.
- Amorphous solids were recovered from NMP, Trifluoroethanol, heptane and water.

Table 7: Results of the approximate solubility assessment experiment

Solvent system	Solub. (mg/mL)	XRPD result
1-Propanol	<10	2
2-Methyl THF	<10	2
2-Propanol	<10	2
Acetone	<10	2
Acetonitrile	<10	2
Anisole	<10	Ins.
Dichloromethane (DCM)	<10	2, PC
DCM:MeOH (90:10 v/v)	≥25	No solids
DCM:MeOH (75:25 v/v)	≥50†	PC
DCM:MeOH (25:75 v/v)	<10	Similar to 1, PC
Dimethylsulfoxide (DMSO)	≥50†	No solids
DMSO:Acetonitirile (50:50 v/v)	<10	2, PC
Ethanol	<10	2
Ethyl Acetate	<10	2
Heptane	<10	Am
Isopropyl Acetate	<10	2
Methanol	<10	2+
Methyl Acetate	<10	2
Methylethyl Ketone (MEK)	<10	2
N,N-Dimethylacetamide (DMA)	≥50†	2*
tert-Butylmethyl Ether (tBME)	<10	2, PC
Tetrahydrofuran (THF)	<10	PC
Toluene	<10	2
Water	<10	Am
Dimethylformamide (DMF)	<10	Ins.
N-methylpyrrolidone (NMP)	≥167†	Am
Trifluoroethanol	≥250†	Am

† Dissolved at 40 °C
\+ Extra peaks
* Predominantly
PC Poorly crystalline
Ins. Insufficient solids
Am Amorphous

Example 5. Crystallization Screen of Compound A Freebase

A crystallization screen of Compound A free base was carried out to identify any additional crystalline forms of the free base. A range of crystallization techniques were investigated

including temperature cycling, slow cooling, anti-solvent addition, evaporation, and solvent drop grinding.

TEMPERATURE CYCLING

The first set of crystallization screening experiments involved temperature cycling of Compound A slurries in various solvent system. The following procedure was used:

- 21 × 10 mg samples of amorphous Compound A were weighed out into 2 mL push cap vials.
- The appropriate solvent system was added to each experiment to form mobile slurries.
- The experiments were stirred and temperature cycled between 40 °C and 5 °C, with a temperature ramp of 0.1 °C/min and 1 hour holds between steps for *c.a.* 48 h.
- After 48 h, the experiments were isolated via centrifugation (during a 5 °C hold), and the resulting solids were analysed by XRPD (Method 4).
- The recovered solids were dried under vacuum at 40 °C for *c.a.* 18 h, then reanalysed by XRPD (Method 4).

Table 8: Experimental details of the crystallization screen – Temperature cycling

Solvent system	Volume added (µL)	Solvent system	Volume added (µL)	Solvent system	Volume added (µL)
2-Methyl THF	500	DCM:MeOH 25:75 v/v	500	DMA	100
2-Propanol	500	DMSO	100	THF	500
Acetone	500	Ethanol	500	Toluene	500
Acetonitrile	500	Ethyl acetate	500	Water	500
DCM	500	Methanol	500	DMF	500
DCM:MeOH 90:10 v/v	200	Methanol:water 50:50 v/v	500	NMP	40
DCM:MeOH 75:25 v/v	100	MEK	500	Trifluoroethanol	40

The results of these experiments are as follows:

- Freebase Pattern 1 (or solids similar to freebase Pattern 1) were recovered from the DCM:MeOH 75:25 v/v and 25:75 v/v experiments
- Freebase Pattern 2 (or solids similar to freebase Pattern 2) were recovered from the 2-methyl THF, 2-propanol, acetone, acetonitrile, DCM, ethanol, ethyl acetate, MEK, DMA, THF, toluene and NMP experiments
- Amorphous solids were recovered from the DCM:MeOH 90:10 v/v, DMSO, methanol:water 50:50 v/v, water and DMF experiments.

- Solids that were too poorly crystalline to assign a pattern were recovered from the methanol experiment.
- A solution was recovered from the trifluoroethanol experiment.
- Both Patterns 1 and 2 generally persisted after drying.
    - The solids recovered from the methanol experiment were determined to be predominantly Pattern 1 after drying.

Table 9: Results of the crystallization screen temperature cycling experiments

Solvent system	XRPD Result		Solvent system	XRPD Result		Solvent system	XRPD Result	
	Wet	Dry		Wet	Dry		Wet	Dry
2-Methyl THF	2	2	DCM:MeOH 25:75 v/v	1*	1*	DMA	2, PC	PC
2-Propanol	2, PC	PC	DMSO	Am	Am	THF	2	2
Acetone	2	2	Ethanol	2	2	Toluene	2, PC	2
Acetonitrile	2	2	Ethyl acetate	2	2	Water	Am	Am
DCM	2	2	Methanol	PC	1*	DMF	Am	Am
DCM:MeOH 90:10 v/v	Am	PC	Methanol:water 50:50 v/v	Am	Am	NMP	2*, PC	2*, PC
DCM:MeOH 75:25 v/v	1, PC	1, PC	MEK	2	2	Trifluoroethanol	N/A (solution)	N/A (solution)

PC: Poorly crystalline
*: Predominantly
Am: Amorphous

EVAPORATION

The next set of crystallization screen experiment involved evaporation of Compound A solutions in various solvents. The following procedure was used:

- 6 × 20 mg samples of amorphous Compound A were weighed out and dissolved in the appropriate solvent system, at ambient temperature.
- The experiments were held at 40 °C to allow the solvents to evaporate.
    - Two experiments fully evaporated after *c.a.* 1 week, the resulting solids were analyzed by XRPD (Method 4), dried under vacuum at 40 °C for 3 days and then reanalyzed by XRPD (Method 4).
    - After *c.a.* 8 weeks the remaining experiments had fully evaporated. Resulting solids were analyzed by XRPD (Method 4), dried under vacuum at 40 °C for *c.a.* 18 h and then reanalyzed by XRPD (Method 4).

Table 10: Experimental details of the crystallization screen – Evaporation

Solvent System	Solvent added (µL)
DCM:MeOH 90:10 v/v	1300
DCM:MeOH 75:25 v/v	500
DMSO	1000
DMA	800
NMP	400
Trifluoroethanol	400

The results of these experiments are as follows:

- Freebase Pattern 2 was recovered from the DCM:MeOH 90:10 v/v experiment after *c.a.* 1 week. This was retained upon drying.
- Freebase Pattern 1 was recovered from the DCM:MeOH 75:25 v/v experiment after *c.a.* 1 week. This was retained upon drying.
- Freebase Pattern 2 was recovered from the DMSO and DMA experiments after *c.a.* 8 weeks. These were retained upon drying.
- Amorphous solids were recovered from the trifluoroethanol experiment after *c.a.* 8 weeks both before and after drying.
- A gum was recovered from the NMP experiment, XRPD analysis was not carried out.

Table 11: Results of the crystallization screen evaporation experiments

Solvent System	XRPD results	
	Wet	Dry
DCM:MeOH 90:10 v/v	FB Pattern 2	FB Pattern 2
DCM:MeOH 75:25 v/v	FB Pattern 1	FB Pattern 1
DMSO	FB Pattern 2	FB Pattern 2
DMA	FB Pattern 2	FB Pattern 2
NMP	N/A (Gum)	N/A (Gum)
Trifluoroethanol	Amorphous	Amorphous

ANTISOLVENT ADDITION

The next set of crystallization screen experiment involved the addition of antisolvent to Compound A solutions in various solvent systems. The following procedure was used:

- 8 × 20 mg samples of amorphous Compound A were weighed out into 1.5 mL screw cap vials.
- Solvent was added in 50 µL aliquots at ambient temperature (*c.a.* 20 °C) until dissolution was observed or 1 mL had been added.
- Once dissolved, antisolvent was added until a slurry was observed or vial capacity was reached.
- Experiments where isolable solids or slurries were present were centrifuged and isolated solids were analyzed by XRPD (Method 4).
- The recovered solids were dried under vacuum at 40 °C for 3 days then reanalyzed by XRPD (Method 4).

Table 12: Experimental details of the crystallization screen – Antisolvent addition

Solvent System	Solvent volume added (µL)	Antisolvent	Antisolvent volume added (µL)
2-Propanol:trifluoroethanol 75:25 v/v	1000	2-Propanol	N/A (Dissolution not observed)
DCM:MeOH 75:25 v/v	450	Methanol	1000
DMSO	600	Water	500
DMA	350	Water	300
DMA:tBME 75:25 v/v	600	tBME	750
NMP	1000	tBME	500
NMP:water 75:25 v/v	1000	Water	N/A (Dissolution not observed)
Trifluoroethanol	200	Water	350

The results of these experiments are as follows:

- An unknown Pattern (assigned as freebase Pattern 3) was recovered from DCM:MeOH.
    - Upon drying these solids converted to poorly crystalline freebase Pattern 1
- Poorly crystalline freebase Pattern 1 solids were recovered from DMA:tBME both wet and dry.
- Solids that were too poorly crystalline to assign a Pattern were recovered from trifluoroethanol:water.
- Predominantly amorphous solids were recovered from DMSO:water and DMA:water.
    - After drying, these solids converted towards freebase Pattern 2 and freebase Pattern 1 respectively.
- XRPD analysis was not carried out on the 2-propanol:trifluoroethanol, NMP:tBME or NMP:water experiments either due to incomplete dissolution after solvent addition or absence of precipitation after antisolvent addition.

Table 13: Results of the crystallization screen antisolvent addition experiments

Solvent System	Antisolvent	XRPD Result	
		Wet	Dry
2-Propanol:trifluoroethanol 75:25 v/v	--	N/A (Dissolution not observed)	N/A (Dissolution not observed)
DCM:MeOH 75:25 v/v	Methanol	Freebase Pattern 3	PC Freebase Pattern 1
DMSO	Water	Predominantly amorphous	Similar to PB Pattern 2
DMA	Water	Predominantly amorphous	PC Freebase Pattern 1
DMA:tBME 75:25 v/v	tBME	PC Freebase Pattern 1	PC Freebase Pattern 1
NMP	tBME	N/A (precipitation not observed)	N/A (precipitation not observed)
NMP:water 75:25 v/v	--	N/A (Dissolution not observed)	N/A (Dissolution not observed)
Trifluoroethanol	Water	Poorly crystalline	Poorly crystalline

PC = Poorly Crystalline

SLOW COOLING

The next set of crystallization screen experiment involved the slow cooling of Compound A solutions from 40 °C to 5 °C. The following procedure was used:

- 20 mg of the prepared amorphous Compound A free base was added to 8 × 1.5 mL screw cap vials.
- The appropriate solvent was added to each vial in 100 µL aliquots until complete dissolution was achieved at 40°C or 1 mL had been added.
- The solutions were then cooled from 40°C to 5°C at 0.05 °C/min.
- At 5°C, samples with solids present were centrifuged and isolated solids were analyzed (damp) by XRPD (Method 4).
- For samples that remained clear solutions at 5°C, anti-solvent was added to facilitate precipitation.
    - These were then stirred further at 5°C for *ca.* 2 h.
    - Any solids present were isolated by centrifugation and analyzed (damp) by XRPD (Method 4).
- All the solids were dried under vacuum at ambient temperature for 3 days, and then re-analyzed by XRPD (Method 4).

Table 14: Experimental details of the crystallization screen – Slow cooling

Solvent System	Vol. added (µL)	tBME added (µL)
IPA:Trifluoroethanol 25:75 v/v	300	0
DCM:MeOH 90:10 v/v	1000	600
DCM:MeOH 75:25 v/v	400	1000
DMSO:Water 75:25 v/v	100	0
DMA	400	0
DMA:tBME 75:25 v/v	500	0
NMP	300	1200
Trifluoroethanol	200	500

The results of these experiments are as follows:

- Poorly crystalline solids were recovered from the DCM:MeOH 75:25 v/v experiment.
- The solids recovered from the DCM:MeOH 90:10 v/v experiment were similar to freebase Pattern 1.
- Freebase Pattern 2 was observed in the solids recovered from the DMA and DMA:tBME 75:25 v/v experiments.
- Amorphous solids were recovered from the IPA:trifluoroethanol 25:75 v/v and trifluoroethanol experiment.
- After drying for *c.a.* 3 days, the solids recovered from the DCM:MeOH 90:10 v/v experiment converted further to Pattern 1.
- The solids recovered from the DMSO:water experiment after drying were consistent with Pattern 2, though with some missing peaks.
    - Initial dissolution was not observed in the DMSO:water: 75:25 v/v experiment, solids were recovered after slurrying, not precipitation.
- No other significant changes were observed post-drying.

Table 15: Results of the crystallization screen slow cooling experiment

Solvent System	XRPD Result		Solvent System	XRPD Result	
	Damp	Dried		Damp	Dried
IPA:Trifluoroethanol (25:75 v/v)	Am	Am	DMA	2	2
DCM:MeOH (90:10 v/v)	Similar to 1	Similar to 1	DMA:tBME (75:25 v/v)	2	2
DCM:MeOH (75:25 v/v)	PC	PC	NMP	ns	ns
DMSO: Water (75:25 v/v)	Am	2 (Missing peaks)	Trifluoroethanol	Am	Am

PC Poorly crystalline
ns No solids
Am Amorphous

SOLVENT DROP GRINDING

The final set of crystallization screen experiments involved solvent drop grinding of Compound A.

The following procedure was used:

- *C.a.* 10 mg of amorphous Compound A was weighed into 25 × 2 mL bead mill vials and 2 steel beads added to each vial.
- 2 µL of solvent system were added to each vial and the experiments were milled using the following program:
  - Milling speed: 5000 rpm
  - Mill time per cycle: 90 s
  - Number of cycles: 10
  - Interval between cycles: 10 s
  - Total milling time: 1 h
- The solids were then analyzed by XRPD (Method 4), dried under vacuum at 40 °C for *c.a.* 18 h then reanalyzed by XRPD (Method 4).

Table 16: Solvent systems of the crystallization screen - Solvent drop grinding

Solvent system	
1-Propanol	Ethyl Acetate
2-Methyl THF	Heptane
2-Propanol	Isopropyl Acetate
Acetone	Methanol
Acetonitrile	Methyl Acetate
Anisole	Methylethyl Ketone (MEK)
Dichloromethane (DCM)	N,N-Dimethylacetamide (DMA)
DCM:MeOH (90:10 v/v)	tert-Butylmethyl Ether (t-BME)

DCM:MeOH (75:25 v/v)	Tetrahydrofuran (THF)
DCM:MeOH (25:75 v/v)	Toluene
Dimethylsulfoxide (DMSO)	Water
DMSO:Acetonitirile (50:50 v/v)	Trifluoroethanol
Ethanol	

The results of these experiments are as follows:

- Freebase Pattern 1 was recovered from 1-propanol, 2-methyl THF, 2-propanol, acetonitrile, DCM:MeOH 75:25 v/v, DCM:MeOH 25:75, methanol and DMA.
- Freebase Pattern 2 was recovered from acetone, anisole, DMSO:acetonitrile 50:50 v/v, ethyl acetate, isopropyl acetate, methyl acetate, MEK and THF.
- Amorphous solids were recovered from DCM, DCM:MeOH 90:10 v/v, DMSO, ethanol, heptane, tBME, toluene and water.
- An unknown Pattern (assigned as freebase Pattern 5) was recovered from trifluoroethanol.
    - This Pattern did not persist after drying, no other significant changes were observed after drying.

Table 17: Results of the crystallization screen solvent drop griding experiments

Solvent system	XRPD result		Solvent system	XRPD result	
	Wet	Dry		Wet	Dry
1-Propanol	1	1	Ethyl Acetate	2	2
2-Methyl THF	1	1	Heptane	Am	Am
2-Propanol	*1	*1	Isopropyl Acetate	2	2
Acetone	2	2	Methanol	*1	*1
Acetonitrile	1	1	Methyl Acetate	2	2
Anisole	2	2	Methylethyl Ketone (MEK)	2	2
Dichloromethane (DCM)	Am	Am	N,N-Dimethylacetamide (DMA)	+*1	+*1
DCM:MeOH (90:10 v/v)	Am	Am	tert-Butylmethyl Ether (tBME)	Am	Am
DCM:MeOH (75:25 v/v)	*1	*1	Tetrahydrofuran (THF)	2	2
DCM:MeOH (25:75 v/v)	*1	*1	Toluene	Am	Am
Dimethylsulfoxide (DMSO)	A	A	Water	Am	Am
DMSO:Acetonitirile (50:50 v/v)	2	2	Trifluoroethanol	5	PC
Ethanol	Am	Am			

+	Extra peaks
*	Predominantly
PC	Poorly crystalline
Am	Amorphous

Example 6. Freebase Pattern 2 Characterization

During the approximate solubility assessment a novel Pattern (assigned freebase Pattern 2) was observed. In order to gain a preliminary understanding of this new form, Pattern 2 solids recovered from the 1-propanol and 2-propanol solubility experiments were dried at 40 °C under vacuum for 18 h then analysed by ^{1}H NMR (Method 10), ^{19}F NMR (Method 10) and TG/DSC (Method 6).

The results are as follows:

- ^{1}H NMR analysis of Compound A Pattern 2 solids recovered from 1-propanol was consistent with analysis carried out on Pattern 1.
- ^{19}F NMR analysis of Compound A Pattern 2 indicates one fluorine environment, consistent with the supplied structure and with Pattern 1.
- TG/DSC analysis of Pattern 2 recovered from 2-propanol indicated a 6.0 % weight loss from the onset of the experiment to 117 °C, followed by a gradual 4.2 % weight loss from *c.a.* 117 °C to 269 °C.
    - A single endothermic event was observed prior to degradation, with an onset temperature of 244 °C and a peak temperature of 251 °C.

FREEBASE PATTERN 2 SCALE-UP

Attempt 1

In order to assess the formation of freebase Pattern 2 via direct slurry conversion from Pattern 1, a scale-up experiment was carried out as follows:

- 200 mg of Pattern 1 Compound A was weighed out and suspended in 10 mL of ethanol (20 mg/mL).
- The experiment was stirred and temperature cycled between 40 °C and 5 °C, with a temperature ramp of 0.1 °C/min and 1 hour holds between steps.
- After *c.a.* 18 h, a subsample of the resultant slurry was removed and centrifuged; isolated solid was analyzed by XRPD (Method 4).
    - XRPD analysis (Method 4) indicated that the subsample was consistent with freebase Pattern 1.
- The experiment was subsequently ended.

Attempt 2

The second attempt of Pattern 2 scale-up was carried out with the amorphous free base as the input material. The procedure is as follows:

- 200 mg of amorphous Compound A were suspended in 10 mL of ethanol (20 mg/mL)
- The experiment was stirred and temperature cycled between 40 °C and 5 °C, with a temperature ramp of 0.1 °C/min and 1 hour holds between steps.
- After *c.a.* 3 days, a subsample of the resultant slurry was removed and centrifuged; isolated solids were analyzed by XRPD (Method 4).
    - XRPD analysis (Method 4) indicated that the subsample was consistent with freebase Pattern 2.
- The rest of the solids (from the bulk) were then isolated via Buchner filtration, analyzed by XRPD (Method 4), dried under vacuum at 40 °C for 18 h, then analyzed by XRPD (Method 4) and TG/DSC (Method 6).

The second Pattern 2 scale-up attempt was carried out with amorphous input material, the results of this experiment are as follows:

- XRPD analysis (Method 4) of the sub sample solids indicated consistency with freebase Pattern 2.
- XRPD analysis (Method 4) of the isolated solids (wet and dried) indicated consistency with freebase Pattern 2.
- TG/DSC analysis (Method 6) of the solids recovered from the scale-up experiment indicated a 2.1 % weight loss from the onset of the experiment to 260 °C.
    - A single endothermic event was observed prior to degradation, with an onset temperature of 246 °C and a peak temperature of 253 °C.

Example 7. Competitive Slurries

Based on the results obtained from the crystallization screen, Freebase Patterns 1 and 2 were the predominant freebase solid forms. To determine which of these two solid forms is more thermodynamically favoured and under what conditions, competitive slurry experiments were carried out using the following procedure:

- 12 × 10 mg samples of received freebase Pattern 1 prepared freebase Pattern 2 were weighed out and combined to make 12 × 1:1 blends of Patterns 1 and 2.
- Solvent was added to each blend in 100 µL aliquots to form mobile slurries.
- The experiments were stirred at either 20 °C or 35 °C for 8 - 9 days.
- After 2 days the 20 °C experiments were subsampled for XRPD analysis (Method 4) and stirred at 20 °C for a further 7 days.

- After 8 days of stirring, the 35 °C experiments were isolated via centrifugation and analyzed by XRPD (Method 4).
    - Dissolution was observed in the 35 °C DCM:MeOH experiment, XRPD analysis was not carried out.
- After 9 days of stirring in total, the 20 °C experiments were isolated via centrifugation and analyzed by XRPD (Method 4).

Table 18: Experimental details of the competitive slurry experiment

Solvent system	Volume added (µL)	
	20 °C	**35 °C**
2-Propanol	500	500
Acetone	500	500
DCM:MeOH 75:25 v/v	400	400
Dimethyl sulfoxide (DMSO)	400	400
Ethyl acetate	500	500
Methanol:water 50:50 v/v	500	500

The results of these experiments are as follows:

20 °C:

- After two days, an unknown Pattern (assigned as freebase Pattern 4) was recovered from the 2-propanol experiment.
  After drying, the solids were observed to have converted to Pattern 1
- Conversion to freebase Pattern 2 was observed in the acetone and DMSO experiments.
    - The solids recovered from the DMSO experiment were poorly crystalline when wet. After drying, the crystallinity had improved.
- Solids similar to freebase Pattern 3 were recovered from the DCM:MeOH 75:25 v/v experiment.
    - Insufficient solids were isolated after 9 days for XRPD analysis (Method 4).
    - The subsample solids were observed to convert towards Pattern 1 upon drying.
- A mixture of freebase Patterns 1 and 2 were recovered from the ethyl acetate and methanol:water 50:50 v/v experiments, this persisted after drying.
- No significant change in form was observed by XRPD (Method 4) after 9 days of stirring in any experiment.

Table 19: XRPD results of the 20 °C competitive slurry experiment

Solvent	XRPD result			
	2 days		9 days	
	Wet	Dry	Wet	Dry
2-Propanol	Pattern 4	Pattern 1	Pattern 4	Pattern 1
Acetone	Pattern 2	Pattern 2	Pattern 2	Pattern 2
DCM:MeOH 75:25 v/v	Similar to FB 3	Similar to FB 1	Insufficient solids	
Dimethyl sulfoxide	PC P2	Pattern 2	PC P2	Pattern 2
Ethyl acetate	P1 + P2	P1 + P2	P1 + P2	P1 + P2
Methanol:water 50:50 v/v	P1 + P2	P1 + P2	P1 + P2	P1 + P2

PC = Poorly Crystalline
FB = Free Base

35 °C:

- Conversion to Pattern 2 was observed in acetone, DMSO, ethyl acetate and methanol:water.
  - The solids recovered from the DMSO and methanol:water experiments were poorly crystalline.
  - Additional peaks were present in the methanol:water experiment diffractogram.
  - The crystallinity of the poorly crystalline pattern 2 solids was observed to have improved upon drying.
- Conversion to Pattern 4 was observed in the 2-propanol experiment, these solids converted to Pattern 1 upon drying.
- Dissolution was observed in the DCM:MeOH 75:25 v/v experiment, XRPD analysis was not carried out.

Table 20: XRPD results of the 35 °C competitive slurry experiment

Solvent	XRPD Result	
	Wet	Dry
2-Propanol	Pattern 4	Pattern 1
Acetone	Pattern 2	Pattern 2
DCM:MeOH 75:25 v/v	N/A (Solution)	
Dimethyl sulfoxide	PC P2	Pattern 2
Ethyl acetate	Pattern 2	Pattern 2
Methanol:water 50:50 v/v	PC P2+	Pattern 2

PC = Poorly Crystalline

Example 8. Freebase Patterns 3 and 4 Characterization

During the crystallization screen and competitive slurry experiments two new freebase patterns (Patterns 3 and 4) were obtained. In order to understand the properties of these solid forms, further characterization was carried out:

- Pattern 3 solids recovered from the DCM:MeOH antisolvent addition experiment and Pattern 4 solids recovered from the 20 °C 2-propanol competitive slurry experiment were dried under vacuum at 40 °C for *c.a.* 3 days.
- After 3 days these solids were analysed by XRPD (Method 4).

The results obtained are as follows:

- XRPD analysis (Method 4) of the Pattern 3 solids (recovered from the DCM:MeOH antisolvent addition experiment) indicated conversion to a Pattern similar to freebase Pattern 1 upon drying.
- XRPD analysis (Method 4) of the Pattern 4 solids (recovered from the competitive slurry experiment in 2-propanol at 20 °C) indicated conversion to freebase Pattern 1 upon drying.

Example 9. Primary Salt Screen of Compound A

The primary salt screen assessed the formation of Compound A salt forms, exploring 12 counterions across 6 solvent systems. The counterions were selected based on their pK_a, molecular weight, toxicity, diversity and market precedence. The screen was carried out using the following procedure:

- 72 × 20 mg of Compound A were weighed out into 2 mL vials.
- The experiments were suspended/dissolved in 300 - 500 µL of solvent.
- 2.05 mole equivalents of counter-ion were added to each vial.
- The experiments were stirred and temperature cycled between 40 °C and 5 °C, with a temperature ramp of 0.1 °C/min and 1 hour holds between steps for *c.a.* 3 days.
- After 3 days, antisolvent (tBME) was added to experiments that were observed to be solutions until precipitation was observed. Temperature cycling continued for a further 16 h.
- The experiments were isolated via centrifugation and analysed by XRPD (Method 4).
    - The solids were also analysed by XRPD (Method 4) after 16 h of drying under vacuum at 40 °C, and after 16 h of 40°C/ 75% RH storage.

- Where material amounts permitted, potential salts were analyzed by ^{1}H NMR (Method 10) and TG/DTA or TG/DSC.

Table 21: Solvent systems and counterions of the Primary salt screen experiments

Counterions	MW (g/mol)	pKa	Merck Class	# of Equiv.	Solvent volume (µL)	Solvent System (v/v)
Hydrochloric acid	36.46	-6	1	2	500	THF:Water 90:10
Sulfuric acid	98.08	-3	1	2	500	
Maleic acid	116.08	1.92; 6.23	1	2	500	Ethyl acetate
Phosphoric acid	98.00	1.96; 7.12; 12.32	1	2	500	
1-Hydroxy-2-naphthoic acid	188.18	2.7; 13.5	2	2	300	Methanol
(+)-L-Tartaric acid	150.09	3.02; 4.36	1	2	300	
Fumaric acid	116.08	3.03; 4.38	1	2	300	Trifluoroethanol
Citric acid	192.13	3.13; 4.76; 6.40	1	2	300	
p-Toluenesulfonic acid	172.2	-1.34	2	2	300	MEK
Methanesulfonic acid	96.10	-1.2	2	2	300	
Malic acid	134.09	3.459; 5.097	1	2	300	DCM:MeOH 75:25
Succinic acid	118.09	4.21; 5.64	1	2	300	

Table 22: Antisolvent volumes of the primary salt screen experiments

Salt Screen	Volume of tBME added (µL)					
	THF:water 90:10 v/v	EtOAc	MeOH	Trifluoro-ethanol	MEK	DCM:MeOH 75:25 v/v
Hydrochloric acid	N/A (slurry)	N/A (slurry)	200	600	N/A (slurry)	200
Sulfuric acid	N/A (slurry)	N/A (slurry)	N/A (slurry)	400	N/A (slurry)	300
Maleic acid	1000	N/A (slurry)	N/A (slurry)	600	N/A (slurry)	1500
Phosphoric acid	N/A (slurry)	N/A (slurry)	N/A (slurry)	400	N/A (slurry)	100
1-Hydroxy-2-naphthoic acid	300	N/A (slurry)	N/A (slurry)	N/A (slurry)	N/A (slurry)	200
(+)-L-Tartaric acid	500	N/A (slurry)	N/A (slurry)	200	N/A (slurry)	N/A (slurry)
Fumaric acid	N/A (slurry)	N/A (slurry)	N/A (slurry)	300	N/A (slurry)	100
Citric acid	1000	N/A (slurry)	N/A (slurry)	200	N/A (slurry)	N/A (slurry)
p-Toluenesulfonic acid	1000	N/A (Slurry)	N/A (Slurry)	400	N/A (Slurry)	200
Methanesulfonic acid	N/A (Slurry)	N/A (Slurry)	400	400	N/A (Slurry)	400
Malic acid	1000	N/A (Slurry)	N/A (Slurry)	500	N/A (Slurry)	200
Succinic acid	N/A (Slurry)	N/A (Slurry)	N/A (Slurry)	400	N/A (Slurry)	200

The primary salt screen assessed the formation of Compound A salt forms, exploring 12 counterions across 6 solvent systems. The counterions were selected based on their pK_a, molecular weight, toxicity, diversity and market precedence. The results of the primary salt screen are as follows:

Table 23: XRPD Results of the primary salt screen

XRPD results	THF:water 90:10 % v/v			Ethyl acetate			Methanol			Trifluoroethanol			Methylethyl ketone			DCM:methanol 75:25 % v/v		
	Wet	Dry	40°C/ 75 %RH	Wet	Dry	40°C/ 75% RH	Wet	Dry	40°C/ 75% RH	Wet	Dry	40°C/ 75% RH	Wet	Dry	40°C/ 75% RH	Wet	Dry	40°C/ 75% RH
Hydrochloric acid	Am	Am	Am	1, PC, PS	1, PC, PS	1, PC, PS	Am	Am	Am	Am	Am	Am	1, PC, PS	1, PC, PS	1, PC, PS	Am	Am	Am
Sulfuric acid	Am	Am	Am	Am	Am	Am	Am	Am	Am	Am	Am	Am	Am	Am	Am	Am	Am	Am
Maleic acid	1, PS	1, PS	1, PS	1, PS	1, PS	1, PS	1, PC, PS	1, PC, PS	1, PC, PS	Am	Am	Am	2 IS, PS	2 IS, PS	2 IS, PS	Am	PC, PS	2 IS, PC, PS
Phosphoric acid	2 IS, PC, PS	2 IS, PC, PS	2 IS, PC, PS	2 IS, PC, PS	2 IS, PC, PS	2 IS, PC, PS	Am	Am	Am	2 IS, PC, PS	Am	Am	Am	Am	Am	Am	1, PC, PS	1, PC, PS
1-Hydroxy-2-naphthoic acid	1, PC. PS	1, PC. PS	1, PC, PS	2, FB	2, FB	2, FB	2, PC. PS	2, PC. PS	2, PC. PS	NS			2	2	2	3, PC. PS	3, PC. PS	3, PC. PS
L-Tartaric acid	1 IS, PC, PS	1 IS, PC, PS	1 IS, PC, PS	1 IS, PC, PS	1 IS, PC, PS	1 IS, PC, PS	Am, PS	Am, PS	Am, PS	Am	Am	Am	1 IS, PC, PS	1 IS, PC, PS	1 IS, PC, PS	1 IS, PC, PS	1 IS, PC, PS	1 IS, PC, PS
Fumaric acid	1, PC, PS	1, PC, PS	1, PC. PS	2, PC, PS	2, PC. PS	2, PC, PS	3, PC, PS	3, PC. PS	3, PC. PS	4, PC, PS	4, PC. PS	4, PC, PS	2, PC. PS	2*, PC. PS	2, PC, PS	3, PC, PS	3, PC. PS	3, PC, PS
Citric acid	1 IS, PC	PS 1 IS, PC. PS	1 IS, PC, PS	1 IS, PC, PS	1 IS, PC, PS	1 IS, PC, PS	1 IS, PC. PS	1 IS, PC. PS	1 IS, PC, PS	Am	1 IS, PC, PS	1 IS, PC. PS	1 IS, PC, PS	1 IS, PC, PS	1 IS, PC, PS	1 IS, PC. PS	1 IS, PC. PS	1 IS, PC. PS
P-Toluene sulfonic acid	1, PC, PS	1, PC, PS	1, PC, PS	1, PC, PS	1, PC, PS	1, PC, PS	1, PC, PS	1, PC, PS	1, PC, PS	2, PC. PS	2, PC. PS	2, PC, PS	1, PC, PS	1, PC, PS	1, PC. PS	3, PC. PS	3, PC, PS	3, PC, PS
Methane sulfonic acid	1, PC. PS	1, PC, PS	1, PC. PS	1, PC, PS	1, PC. PS	1, PC, PS	1, PC. PS	1, PC. PS	1, PC. PS	1, PC, PS	1, PC. PS	1, PC, PS	1, PC. PS	1, PC. PS	1, PC, PS	1, PC, PS	1, PC. PS	1, PC, PS
Malic acid	1 IS, PC, PS	1 IS, PC. PS	1 IS, PC, PS	1 IS, PC, PS	1 IS, PC, PS	1 IS, PC, PS	2 IS, PC. PS	2 IS, PC. PS	2 IS, PC, PS	1 IS, PC, PS	1 IS, PC, PS	1 IS, PC, PS	1 IS, PC, PS	1 IS, PC, PS	1 IS, PC, PS	1 IS, PC. PS	1 IS, PC. PS	1 IS, PC. PS
Succinic acid	NS			2 IS, PC, PS	2 IS, PC, PS	2 IS, PC, PS	1, PC, PS	Am	Am	2 IS, PC. PS	2 IS, PC, PS	2 IS, PC, PS	2 IS, PC, PS	2 IS, PC, PS	2 IS, PC, PS	3 IS, PC, PS	3 IS, PC, PS	3 IS, PC, PS

FB	Freebase	PC	Partially crystalline	Am	Amorphous	IS	Potentially Isostructural
PS	Potential salt	1,2,3...	Pattern Number	NS	Insufficient/no solids	*	Extra peak

Hydrochloric acid:

- An HCl salt (assigned as hydrochloride Pattern 1 salt) was recovered from the ethyl acetate and MEK experiments.
    - Amorphous solids were recovered from all other HCl experiments.
- The differences between the ^{1}H NMR spectra (Method 10) of the solids recovered from the ethyl acetate experiment and Compound A free base were indications of salt formation.
    - Peaks corresponding to 0.13 molar equivalents (1.22 wt%) of ethyl acetate were also detected.
- TG/DT analysis (Method 7) of the solids recovered from the MEK experiment detected a 5.9 % weight loss from the onset of the experiment to *c.a.* 89 °C, then a 1.6 % weight loss from *c.a.* 89 °C to *c.a.* 176 °C and a 1.8 % weight loss from *c.a.* 176 °C to *c.a.* 222 °C.
- Two shallow endothermic events were observed before the onset of degradation, the first at 45 °C and the second at 195 °C.

Sulfuric acid:

- Amorphous solids were recovered from all sulfuric acid experiments.

Maleic acid:

- Two potential salt forms were recovered from the maleic acid experiments, the first (maleate Pattern 1) from THF:water 90:10 v/v, ethyl acetate and methanol and the second (maleate Pattern 2) from MEK and DCM:MeOH 75:25 v/v.
    - The solids recovered from DCM:MeOH (75:25 v/v) were amorphous when wet and dried to maleate Pattern 2.
    - Though salt formation was confirmed by ^{1}H NMR analysis (Method 2), the diffractogram of maleate Pattern 2 was comparable with potential salts from other counterions. This is an indication of isostructural salt formation.
    - Amorphous solids were recovered from the maleic acid experiment in trifluoroethanol.
- The differences between the ^{1}H NMR spectra (Method 10) of the solids recovered from the ethyl acetate experiment (maleate Pattern 1) and Compound A free base were indications of salt formation.
    - Peaks corresponding to 1.1 equivalents of maleic acid and 0.03 molar equivalents (0.27 wt%) of ethyl acetate were detected.

- TG analysis (Method 6) of the solids recovered from the ethyl acetate experiment (maleate Pattern 1) detected a 5.51% weight loss from the onset of the experiment to *c.a.* 85 °C, then a 7.07 % weight loss from *c.a.* 117 °C to *c.a.* 245 °C.
- TG/DT analysis (Method 7) of the solids recovered from the ethyl acetate experiment (maleate Pattern 1) detected three endothermic events, the first with an onset temperature of *c.a.* 50 °C and a peak temperature of *c.a.* 64 °C, the second with an onset temperature of *c.a.* 170 °C and a peak temperature of *c.a.* 178 °C and the third with an onset temperature of *c.a.* 203 °C and a peak temperature of *c.a.* 218 °C.
- The differences between the ^{1}H NMR spectra (Method 10) of the solids recovered from the MEK experiment (maleate Pattern 2) and Compound A free base were indications of salt formation.
    - Peaks corresponding to 1.4 equivalents of maleic acid and 0.1 molar equivalents (0.79 wt%) of MEK were detected.

Phosphoric acid:

- Two potential salt forms were recovered from the phosphoric acid experiments, the first (phosphate Pattern 1) from DCM:MeOH 75:25 v/v and the second (phosphate Pattern 2) from THF:water 90:10 v/v, ethyl acetate and trifluoroethanol.
    - The phosphate Pattern 2 solids recovered from trifluoroethanol did not persist after drying.
    - Phosphate Pattern 2 was found to be isostructural with other salts.
    - Amorphous solids were recovered from the phosphoric acid experiments in methanol and MEK
- The differences between the ^{1}H NMR spectra (Method 10) of the solids recovered from the DCM:MeOH

Differences between the ^{1}H NMR of the solids recovered from the DCM:MeOH 75:25 v/v experiment (phosphate Pattern 1) and Compound A free base were indications of salt formation.

- Peaks corresponding to 0.02 molar equivalents (0.06 wt%) of tBME were detected.

- TG analysis (Method 6) of the solids recovered from the DCM:MeOH experiment (phosphate Pattern 1) detected a 7.86% mass loss from the onset of the experiment to *c.a.* 102 °C, then a gradual 1.86 % mass loss from 102 °C to *c.a.* 264 °C.

- Three endothermic events were detected prior to degradation: the first with an onset temperature of 36 °C and a peak temperature of 44 °C; the second event was shallow and occurred between 80 °C and 110 °C; the third event had an onset temperature of 199 °C and a peak temperature of 221 °C.

- The differences between the ^{1}H NMR spectra (Method 10) of the solids recovered from the THF:water 90:10 v/v experiment (phosphate Pattern 2) and Compound A free base were indications of salt formation.
  - Peaks corresponding to 0.04 molar equivalents (0.29 wt%) of THF were detected.

1-Hydroxy-2-naphthoic acid:

- Three potential salt forms were recovered from the 1-hydroxy-2-naphthoic acid experiments, the first (1-hydroxy-2-naphthoate Pattern 1) from THF:water 90:10 v/v, the second (1-hydroxy-2-naphthoate Pattern 2) from methanol and the third (1-hydroxy-2-naphthoate Pattern 3) from DCM:MeOH 75:25 v/v.
  - Freebase Pattern 2 was recovered from the 1-hydroxy-2-naphthoic acid experiments in ethyl acetate and MEK.
  - No solids were recovered from the 1-hydroxy-2-naphthoic acid experiment in trifluoroethanol.
- The differences between the ^{1}H NMR spectra (Method 10) of the solids recovered from the 1-hydroxy-2-naphtoic acid in THF:water 90:10 v/v experiment (1-hydroxy-2-naphthoate Pattern 1) and Compound A free base were indications of salt formation.
  - Peaks corresponding to 1 molar equivalent of 1-hydroxy-2-naphthoic acid, 0.49 molar equivalents (3.82 wt%) of THF and 0.12 molar equivalents (1.13 wt%) of tBME were detected.
- The differences between the ^{1}H NMR spectra (Method 10) of the solids recovered from the 1-hydroxy-2-naphthoic acid in methanol experiment (1-hydroxy-2-naphthoate Pattern 2) and Compound A free base were indications of salt formation.
  - Peaks corresponding to 1.2 molar equivalents of 1-hydroxy-2-naphthoic acid were detected. No residual solvents were detected.
- The differences between the ^{1}H NMR spectra (Method 10) of the solids recovered from the 1-hydroxy-2-naphthoic acid in DCM:MeOH 75:25 v/v experiment (1-

hydroxy-2-naphthoate Pattern 3) and Compound A free base were indications of salt formation.

- Peaks corresponding to 1.1 molar equivalents of 1-hydroxy-2-naphthoic acid 0.05 molar equivalents (0.48 wt%) of tBME were detected.

- TG analysis (Method 6) of the solids recovered from the DCM:MeOH experiment (1-hydroxy-2-naphthoate Pattern 3) detected a 1.2 % mass loss from the onset of the experiment to *c.a.* 63 °C and a 13.1 % mass loss from 158 °C to 226 °C.
  - Two endothermic events were observed, the first with an onset of 191 °C and a peak of 202 °C and the second with an onset of 218 °C and a peak of 244 °C.

L-tartaric acid:

- A potential salt form (tartrate Pattern 1) was recovered from the THF:water 90:10 v/v, ethyl acetate, MEK and DCM:MeOH 75:25 v/v experiments.
  - Amorphous solids were recovered from all other tartrate experiments.

  Though salt formation was confirmed via ^{1}H NMR analysis (Method 10), tartrate Pattern 1 was found to be isostructural with other salts.
- The differences between the ^{1}H NMR spectra (Method 10) of the solids recovered from the L-tartaric acid in DCM:MeOH experiment and Compound A free base were indications of salt formation.
  - Peaks corresponding to 1.9 molar equivalents of L-tartaric acid were detected. No residual solvents were detected
- TG analysis (Method 6) of the solids recovered from the DCM:MeOH experiment detected a 5.5 % mass loss from the onset of the experiment to *c.a.* 101 °C and a 18.4 % mass loss from 168 °C to 241 °C.
  - Multiple endothermic events were observed between 190 °C and 240 °C.

Fumaric acid:

- Four potential salt forms were recovered from the fumaric acid experiments, the first (fumarate Pattern 1) from THF:water 90:10 v/v, the second (fumarate Pattern 2) from ethyl acetate and MEK, the third (fumarate Pattern 3) from methanol and DCM:MeOH 75:25 v/v and the fourth (fumarate Pattern 4) from trifluoroethanol.
- The differences between the ^{1}H NMR spectra (Method 10) of the solids recovered from the fumaric acid in THF:water 90:10 v/v experiment (fumarate Pattern 1) and Compound A free base were indications of salt formation.
  - Peaks corresponding to 1.4 molar equivalents of fumaric acid were detected.

- Trace amounts of THF were detected, too low to quantify.

- The differences between the ^{1}H NMR spectra (Method 10) of the solids recovered from the fumaric acid in MEK experiment (fumarate Pattern 2) and Compound A free base were indications of salt formation.
  - Peaks corresponding to 1.3 molar equivalents of fumaric acid were detected.
  - No residual solvents were detected.
- The differences between the ^{1}H NMR spectra (Method 10) of the solids recovered from the fumaric acid in methanol experiment (fumarate Pattern 3) and Compound A free base were indications of salt formation.
  - Peaks corresponding to 1.5 molar equivalents of fumaric acid and 0.08 molar equivalents (0.28 wt%) of methanol were detected.
- TG analysis (Method 6) of the solids recovered from the methanol experiment (fumarate Pattern 3) indicated a 3.44 % mass loss from the onset of the experiment to *c.a.* 66 °C, theoretically equivalent to 1.8 molar equivalents of water. A gradual 1.28 % mass loss was observed between 66 °C and 207 °C, followed by a 9.33 % mass loss from 207 °C to 278 °C.
  - Two endothermic events were also observed: the first event had an onset temperature of 39 °C and a peak temperature of 50 °C; the second, broader, endothermic event had an onset temperature of 183 °C and a peak temperature of 200 °C.
- The differences between the ^{1}H NMR spectra (Method 10) of the solids recovered from the fumaric acid in trifluoroethanol experiment (fumarate Pattern 4) and Compound A free base were indications of salt formation.
  - Peaks corresponding to 1.1 molar equivalents of fumaric acid, 0.04 molar equivalents (0.46 wt%) of trifluoroethanol and 0.02 molar equivalents (0.21 wt%) of tBME were detected.

Citric acid:

- A potential salt form (citrate Pattern 1) was recovered from all citric acid experiments.
  - The solids recovered from the citric acid experiment in trifluoroethanol were amorphous when wet and dried to citrate Pattern 1
  - Though salt formation was confirmed via ^{1}H NMR analysis (Method 10), citrate Pattern 1 was found to be isostructural with other salts.

- The differences between the ^{1}H NMR spectra (Method 10) of the solids recovered from the citric acid in MEK experiment (citrate Pattern 1) and Compound A free base were indications of salt formation.
  - Peaks corresponding to 1.06 molar equivalents of citric acid and 1.1wt% of MEK were detected.
- TG analysis (Method 6) of the solids recovered from the MEK experiment indicated a total mass loss of *ca.* 5.02% from the onset to *c.a.* 124 °C.
  - Endothermic events were observed at peak onsets *ca.* 25 °C, 67 °C (peak at 79 °C) and 149 °C (peak at 169 °C).

ρ-Toluene sulfonic acid:

- Three potential salt forms were recovered from the p-toluene sulfonic acid experiments, the first (tosylate Pattern 1) from THF:water 90:10 v/v, ethyl acetate, methanol and MEK, the second (tosylate Pattern 2) from trifluoroethanol and the third (tosylate Pattern 3) from DCM:MeOH 75:25 v/v.
- The differences between the ^{1}H NMR spectra (Method 10) of the solids recovered from the p-toluene sulfonic acid in MEK experiment (tosylate Pattern 1) and Compound A free base were indications of salt formation.
  - Peaks corresponding to *c.a.* 1.5 molar equivalents of p-toluene sulfonic acid were detected, however due to overlapping peaks, it could not be accurately quantified.
  - Peaks corresponding to 0.31 molar equivalents (2.46 wt%) of MEK were also detected.
- The differences between the ^{1}H NMR spectra (Method 10) of the solids recovered from the p-toluene sulfonic acid in trifluoroethanol experiment (tosylate Pattern 2) and Compound A free base were indications of salt formation.
  - *C.a.* 2 molar equivalents of p-toluene sulfonic acid were detected, based on subtraction of API signals due to peak overlap.
  - Peaks corresponding to 0.16 equivalents (1.51 wt%) of tBME were also detected.
- The differences between the ^{1}H NMR spectra (Method 10) of the solids recovered from the p-toluene sulfonic acid in DCM:MeOH 75:25 v/v experiment (tosylate Pattern 3) and Compound A free base were indications of salt formation.

- *C.a.* 2.2 molar equivalents of p-toluene sulfonic acid were detected, based on subtraction of API signals due to peak overlap.
- Peaks corresponding to 0.01 molar equivalents (0.12 wt%) of DCM and 0.01 equivalents (0.07 wt%) of tBME were detected.

- TG/DT analysis (Method 6) of the solids recovered from the DCM:MeOH 75:25 v/v experiment (tosylate Pattern 3) detected a 2.17 % weight loss from the onset of the experiment to *c.a.* 67 °C, theoretically equivalent to 1.1 equivalents of water.
  - A single endothermic event was observed prior to degradation, with an onset temperature of 288 °C and a peak temperature of 295 °C.

Methanesulfonic acid:

- A potential salt form (mesylate Pattern 1) was recovered from all methanesulfonic acid experiments
- The differences between the ^{1}H NMR spectra (Method 10) of the solids recovered from the methane sulfonic acid in DCM:MeOH 75:25 v/v experiment and Compound A free base were indications of salt formation.
  - Peaks corresponding to 2 molar equivalents of methane sulfonic, 0.03 molar equivalents (0.24 wt%) of DCM, 0.14 equivalents (0.51 wt%) of methanol and 0.17 equivalents (1.66 wt%) of tBME were detected.
- TG/DT analysis (Method 6) of the solids recovered from the DCM:MeOH 75:25 v/v experiment (mesylate Pattern 1) detected a 61.88 % weight loss from the onset of the experiment to *c.a.* 228 °C, followed by a 6.21 % weight loss from 228 °C to *c.a.* 295 °C.
  - Two endothermic events were observed prior to degradation, the first with an onset temperature of 96 °C and a peak temperature of 119 °C and the second with an onset temperature of 229 °C and a peak of 230 °C.

L-malic acid:

- Two potential salt forms were recovered from the L-malic acid experiments, the first (malate Pattern 1) from THF:water 90:10 v/v, ethyl acetate, trifluoroethanol, MEK and DCM:MeOH 75:25 v/v and the second (malate Pattern 2) from methanol.
  - Though salt formation was confirmed via ^{1}H NMR analysis (Method 10), both malate Patterns 1 and 2 were found to be isostructural with other salts,

- The differences between the ^{1}H NMR spectra (Method 10) of the solids recovered from the L-malic acid in ethyl acetate experiment (malate Pattern 1) and Compound A free base were indications of salt formation.
  - L-malic acid was detected, however due to overlapping peaks could not be quantified.
  - Peaks corresponding to 0.02 molar equivalents (0.16 wt%) of ethyl acetate were detected.
- TG analysis (Method 6) of the solids recovered from ethyl acetate (malate Pattern 1) detected a 4.43 % mass loss from the onset of the experiment to *c.a.* 102 °C (theoretically equivalent to 2.3 molar equivalents of water) and a 9.68 % mass loss from *c.a.* 170 °C to *c.a.* 233 °C.
  - Three endothermic events were detected, the first with an onset temperature of 65 °C and a peak temperature of 75 °C, the second with an onset temperature of 174 °C and a peak temperature of 202 °C and the third with an onset temperature of 218 °C and a peak temperature of 222 °C.
- The differences between the ^{1}H NMR spectra (Method 10) of the solids recovered from the L-malic acid in methanol experiment (malate Pattern 2) and Compound A free base were indications of salt formation.
  - L-malic acid was detected, however due to overlapping peaks could not be quantified.
  - 0.29 molar equivalents (1.03 wt%) of methanol were detected.

Succinic acid:

- Three potential salt forms were recovered from the succinic acid experiments, the first (succinate Pattern 1) from methanol, the second (succinate Pattern 2) from ethyl acetate, trifluoroethanol and MEK and the third (succinate Pattern 3) from DCM:MeOH 75:25 v/v
  - Succinate Pattern 1 did not persist after drying.
  - Though salt formation was confirmed via ^{1}H NMR analysis (Method 10), succinate Patterns 2 and 3 were found to be isostructural with other salts.
  - No solids were recovered from the Succinic acid experiment in THF:water 90:10 v/v

- The differences between the ^{1}H NMR spectra (Method 10) of the solids recovered from the succinic acid in methanol experiment (succinate Pattern 1) and Compound A free base were indications of salt formation.
  - 1.5 molar equivalents of succinic acid were detected, however due to partially overlapping signals the true value is likely to be slightly lower than 1.5 molar equivalents.
  - Peaks corresponding to 0.02 molar equivalents (0.06 wt%) of methanol were also detected.
- The differences between the ^{1}H NMR spectra (Method 10) of the solids recovered from the succinic acid in ethyl acetate experiment (succinate Pattern 2) and Compound A free base were indications of salt formation.
  - 1.4 molar equivalents of succinic acid were detected, however due to partially overlapping signals the true value is likely to be slightly lower than 1.4 molar equivalents.
  - Peaks corresponding to 0.02 molar equivalents (0.15 wt%) of ethyl acetate were also detected.
- TG analysis (Method 6) of the solids recovered from the ethyl acetate experiment (succinate Pattern 2) detected a 5.75 % mass loss from the onset of the experiment to *c.a.* 98 °C (theoretically equivalent to 3 molar equivalents of water) and a 14.31 % mass loss from *c.a.* 182 °C to *c.a.* 317 °C.
  - Three endothermic events were observed before degradation, the first with an onset temperature of 62 °C and a peak temperature of 72 °C, the second with an onset temperature of 136 °C and a peak temperature of 143 °C and the third, very broad event, had an onset temperature of 155 °C and a peak temperature of 169 °C.

Example 10. Mini Scale-ups of Selected Salt Forms

Following the primary salt screen, 10 of the potential salt forms were selected for further assessment. These were re-prepared on a 50 mg scale using the following procedures:

- *C.a.* 50 mg of Compound A was added to 10 × 1.5 mL screw cap vials and suspended/dissolved in the appropriate solvent system.
- The samples were stirred at 40°C.

- The required stoichiometric amount of counter-ion was added to each experiment, and stirring continued at 40°C.
    - For the experiments that were cloudy/clear solutions after counterion addition, anti-solvent (tBME) was added to facilitate precipitation.
- The experiments were then temperature cycled between 40°C and 5°C, with a ramp/hold of 0.1 °C/min and 1 hour.
- After *c.a.* 20 hours, the experiments (all slurries) were subsampled for XRPD analysis (Method 4) to check the solid form.
- Additional solvent was added to experiments that were thick slurries in order to improve mixing.
    - For experiments that were not the target form (most were free base forms), additional counterion was also added to facilitate salt formation.
    - All the experiments were allowed to continue temperature cycling as above.
- After another *c.a.* 24 h of cycling, the experiments were again subsampled for XRPD analysis (Method 4) to check the solid form.
    - The experiments that showed the target form were isolated via centrifugation and solids dried under vacuum at 40°C.
    - For experiments that were not the target form, 2.25 vol. of water was added, as these salt forms were suspected to be hydrates.
- The experiments were allowed to continue temperature cycling (as before) for an additional 24 h.
- After 24 h, the solids were isolated via centrifugation, dried under vacuum at 40°C and analysed by XRPD (Method 4).

Table 24: Experimental conditions of the mini scale-ups of selected salt forms

Target Salt Form	Mole Eq. of Acid		Solvent System	Volume added (µL)		
	Initial	Final		Solvent (total)	Antisolvent (tBME)	water
Tosylate P3	2.05	--	DCM:MeOH (75:25 v/v)	500	700	0
Hydrochloride P1	2.0	2.1	Ethyl acetate	649.5	0	126
Maleate P1	2.0	2.1	Ethyl acetate	1600	0	120
Phosphate P1	2.0	2.1	DCM:MeOH (75:25 v/v)	400	400	122
Hydroxynaphthoate P3	1.1	--	DCM:MeOH (75:25 v/v)	600	600	0
Fumarate P3	1.1	--	Methanol	1000	0	0
Malate P1	1.1	1.5	Ethyl Acetate	1500	0	114
Succinate P2	1.1	1.5	Ethyl acetate	1200	0	116
L-Tartrate P1	2.0	2.1	DCM:MeOH (75:25 v/v)	200	300	122
Citrate P1	1.1	1.5	MEK	1200	0	120

The results of these experiments are as follows:

Table 25: Results of the mini scale-ups of selected salt forms

Target Salt	Solvent System	Acid addition + Temp cycle		More acid + Temp cycle		Water addition + Temp cycle		Dried solids
		Obs.	XRPD	Obs.	XRPD	Obs.	XRPD	XRPD
Tosylate P3	DCM:MeOH (75:25 v/v)	Slurry	Tosylate P3, PC	N/A	N/A	Slurry	N/A	Tosylate P3, PC
Hydrochloride P1	Ethyl acetate	Slurry	P2, FB	Slurry	P2, FB	Gel-like	HCl P1 + FB2, PA	Am
Maleate P1	Ethyl acetate	Slurry/gel	Am	Gel-like	Am	Solid on walls	Maleate P1*, PC	Maleate P1, PC
Phosphate P1	DCM:MeOH (75:25 v/v)	Slurry	Am	Gel/slurry	Am	Gum/ solids	Phosphate P1, PA	Phosphate P1, PA
Hydroxy naphthoate P3	DCM:MeOH (75:25 v/v)	Slurry	Hydroxy naphthoate P3, PA	N/A	N/A	N/A	N/A	Hydroxy naphthoate P3, PA
Fumarate P3	Methanol	Slurry	Fumarate P3, PC	N/A	N/A	N/A	N/A	Fumarate P5, PC
Malate P1	Ethyl Acetate	Slurry	P1, FB	Slurry	P1, FB	Solids on walls	Malate P3, PC	Malate P3, PA
Succinate P2	Ethyl acetate	Slurry	P1, FB	Slurry	P1, FB	Solid on walls	Succinate P4, PC	Succinate P4, PA
L-Tartrate P1	DCM:MeOH (75:25 v/v)	Slurry	Am	Slurry	Am	Gum/ solids	Tartrate P1, PA	Tartrate P1, PA
Citrate P1	MEK	Slurry	P2, FB	Slurry	Am	Gum/ solids	Citrate P1, PA	Citrate P1, PA

Am=Amorphous
FB = Freebase
PC = Potential crystalline salt
PA = Partially/ poorly crystalline
* Minor peak shifting

Tosylate Pattern 3:

- XRPD analysis (Method 4) of both damp and dried solids were consistent with the reference diffractogram for tosylate Pattern 3 salt.

- A mass loss of *ca.* 1.7% was observed between the outset and *ca.* 111 °C by TG/DTA (Method 7).
    - No thermal events were observed until the melting and degradation event observed above 250°C.
- The ^{1}H NMR spectrum (Method 10) showed peak shifts that were comparable with the reference spectrum for tosylate Pattern 3 salt.
    - Peaks corresponding to *c.a.* 2.1 mole equiv. of counterion and 0.18 %w/w of methanol were observed in the spectrum.
    - Based on TGA/DTA (Method 7) and ^{1}H NMR analysis (Method 10), Tosylate Pattern 3 appears to be an anhydrous form.

Hydrochloride Pattern 1:

- XRPD analysis (Method 4) showed the first two subsamples to be poorly crystalline with peaks consistent with Pattern 2 of the free base material.
- Salt formation was apparent after the addition of H_2O; the diffractogram was consistent with the reference hydrochloride Pattern 1 salt, but with reduced crystallinity.
    - Some peaks corresponding to Pattern 2 of the free base material were also observed.
    - Dried solids were predominantly amorphous.

Maleate Pattern 1:

- XRPD analysis (Method 4) showed the first two subsamples to be predominantly amorphous.
- Salt formation was apparent after the addition of H_2O.
- The dried diffractogram was consistent with the reference maleate Pattern 1 salt (peak shifting/small peak differences compared with wet material).
- A mass loss of *ca.* 5.87% was observed between the outset and *ca.* 97°C by TG/DTA (Method 7), followed by a 6.97% loss between 125°C and 251°C.
    - Three endothermic events were observed, the first with an onset temperature of 51°C and a peak temperature of 63°C. The second event had an onset temperature of 171°C and a peak temperature of 179°C and the third event had an onset temperature of 202°C and a peak temperature of 215°C.

Phosphate Pattern 1:

- XRPD analysis (Method 4) showed the first two subsamples to be predominantly amorphous.
- Salt formation was apparent after the addition of H_2O; the diffractogram was consistent with the reference phosphate Pattern 1 salt, with partial crystallinity.
    - The dried solids were predominantly amorphous.

1-Hydroxy-2-naphthoate Pattern 3:

- XRPD analysis (Method 4) of both damp and dried solids were consistent with the reference diffractogram for 1-hydroxy-2-napthoate Pattern 3 salt, with partial crystallinity.
    - The dried solids were predominantly amorphous.

Fumarate Pattern 3:

- XRPD analysis (Method 4) of the initial subsample showed a similar pattern to the reference fumarate Pattern 3 salt.
- After further temperature cycling, conversion to a previously an unknown Pattern (assigned as fumarate Pattern 5) was observed. This was retained after drying.

Malate Pattern 1:

- XRPD analysis (Method 4) showed the first two subsamples to be consistent with Pattern 1 of the free base material, with the second being poorly crystalline.
- The diffractogram of the subsample taken after water addition showed an unknown pattern (assigned as malate Pattern 3). This became partially crystalline after drying.

Succinate Pattern 2:

- XRPD analysis (Method 4) showed the first two subsamples to be consistent with Pattern 1 of the free base material, with the second being poorly crystalline.
- The diffractogram of the subsample taken after water addition showed an unknown pattern (assigned as succinate Pattern 4). This became poorly crystalline after drying.

Tartrate Pattern 1:

- XRPD analysis (Method 4) showed the first two subsamples to be predominantly amorphous.
- Salt formation was apparent after the addition of H_2O; the diffractogram was consistent with the reference tartrate Pattern 1 salt. The solids became predominantly amorphous after drying.

Citrate Pattern 1:

- XRPD analysis (Method 4) showed the first subsample to be consistent with Pattern 2 of the free base material, with the second being predominantly amorphous.
- Salt formation was apparent after the addition of H_2O; the diffractogram was consistent with the reference citrate Pattern 1 salt, but with reduced crystallinity.

Example 11. Aqueous Solubility

Following the mini scale up experiments, experiments were carried out to determine the aqueous solubility of the most promising salt and freebase forms. In order to fund the aqueous solubility experiments, the required salts were prepared on a 200 mg scale using the following procedure:

- 3 × 200 mg of Compound A was weighed out and suspended/dissolved in the required volume of solvent at 40 °C.
- A stoichiometric amount of counter-ion was added to each experiment, and these were then stirred for 1 hour at 40 °C.
    - 2.1 mL of antisolvent (tBME) was added to the tosylate experiment to create a thick slurry.
- The experiments were temperature cycled between 40 °C and 5 °C with a ramp of 0.1 °C/min and 1 hour hold between steps.
- After *c.a.* 19 h of cycling, the solids were isolated via centrifugation, analyzed by XRPD (Method 4) to check the form, and then dried under vacuum at 40 °C for *c.a.* 3 days.
    - The dried solids were re-analyzed by XRPD (Method 4).

Table 26: Experimental conditions of the aqueous solubility salt preparations

Target Salt Form	Counter-ion stoichiometry (Equivalents)	Solvent	Volume added
Maleate Pattern 1	2.05	Ethyl acetate	2 mL (+ 0.45 mL
Tosylate Pattern 3	2.05	DCM:MeOH 75:25 v/v	1.5 mL
Fumarate Pattern 3	1.05	Methanol	3 mL

The aqueous solubility experiment was carried out on the salts (prepared above) and free base Patterns 1 and 2, according to the following procedure:

- 2 × 50 mg samples of each material was suspended in 2.5 mL of water and stirred at 20 °C.

- After 30 minutes, one sample of each material was isolated via centrifugation. pH measurements were taken of the mother liquors and the solids were analyzed by XRPD (Method 4).
    - HPLC analysis (Method 14) was also carried out on the mother liquors to determine the concentrations.
- After 24 h, the other sample of each material was also isolated via centrifugation. pH measurements were taken of the mother liquors and the solids were analyzed by XRPD (Method 4).
    - HPLC analysis (Method 14) was also carried out on the mother liquors to determine the concentrations.

The results of these preparations are as follows:

- Maleate Pattern 1 and tosylate Pattern 3 were successfully produced from their respective experiments.
- A previously unobserved Pattern (assigned as fumarate Pattern 6) was recovered from the fumarate Pattern 5 preparation experiment.
    - The fumarate Pattern 6 solids were used as input for the aqueous solubility experiment.

The results of the aqueous solubility experiment proper are as follows:

- pH analysis indicated a 0.54 drop in pH between the 30 min and 24 h time points in the Tosylate experiment.
    - All other changes in pH were smaller.
- XRPD analysis (Method 4) showed minimal changes in diffractograms between the 30 min and 24 h timepoints for all the experiments.
    - Several diffractograms were similar but not completely consistent with their input diffractograms.
    - A diffractogram similar to maleate Pattern 1 was recovered from the maleate Pattern 1 experiment. This was assigned as maleate Pattern 1*
- HPLC analysis (Method 14) of the mother liquors indicated a concentration of <0.04 mg/mL for all the experiments at both the 30 min and 24 h timepoint.

Table 27: Results of the aqueous solubility experiment

Input Pattern	30 min			24 h		
	pH	XRPD	Concentration (mg/mL)	pH	XRPD	Concentration (mg/mL)
Maleate P1	2.50	Maleate P1*	0.0336	2.49	Maleate 1*	0.0156
Tosylate P3	4.29	Tosylate P3	0.0014	3.75	Tosylate 3	0.0111
Fumarate P6	3.28	Similar to Fumarate P5 + traces P6	0.0308	3.08	Similar to Fumarate P5 + traces P6	0.0032
Freebase P1	8.41	Similar to FB 1	Not detected	8.56	Similar to FB 1	0.0001
Freebase P2	8.50	FB 2	Not detected	8.53	FB 2	Not detected

Example 12. Secondary Screen of Selected Solid Forms

The freebase Pattern 2 and tosylate Pattern 3 salt forms of Compound A were reprepared on a 200 mg scale to allow more detailed characterisation to be carried out. The following procedure was used:

FREEBASE PATTERN 2:

- *ca.* 200 mg of amorphous Compound A was suspended in 12.4 mL of ethanol.
- The slurry was temperature cycled from 5 to 40 °C for ca. 20 h.
- The solids were recovered by Buchner filtration and dried at 40 °C under vacuum for c.a. 18 h.
- Dried solids were characterized by XRPD (Method 4) to confirm Pattern 2.

TOSYLATE PATTERN 3:

- *ca.* 500 mg of amorphous Compound A and 2.05 equivalents of p-toluenesulfonic acid were suspended in 3.75 mL of DCM:MeOH 75:25 v/v at 40 °C.
- 5.25 mL of tBME was added, forming a slurry.
- The slurry was temperature cycled with stirring from 5 to 40 °C for ca. 20 h.
- Solids were recovered by Buchner filtration and analyzed by XRPD (Method 4).
- After confirming that Pattern 3 had been obtained, solids were dried under vacuum at 40 °C for c.a. 18 h and re-analyzed by XRPD (Method 4).

Dried solids of both freebase Pattern 2 and tosylate Pattern 3 were characterized by XRPD (Method 4), TG/DSC (Method 6), Standalone DSC (Method 8), ^{1}H + ^{19}F NMR (Method 10), FT-IR (Method 11), PLM (Method 5), KF (Method 9), HPLC (Method 14) and DVS (Method 12).

From all the screening studies carried out so far, the most promising forms of Compound A were determined to be freebase Pattern 2 and tosylate Pattern 3. These forms were reprepared

on a 200 mg scale to allow more detailed characterisation to be carried out. The results of these experiments are as follows:

FREEBASE PATTERN 2

- XRPD analysis (Method 4) indicated the recovered solids were consistent with freebase Pattern 2 both wet and dry.
- TG/DSC analysis (Method 6) of free base Pattern 2 indicated a 0.71 % weight loss from the onset of the experiment to *c.a.* 220 °C.
  - One endothermic event was observed, with an onset temperature of 244 °C and a peak temperature of 252 °C.
- During the DSC first heat (Method 8), an endothermic event with an onset temperature of 246 °C and a peak temperature of 253 °C was observed.
  - In the cooling step, a glass transition was observed with a midpoint of 144 °C.
  - During the second heat step, a glass transition was observed with a midpoint of 151 °C.
- ^{1}H NMR analysis (Method 10) of Compound A Pattern 2 was consistent with analysis carried out on Pattern 1. No residual ethanol was observed.
- ^{19}F NMR (Method 10) showed a single fluorine environment, consistent with molecular structure.
- FT-IR spectrum (Method 11) of freebase Pattern 2 was consistent with that of freebase Pattern 1.
- PLM analysis (Method 5) showed small particles with some aggregation. Some birefringence observed.
- Karl Fisher titration (Method 9) indicated an average water content of 0.6%.
- HPLC analysis (Method 14) indicated a purity of 98.06 %area.
- DVS analysis (Method 12) showed water uptake of 12.2 % at 80 % RH, indicating moderately hygroscopicity. After DVS analysis, XRPD analysis (Method 4) of the residual solids was consistent with the input form, but with a slight decrease in crystallinity. A maximum hysteresis of 6.6 % was observed and the mass uptake was reversible.

TOSYLATE PATTERN 3

- XRPD analysis (Method 4) indicated the recovered solids were consistent with tosylate Pattern 3 both wet and dry.

- TG/DSC analysis (Method 6) of tosylate Pattern 3 indicated a mass loss of ca. 1.7% between the outset and ca. 111°C.
  - No thermal events were observed until the melting and degradation event with onset temperature of 291°C and a peak temperature of 296 °C.
- During the DSC (Method 8) first heat, an endothermic event with an onset temperature of 293 °C and a peak temperature of 297 °C was observed.
  - In the cooling step, a glass transition was observed with a midpoint of 159 °C and in the second heat a glass transition was observed with a midpoint of 170 °C.
- ^{1}H NMR analysis (Method 10) was consistent with the structure of Compound A, with peak shifting indicating salt formation. Peaks corresponding to 1.8 equivalents of tosylate counterion was observed. No residual solvent was observed.
- 19F NMR (Method 10) detected 1 fluorine environment, consistent with the expected result.
- FT-IR spectrum (Method 11) was collected for tosylate Pattern 3 for reference.
- PLM analysis (Method 5) showed small particles with some aggregation. Slight birefringence observed.
- Karl Fisher titration (Method 9) showed an average water content of 2.4%.
- HPLC analysis (Method 14) indicated solid purity of 97.81 %area.
- DVS analysis (Method 12) indicated a water uptake of 5.3 % at 80 % RH, indicating moderate hygroscopicity. After DVS analysis, XRPD analysis (Method 4) of the resulting solids was consistent with the input form, but with a slight decrease in crystallinity. A maximum hysteresis of 0.2 % was observed and the mass uptake was reversible.

1-WEEK STABILITY STUDY

As a part of the secondary screen, 1-week stability studies were carried out on both freebase Pattern 2 and tosylate Pattern 3. The following procedure was used:

- 3 × 20 mg samples of both materials were weighed out, one sample of each was stored under the following conditions:
  - 40 °C/75 % RH (Open vial)
  - 80 °C (Closed vial)
  - Ambient temperature, light and humidity (Open vial)

- These experiments were stored under their respective conditions for 1 week after which they were analyzed by XRPD (Method 4) and HPLC (for purity) (Method 14).

As a part of the secondary screen, 1-week stability study was carried out on both freebase Pattern 2 and tosylate Pattern 3. The results of this experiment are as follows:

- Freebase Pattern 2 showed no change in solid form or crystallinity by XRPD (Method 4) under any of the tested conditions.
  - A <1 %area loss in solid purity was observed under all conditions.
- Tosylate Pattern 3 showed no change in solid form or crystallinity by XRPD (Method 4) under any of the tested conditions.
  - No significant change in purity was observed under any of the examined conditions.

Table 28: Results of the 1-week stability studies

Input Form	Storage Condition	Purity (%area)	XRPD Results
Freebase Pattern 2	Input (Reference)	98.06	**FB 2**
	Ambient	97.96	**FB 2**
	80 °C	97.87	**FB 2**
	40 °C/ 75% RH	97.30	**FB 2**
Tosylate Pattern 3	Input (Reference)	97.81	**Tosylate 3**
	Ambient	97.87	**Tosylate 3**
	80 °C	97.94	**Tosylate 3**
	40 °C/ 75% RH	97.61	**Tosylate 3**

PH SOLUBILITY ASSESSMENT

As a part of the secondary screen, pH solubility assessment was carried out on both freebase Pattern 2 and tosylate Pattern 3. The following procedure was used:

- 10 mg of both materials were each weighed into 3 × 1.5 mL vials.
- 500 µL of the required buffer was added to each vial to obtain mobile slurries, and the experiments were stirred at 20 °C. The buffers assessed were:
  - pH 1.2 = HCl/KCl
  - pH 4.5 = Acetate
  - pH 6.8 = Phosphate
- After 1 h and 22 h, the pH of the slurries were measured and adjusted if required.

- After a total of 24 h, a final pH measurement was taken (no adjustment) and the solids were isolated via centrifugation.
- The isolated solids were analyzed by XRPD (Method 4) and the liquors by HPLC (concentration) (Method 14).

As a part of the secondary screen, a pH solubility assessment was carried out on both freebase Pattern 2 and tosylate Pattern 3. The results of these experiment are as follows:

Freebase Pattern 2:

- At pH 1.2, freebase Pattern 2 was observed to become amorphous.
  - Solubility of 0.0273 mg/mL was observed.
- Freebase Pattern 2 persisted at pH 4.5, however a decrease in crystallinity and emergence of extra peaks were observed.
  - Solubility of 0.0022 mg/mL was observed.
- At pH 6.8, freebase Pattern 2 was observed to persist.
  - Solubility of 0.0023 mg/mL was observed.

Tosylate Pattern 3:

- At pH 1.2, tosylate Pattern 3 was observed to persist.
  - Solubility of 0.0303 mg/mL was observed.
- At pH 4.5, tosylate Pattern 3 was observed to persist.
  - Solubility of 0.0058 mg/mL was observed.
- At pH 6.8, tosylate Pattern 3 was observed to become amorphous.
  - Solubility of 0.0020 mg/mL was observed.

Table 29: Results of the pH solubility assessment

Form	Target pH	1 h pH		22 h		24 h	Solubility / mg/mL	XRPD
		Measured	Adjusted	Measured	Adjusted	Measured		
Freebase Pattern 2	1.2	1.38	1.29	1.37	1.28	1.35	0.0273	**A**
	4.5	4.66	4.53	4.46	N/A	4.51	0.0022	**FB 2+, PC**
	6.8	6.86	N/A	6.83	N/A	6.88	0.0023	**FB 2**
Tosylate pattern 3	1.2	1.18	N/A	1.17	N/A	1.20	0.0303	**Tosylate 3**
	4.5	4.54	N/A	4.46	N/A	4.49	0.0058	**Tosylate 3**
	6.8	6.74	N/A	6.54	6.73	6.82	0.0020	**A**

+ = Extra peaks
FB 2 = Freebase Pattern 2
PC = Poorly crystalline
Tosylate 3 = Tosylate Pattern 3
A = Amorphous

Example 13. XRPD Analysis of Compound A Batch A and Batch B

Two samples of solid form Compound A free base were analyzed by XRPD according to XRPD Method 1. Batch A (from polymorph screening) was determined to be crystalline and the XRPD pattern was defined as P2 Form (FIG. 113) from polymorph screening. The X-ray diffraction pattern of Batch B is shown in FIG. 114. The XRPD peaks for Batch A and Batch B are shown in Table 1 and Table 2, respectively, above.

DSC for Batch B was carried out according to DSC Method 2. DSC (FIG. 115) registered an onset temperature of 253.93°C and a peak temperature of 256.87°C, which also confirms that Compound A is crystalline. TGA for Batch B was carried out according to TGA Method 3. TGA (FIG. 116) result showed a weight loss of 0.31% at 150°C.

Example 14. Preparation of a crystalline ethanol solvate form of Compound A

Activated carbon was added to a solution of crude Compound A in DCM and ethanol (80:20). The mixture was filtered to remove the activated carbon, the filter was rinsed with a mixture of DCM and ethanol, and the combined filtrate and rinse was concentrated to induce crystallization. The product was collected by filtration, the cake was washed with a mixture of DCM and ethanol, and the wet cake was dried to afford a solid. XRPD patterns were obtained according to Method 15. DSC and DVS analyses were also carried out.

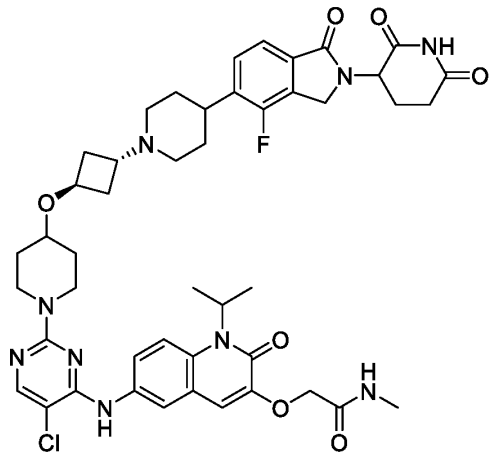
EQUIVALENTS

While the present invention has been described in conjunction with the specific embodiments set forth above, many alternatives, modifications and other variations thereof will be apparent to those of ordinary skill in the art. All such alternatives, modifications and variations are intended to fall within the spirit and scope of the present invention.

CLAIMS

What is claimed is:

1. A solid form of Compound A:



(Compound A).

2. The solid form of claim 1, wherein the solid form is crystalline.

3. The solid form of claim 1, wherein the solid form is amorphous.

4. The solid form of claim 1 or 2, wherein the solid form is a crystalline polymorphic form characterized by two or three XRPD signals selected from the group consisting of 8.2 °2θ, 8.7 °2θ, and 13.9 °2θ (±0.2 °2θ; Cu Kα1 radiation).

5. The solid form of claim 1 or 2, wherein the solid form is a crystalline polymorphic form characterized by XRPD signals at 8.2 °2θ, 8.7 °2θ, and 13.9 °2θ (±0.2 °2θ; Cu Kα1 radiation).

6. The solid form of claim 1 or 2, wherein the solid form is a crystalline polymorphic form characterized by XRPD spectra substantially similar to that shown in FIG 3B.

7. The solid form of claim 1 or 2, wherein the solid form is a crystalline polymorphic form characterized by one, two, three, four, five, six, seven, eight, nine, or ten XRPD signals selected from those in Table 1.

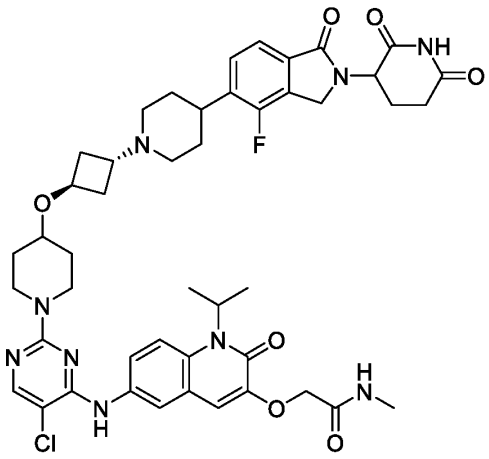
8. The solid form of claim 1 or 2, wherein the solid form is a crystalline polymorphic form characterized by one, two, three, four, five, six, seven, eight, nine, or ten XRPD signals selected from those in Table 2.

9. The solid form of claim 1 or 2, wherein the solid form is a crystalline polymorphic form characterized by XRPD spectra substantially similar to that shown in FIG 3A.

10. The solid form of claim 1 or 2, wherein the solid form is a crystalline polymorphic form characterized by XRPD spectra substantially similar to that shown in FIG 73B.

11. The solid form of claim 1 or 2, wherein the solid form is a crystalline polymorphic form characterized by XRPD spectra substantially similar to that shown in FIG 74B.

12. A hydrochloride salt of Compound A:



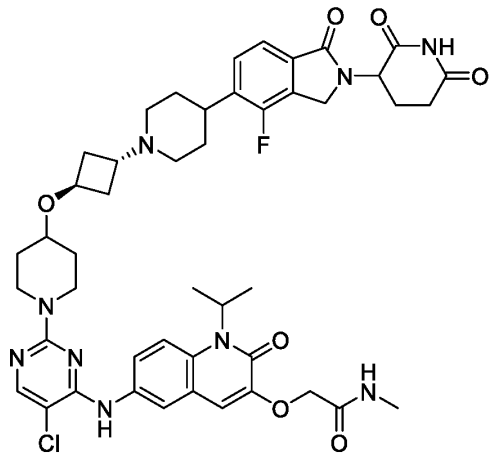
(Compound A).

13. The hydrochloride salt of claim 12, wherein the hydrochloride salt is crystalline.

14. The hydrochloride salt of claim 12, wherein the hydrochloride salt is amorphous.

15. The hydrochloride salt of claim 12 or 13, wherein the hydrochloride salt is a crystalline polymorphic form characterized by XRPD spectra substantially similar to that shown in FIG 75D.

16. A maleate salt of Compound A:



(Compound A).

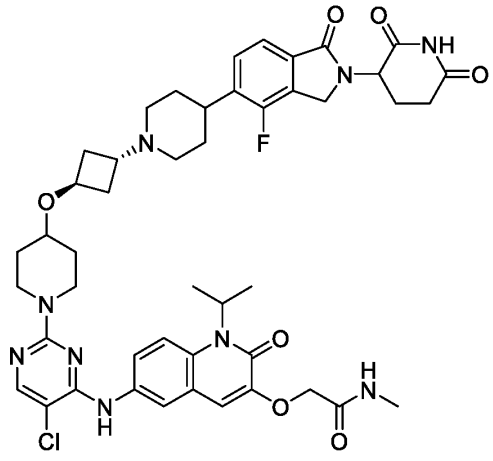
17. The maleate salt of claim 16, wherein the maleate salt is crystalline.

18. The maleate salt of claim 16, wherein the maleate salt is amorphous.

19. The maleate salt of claim 16 or 17, wherein the maleate salt is a crystalline polymorphic form characterized by XRPD spectra substantially similar to that shown in FIG 77C.

20. The maleate salt of claim 16 or 17, wherein the maleate salt is a crystalline polymorphic form characterized by XRPD spectra substantially similar to that shown in FIG 77D.

21. A phosphate salt of Compound A:



(Compound A).

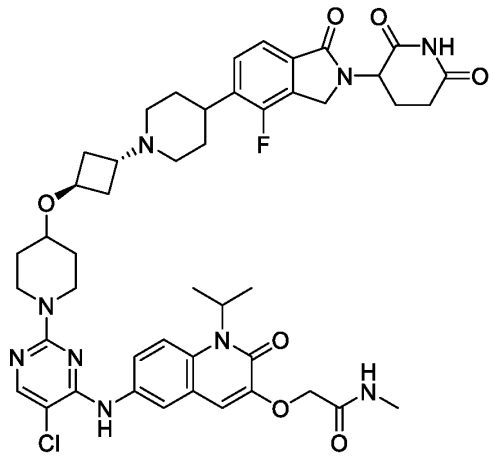
22. The phosphate salt of claim 21, wherein the phosphate salt is crystalline.

23. The phosphate salt of claim 21, wherein the phosphate salt is amorphous.

24. The phosphate salt of claim 21 or 22, wherein the phosphate salt is a crystalline polymorphic form characterized by XRPD spectra substantially similar to that shown in FIG 78C.

25. The phosphate salt of claim 21 or 22, wherein the phosphate salt is a crystalline polymorphic form characterized by XRPD spectra substantially similar to that shown in FIG 78D.

26. A 1-hydroxy-2-naphthoate salt of Compound A:



(Compound A).

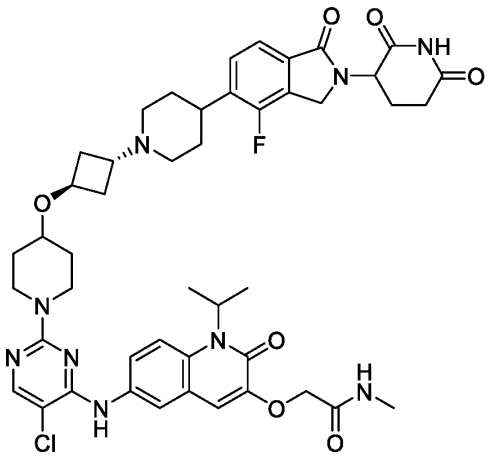
27. The 1-hydroxy-2-naphthoate salt of claim 26, wherein the 1-hydroxy-2-naphthoate salt is crystalline.

28. The 1-hydroxy-2-naphthoate salt of claim 26 or 27, wherein the 1-hydroxy-2-naphthoate salt is a crystalline polymorphic form characterized by XRPD spectra substantially similar to that shown in FIG 79C.

29. The 1-hydroxy-2-naphthoate salt of claim 26 or 27, wherein the 1-hydroxy-2-naphthoate salt is a crystalline polymorphic form characterized by XRPD spectra substantially similar to that shown in FIG 79D.

30. The 1-hydroxy-2-naphthoate salt of claim 26 or 27, wherein the 1-hydroxy-2-naphthoate salt is a crystalline polymorphic form characterized by XRPD spectra substantially similar to that shown in FIG 79E.

31. A tartrate salt of Compound A:



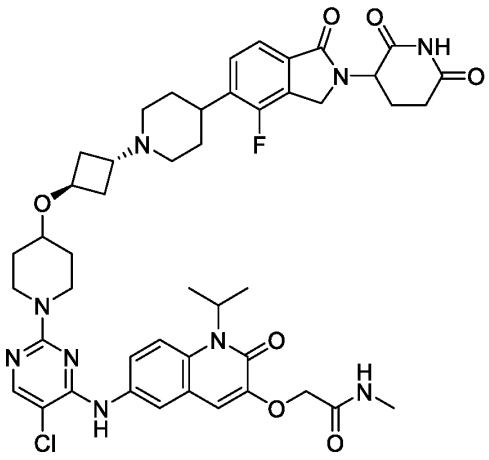
(Compound A).

32. The tartrate salt of claim 31, wherein the tartrate salt is crystalline.

33. The tartrate salt of claim 31, wherein the tartrate salt is amorphous.

34. The tartrate salt of claim 31 or 32, wherein the tartrate salt is a crystalline polymorphic form characterized by XRPD spectra substantially similar to that shown in FIG 80C.

35. A fumarate salt of Compound A:



(Compound A).

36. The fumarate salt of claim 35, wherein the fumarate salt is crystalline.

37. The fumarate salt of claim 35 or 36, wherein the fumarate salt is a crystalline polymorphic form characterized by XRPD spectra substantially similar to that shown in FIG 81C.

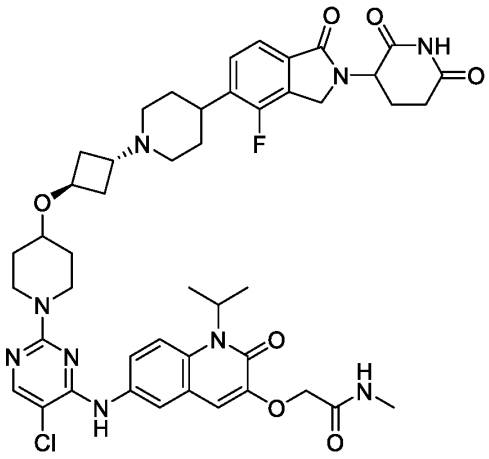
38. The fumarate salt of claim 35 or 36, wherein the fumarate salt is a crystalline polymorphic form characterized by XRPD spectra substantially similar to that shown in FIG 81D.

39. The fumarate salt of claim 35 or 36, wherein the fumarate salt is a crystalline polymorphic form characterized by XRPD spectra substantially similar to that shown in FIG 81E.

40. The fumarate salt of claim 35 or 36, wherein the fumarate salt is a crystalline polymorphic form characterized by XRPD spectra substantially similar to that shown in FIG 81F.

41. The fumarate salt of claims 35 or 36, wherein the fumarate salt is a crystalline polymorphic form characterized by XRPD spectra substantially similar to that shown in FIG 99A.

42. A citrate salt of Compound A:



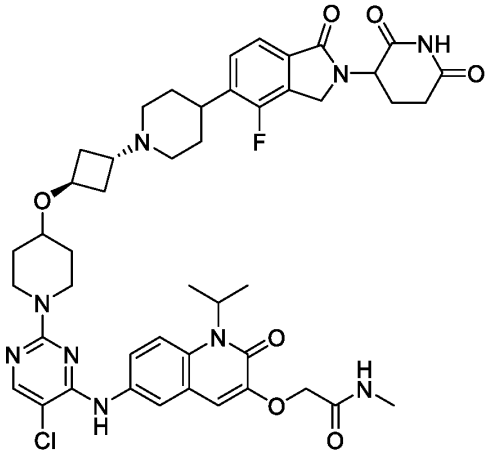
(Compound A).

43. The citrate salt of claim 42, wherein the citrate salt is crystalline.

44. The citrate salt of claim 42, wherein the citrate salt is amorphous.

45. The citrate salt of claim 42 or 43, wherein the citrate salt is a crystalline polymorphic form characterized by XRPD spectra substantially similar to that shown in FIG 82D.

46. A tosylate salt of Compound A:



(Compound A).

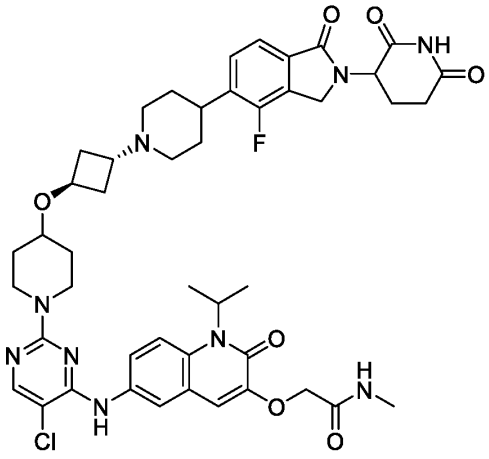
47. The tosylate salt of claim 46, wherein the tosylate salt is crystalline.

48. The tosylate salt of claim 46 or 47, wherein the tosylate salt is a crystalline polymorphic form characterized by XRPD spectra substantially similar to that shown in FIG 83C.

49. The tosylate salt of claim 46 or 47, wherein the tosylate salt is a crystalline polymorphic form characterized by XRPD spectra substantially similar to that shown in FIG 83D.

50. The tosylate salt of claim 46 or 47, wherein the tosylate salt is a crystalline polymorphic form characterized by XRPD spectra substantially similar to that shown in FIG 83E.

51. A mesylate salt of Compound A:

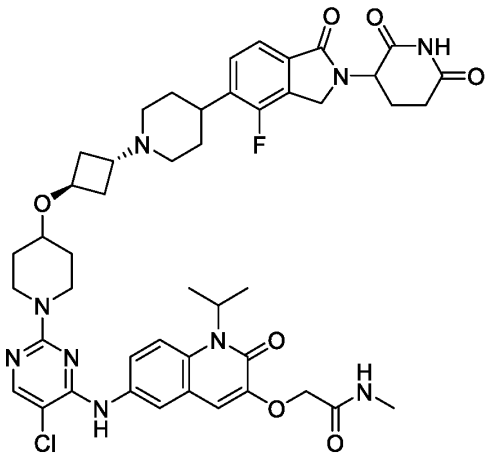


(Compound A).

52. The mesylate salt of claim 51, wherein the mesylate salt is crystalline.

53. The mesylate salt of claim 51 or 52, wherein the mesylate salt is a crystalline polymorphic form characterized by XRPD spectra substantially similar to that shown in FIG 84C.

54. A malate salt of Compound A:



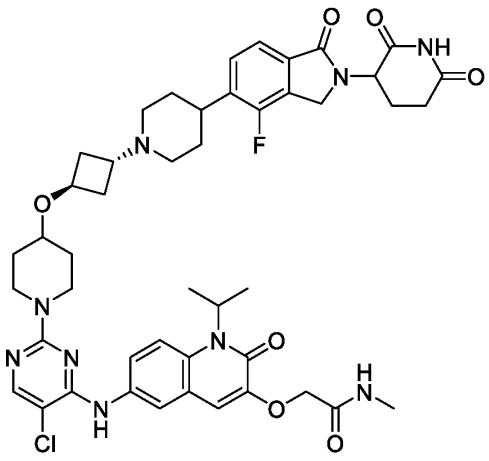
(Compound A).

55. The malate salt of claim 54, wherein the malate salt is crystalline.

56. The malate salt of claim 54 or 55, wherein the malate salt is a crystalline polymorphic form characterized by XRPD spectra substantially similar to that shown in FIG 85C.

57. The malate salt of claim 54 or 55, wherein the malate salt is a crystalline polymorphic form characterized by XRPD spectra substantially similar to that shown in FIG 85D.

58. A succinate salt of Compound A:



(Compound A).

59. The succinate salt of claim 58, wherein the succinate salt is crystalline.

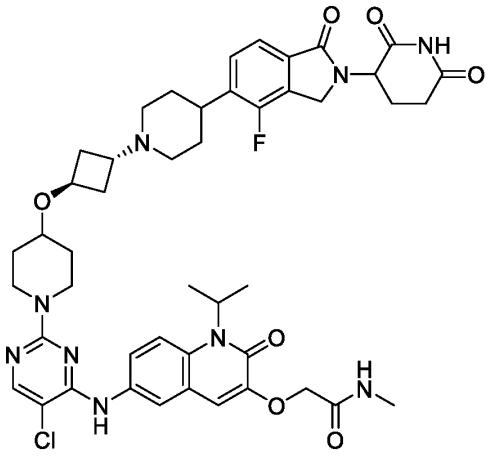
60. The succinate salt of claim 58, wherein the succinate salt is amorphous.

61. The succinate salt of claim 58 or 59, wherein the succinate salt is a crystalline polymorphic form characterized by XRPD spectra substantially similar to that shown in FIG 86D.

62. The succinate salt of claim 58 or 59, wherein the succinate salt is a crystalline polymorphic form characterized by XRPD spectra substantially similar to that shown in FIG. 86C.

63. The succinate salt of claim 58 or 59, wherein the succinate salt is a crystalline polymorphic form characterized by XRPD spectra substantially similar to that shown in FIG. 86E.

64. An ethanol solvate of Compound A:



(Compound A).

65. The ethanol solvate of claim 64, wherein the ethanol solvate is crystalline.

66. The ethanol solvate of claim 64, wherein the ethanol solvate is a crystalline polymorphic form characterized by XRPD spectra substantially similar to that shown in FIG. 118.

67. The ethanol solvate of claim 64, wherein the ethanol solvate is a crystalline polymorphic form characterized by XRPD spectra substantially similar to that shown in FIG. 119.

68. A method of treating a disease or disorder in a subject comprising administering to the subject a therapeutically effective amount of a solid form or salt of any one of the preceding claims.

69. The method of claim 68, wherein the disease or disorder is associated with aberrant BCL6 expression and or activity.

70. The method of claim 68, wherein the disease or disorder is cancer.

71. The method of claim 70, wherein the cancer is advanced lymphoma, relapsed/refractory (R/R) lymphoma, malignant lymphoma, Burkitt's lymphoma, non-Hodgkin's lymphoma, advanced non-Hodgkin Lymphoma, B-cell advanced non-Hodgkin Lymphoma, Large B-cell Lymphoma, follicular lymphoma, intravascular large B-cell lymphoma, transformed follicular lymphoma, angioimmunoblastic T-cell lymphoma, diffuse large B-cell lymphoma (DLBCL), high grade B-cell lymphoma, germinal center B-cell (GCB) DLBCL, activated B-cell (ABC) DLBCL, non-Hodgkin's lymphoma not otherwise specified, solid tumors (e.g. breast cancer, lung cancer, ovarian cancer, neuroblastoma, and glioblastoma), Kaposi advanced non-Hodgkin's lymphoma (NHL), relapsed/refractory (R/R) non-Hodgkin's lymphoma (NHL), relapsed/refractory (R/R) B cell non-Hodgkin's Lymphoma, advanced relapsed/refractory (R/R) non-Hodgkin's lymphoma (NHL), nodal T-follicular helper cell lymphoma - angioimmunoblastic type (nTFHL-AI) / advanced angioimmunoblastic T-cell lymphoma (AITL), relapsed/refractory (R/R) nodal T-follicular helper cell lymphoma - angioimmunoblastic type (nTFHL-AI) / angioimmunoblastic T-cell lymphoma (AITL), nodal T-follicular helper cell lymphoma (nTFHL), relapsed/refractory (R/R) nodal T-follicular helper cell lymphoma (nTFHL), advanced nTFHL, R/R nTFHL, nodal T-follicular helper cell lymphoma-angioimmunoblastic type (nTFHL-AI), advanced nTFHL-AI, R/R nTFHL-AI, T-lineage lymphoblastic Lymphoma (T-LL), Peripheral T-cell lymphoma, or Pre-B Lymphoma.

72. The method of claim 71, wherein the solid tumors are selected from breast cancer, lung cancer, ovarian cancer, neuroblastoma, and glioblastoma.